THE ROLE OF TRANSFORMING GROWTH FACTOR BETA IN HEPATIC ENCEPHALOPATHY PATHOGENESIS

A Dissertation

by

MATTHEW ALEXANDER MCMILLIN

Submitted to the Office of Graduate and Professional Studies of
Texas A&M University
in partial fulfillment of the requirements for the degree of

DOCTOR OF PHILOSOPHY

Chair of Committee,	Sharon DeMorrow
Committee Members,	Cynthia Meininger
	Pier Luigi Di Patre
	Russell Sanchez
Head of Department,	Alejandro Arroliga

December 2013

Major Subject: Neuroscience

ABSTRACT

Hepatic encephalopathy (HE) is a neurological complication that arises due to liver dysfunction and is associated with increased circulating ammonia and a systemic immune response. Treatment paradigms have attempted to minimize the metabolic and inflammatory consequences of liver failure. However, investigations into the specific cell signaling mechanisms between the liver and brain that induce these pathological processes are currently lacking. Both TGFβ1 and Shh are known to be upregulated in the liver and present in the circulation following liver damage. These studies employed the azoxymethane (AOM) model of acute liver failure in mice, the bile duct ligation (BDL) model of minimal HE in rats, and patients with liver cirrhosis who had HE to study cell signaling and pathological processes present during HE. Studies of specific cellular signaling mechanisms were performed in isolated primary neurons and immortalized brain endothelial cells. All pharmacological manipulations of hedgehog signaling, TGFβ signaling, and clodronate-liposome depletion of microglia were performed in AOM mice. Gli1 was upregulated in AOM, BDL, and HE patient cortices. Shh was upregulated in the liver and serum during HE, but had no effect on neurological decline. Liver TGFβ1 signaling was upregulated and had increased expression in cortical neurons. TGFβ1 suppressed neuronal Gli1 via SMAD3. The use of neutralizing antibodies against TGFβ generated neuroprotection during HE. The BBB was disrupted

during AOM-induced HE and neutralizing antibodies against TGFβ significantly reduced permeability. Studies using bEnd.3 cells found that TGFβ1 suppressed Claudin-5 and increased MMP9 through a SMAD3-dependent mechanism. Depletion of microglia with clodronate liposomes in AOM mice was protective. Cortical CCL3/CCR1 axis signaling was elevated during HE and was reduced with neutralizing antibodies against TGFβ. Also, treatment with neutralizing antibodies against TGFβ reduced microgliosis and microglia activation. CCL3 KO mice had no changes in neurological decline compared to wild-type mice. Elevation of Gli1 or suppression of TGFβ1 was neuroprotective during HE. TGFβ1 increased BBB permeability and generated microglia activation and microgliosis during HE though this effect was not through the CCL3/CCR1 signaling axis. Gli1 or TGFβ1 may be therapeutic targets for the treatment and management of HE.

DEDICATION

This work is dedicated to my loving wife, Tammy, who supported me in every possible way and helped make this possible. Without her I would have never pursued a formal graduate degree and would not be where I am today.

Also, I would like to dedicate this work to my parents, Mark and Lorraine, who have helped support me both financially and emotionally over my many years of study.

Finally, this could not have been possible without my friends and family who were always there for me.

ACKNOWLEDGEMENTS

I would like to acknowledge my dissertation mentor and friend, Dr. Sharon DeMorrow. Her ability to help me grow from a psychology student who knew little about cellular and molecular biology to having a full dissertation in this area would not have been possible without her guidance and patience.

I also would like to acknowledge my fellow lab members and the summer students who helped both intellectually and technically on this project. These include Cheryl Galindo, Gabriel Frampton, Hae Yong Pae, Rachel Petrofes Chapa, Dr. Matthew Quinn, Dr. Dinorah Leyva-Illades, Amber Jacobs, Andrew Seiwell, Leticia Fuentes and Eric Whittington.

I also would like to acknowledge my committee members Dr. Cynthia Meininger, Dr. Russell Sanchez, and Dr. Pier Luigi Di Patre who challenged and kept me on track to help me complete this work.

Finally, I would like to acknowledge Scott & White Memorial Hospital and the NIH for helping fund this project. Also, I would like to acknowledge the Central Texas Veterans Health Care System for providing us lab space and resources to perform this work.

TABLE OF CONTENTS

LIST OF FIGURES

FIGURE Page

LIST OF TABLES

1. INTRODUCTION

The liver is the largest internal organ in the body making up between 2% and 3% of total body weight and is one of the most important organs involved in maintenance of physiological homeostasis(1). The liver is also the most highly vascularized organ receiving 25% of total cardiac output due to its dual blood supply from the hepatic artery and the portal vein(1). The blood from these two sources mixes within hepatic sinusoids before entering the hepatic venous system and passing into the systemic circulation. This association with the blood supply allows the liver to perform many functions including metabolism of carbohydrates, proteins, and lipids, clearance of toxins and pathogens, and immune response regulation(2). In addition to these, the liver also produces bile, regulates plasma proteins and glucose, and is involved in the biotransformation of drugs and toxins(3).

Damage to the liver disrupts all of the aforementioned processes and leads to dysfunction in maintenance of homeostasis. Liver failure arises from both chronic and acute liver insults, which result in differential liver pathology and disease processes. Chronic liver damage is commonly associated with hepatitis C, alcoholic cirrhosis, nonalcoholic fatty liver disease, nonalcoholic steatohepatitis and hemochromatosis, which collectively affect around 40 million people in the United States(4). On the other hand acute liver failure (ALF) is a significantly more rare disorder but is associated with higher mortality(5). The

causes of ALF differ significantly based on geographical location, with ALF in the United States and western Europe being predominantly caused by drug-induced liver injury, while ALF in other areas is predominantly caused by hepatitis A, B, and E(6). In the United States, acetaminophen-induced toxicity leads to 26,000 hospitalizations and close to 500 deaths per year(7, 8). While acetaminophen toxification is the leading cause of toxin based ALF in the United States, multiple drugs including statins, non-steroidal anti-inflammatory drugs, antituberculosis drugs, antibiotics, anti-epileptic drugs, and other drugs have been reported to cause ALF(9). There have been other rare cases of ALF, which result from hyperthermic injury, Wilson's disease, ischemic injury from systemic hypotension during sepsis or cardiac failure, Budd-Chiari syndrome, and specific toxin exposure such as the *Amanita spp* mushroom(10).

While the causes of both chronic liver failure and ALF vary greatly, the molecular basis for liver failure is based upon the same general principles. In the case of Wilson's disease, a rare hereditary condition caused by a loss of function mutation in the copper transporting ATPase ATP7B, there is increased copper accumulation in the mitochondria of hepatocytes, which causes mitochondrial dysfunction with subsequent damage to these cells(11). During nonalcoholic steatohepatitis it has been previously shown that there is an upregulation of tumor necrosis factor-alpha (TNFα), which causes apoptosis of hepatocytes(12). Acetaminophen toxicity, on the other hand, leads to mitochondria dysfunction and nuclear DNA fragmentation, which cause

hepatocyte necrosis with subsequent liver failure(13). Thus, in genetic, chronic, and acute liver pathologies that lead to liver failure there is dysfunction and death of hepatocytes, which lead to loss of liver function and liver failure.

Both acute and chronic liver failure have the ability to generate a multitude of effects inside and outside the liver. Inside the liver there is a loss of metabolic function, hypoglycemia due to decreased gluconeogenesis, lactic acidosis caused by reduced lactate clearance, reduced ammonia clearance, and coagulopathy(5). Outside of the liver there is a systemic inflammatory response(14), increased energy expenditure(15), acute lung injury, reduced glucocorticoid production(16), increased cardiac output with subclinical myocardial injury(17), pancreatitis, kidney dysfunction(18), immune impairment increasing susceptibility to sepsis, and immunoparesis(19). In addition to this, the development of a neurological condition called hepatic encephalopathy (HE) is evident, which is correlated with cerebral edema and increased intracranial pressure(5, 20). HE is a deadly complication that arises from liver failure and has its own unique pathological mechanisms.

Due to the fact that liver failure and dysfunction can arise from different mechanisms, HE is divided into three main clinical categories. Type A HE arises from ALF, type B HE is caused by portal-systemic shunting with no liver disease, and type C is caused by chronic liver disease and cirrhosis(21). In addition to this, HE manifests with four different clinical grades, which are known as the West Haven Criteria. Grade 1 is classified with a lack of awareness, euphoria,

anxiety and reduced attention span. Grade 2 manifests with lethargy, mild disorientation for time or place, minor personality changes and inappropriate behavior. Confusion, significant disorientation, and a loss of comprehension of verbal stimuli occur at grade 3. This progresses to grade 4 where a patient will stop responding to verbal cues or noxious stimuli and subsequently becomes comatose(21).

While there is no true rodent model to replicate human disease in its entirety, there are certain models that have become accepted and used in the HE field to help understand and manipulate pathological factors. Type A HE has the greatest number of models, with most of them being developed in rats. Rat models of type A HE anhepatic models include hepatic devascularization(22), hepatectomy(23), and portacaval anastomosis with ammonia(24). Hepatoxin models in rats include galactosamine, acetaminophen and thioacetamide(25, 26). The only model proven to generate liver failure with consistent neurological decline in mice is the hepatotoxin model azoxymethane (AOM) (27). The AOM mouse model is a newer model of HE that has been characterized in both liver and brain and displays rapid encephalopathy progression and brain edema(28). Since this model is in mice, it allows for greater genetic manipulations to be performed. Type B HE has no models in mice, but can be induced in rats by portacaval anastomosis and graded portal vein stenosis(29). Type C HE again has no models in mice, but in rats bile duct ligation (BDL) generates some elements of this type of HE. The BDL rat model of biliary cirrhosis leads to

reduced locomotor activity and elevated levels of circulating ammonia, characteristics of lower grade HE, 4-6 weeks following surgery(30, 31).

Interestingly, the amount of liver damage present in patients does not always correlate with HE development or severity indicating that other factors outside the liver play a significant role in HE(32). That being said many treatments are aimed at reducing ammonia, such as lactulose and nonabsorbable antibiotics, which help remove ammonia from the circulation and reduce its production by eliminating components of the gut microbiota respectively(33, 34). Outside of this, hypothermia and mannitol can be used to reduce intracranial pressure with hypothermia giving the added benefits of reducing inflammation and restoring cerebral blood flow(35-39). Liver transplantation is generally the most efficacious treatment for HE, as patients who had liver failure with no liver transplantation have only an 18% survival one year after developing liver failure, though therapeutics like *N*-acetylcysteine, which is an antioxidant and used to treat acetaminophen toxicity, have been shown to significantly improve transplant-free survival to 35%(40). Even with the advances made in liver transplantation and novel therapeutics, recent statistics show survival following liver failure to be only around 65%(41, 42). Thus, the development of new therapeutics that are cost effective for the management of HE is greatly warranted, but to do so requires greater understanding of the mechanisms that cause this disease.

The primary mechanism classically thought to be involved in exacerbating HE pathology involves increases in circulating and intracranial concentrations of ammonia. Following liver damage and subsequent disruption of the urea cycle, levels of ammonia are increased in the circulation. This increased concentration of ammonia is able to enter the brain where astrocytes metabolize this molecule(43). Ammonia metabolism by astrocytes causes metabolic stress in astrocytes leading to cytotoxic edema and, in clinical HE, the development of Alzheimer's type II astrocytes in the basal ganglia(44). Furthermore, low concentrations of ammonia have been demonstrated to enhance GABAergic neurotransmission while at the same time downregulating glutamatergic neurotransmission via postsynaptic downregulation of NMDA receptors(45, 46). Thus, there is support that some of the cognitive and motor deficits that are present could be caused by suppression of neural circuits and astrocyte dysfunction caused by ammonia. However, there are some significant issues that point to other factors playing a more prevalent role in HE. First of all, arterial ammonia levels do not correlate strongly with HE severity in a study of cirrhotic patients with severe HE(47). Also, studies investigating hyperammonia have found that patients do express some similarities to HE, such as cerebral edema and swelling of astrocytes, but there were also observations of ventriculomegaly and atrophy of the cerebral cortex, which are not observed during HE(48). In addition to these structural changes in the brain, ammonia has been demonstrated to correlate with increased seizure activity, as patients

with generalized tonic-clonic seizures have elevated levels of plasma ammonia(49). Thus, it is apparent that ammonia is not capable of replicating all aspects of HE pathology and, because of this, must work in synergism with other pathological processes.

A second hypothesis into the major etiological cause of HE has identified inflammation to play a prominent role. Liver failure due to infection demonstrated that both the infection itself as well as the subsequent hepatocyte cell death are able to promote a systemic inflammatory response(14, 50). That being said, the cause of liver failure greatly influences the magnitude of the inflammatory response that is generated(51). Patients who had ALF and systemic inflammatory response syndrome were more likely to go on to develop HE compared to patients with ALF who did not have systemic inflammatory response syndrome(52). In a model of hepatic devascularization, microglia activation is observed along with upregulation of proinflammatory cytokines TNFα, IL-1β, and IL-6 in the brain(53). Elevated mRNA expression of proinflammatory cytokines has been found to predict increased HE severity and correlates with brain edema(54). These proinflammatory cytokines have been demonstrated to be pathogenic as TNFα and IL-1 β receptor gene deletion in AOM mice was found to reduce HE onset and subsequent brain edema(55). In addition to this, microglia activation has been observed clinically in patients who had ALF from infection from viral hepatitis(56) and in patients with liver cirrhosis who died from hepatic coma(57). Strategies to suppress microglia activation via

minocycline administration have been demonstrated to be protective in rats that had undergone hepatic devascularization with the subsequent development of HE via the suppression of proinflammatory cytokines(54, 58). Interestingly, ammonia also has the ability to induce inflammation and microglia activation and could be one mechanism driving progression of HE(57, 59). However, there is also increased lactate in the brain, which has been found to activate microglia and lead to release of TNFα and IL-6 from microglia cell cultures(60). In addition to lactate, manganese accumulation occurs in the brains of patients with cirrhosis but has not been shown in patients with ALF(61, 62). Manganese has been demonstrated to regulate inflammatory cytokine output, hydrogen peroxide release, and nitric oxide release from microglia(63, 64). These studies support that there is a significant involvement of inflammation in HE pathology. However, at this time there are few studies investigating cell signaling proteins that are directly and indirectly involved with inflammation and whose expression are upregulated during HE.

Sonic hedgehog (Shh) is a mammalian hedgehog protein that has been found to play important roles in nervous system development, blood-brain barrier (BBB) maintenance, immune function, and liver remodeling following injury(65-67). Shh protein is expressed centrally in neurons, oligodendrocytes, and other cells, while Indian hedgehog (Ihh) is expressed primarily in the heart and bone and Desert hedgehog (Dhh) is expressed in the gonads and peripheral nerves(68). Shh is cleaved into its C and N terminus and secreted from a host

cell where the N terminus is the active protein that exerts its effects by binding its membrane bound receptor, patched, on a target cell(69, 70). This removes the inhibitory effect of patched on a transmembrane bound effector protein called smoothened, which ultimately causes the activation and nuclear translocation of the Gli family of transcription factors (71, 72). In regards to liver damage, it has been shown in mice that have ingested ethionine, a hepatotoxin, that hedgehog signaling is upregulated in the liver and this upregulation increases with exacerbated liver damage(73). This damage to the liver and upregulation of Shh is primarily in hepatocytes and is in response to stimuli that cause apoptosis(74). Shh signaling cannot be transduced in hepatocytes due to a lack of patched expression, thus Shh signaling occurs at neighboring and distant cells that facilitate liver remodeling(75). In fact, following BDL it has been shown that exosome-enriched microparticles containing hedgehog ligands are found in the bile and plasma, supporting that following liver damage hedgehog ligands can be released from the liver and induce paracrine signaling at distant sites(76). One of these potential distant sites is the BBB whose endothelial cells express hedgehog receptors and were found to have reduced permeability upon exposure to hedgehog ligands(66). In addition to this, the same study found that hedgehog signaling was able to reduce proinflammatory cytokine profiles and protect against experimental autoimmune encephalomyelitis(66). Thus, this gives support to the view that following liver damage Shh is upregulated in the

liver and has the capability to be released to affect distant targets to promote both BBB integrity and reduce proinflammatory cytokine expression.

Another signaling factor that has been demonstrated to be upregulated following liver damage is transforming growth factor beta 1 (TGFβ1). TGFβ1 is a signaling protein involved in many processes, including immune system modulation, cell proliferation, cell differentiation, and apoptosis(77, 78). TGFβ1 transduces its signal by binding to its receptor TGFβRII, which then phosphorylates and forms a dimer with TGFβRI(79). This receptor tyrosine kinase phosphorylates either SMAD2 or SMAD3, which then associate with the co-SMAD, SMAD4(80). This signaling complex translocates to the nucleus where it can bind DNA and affect transcription(81).

In regard to liver damage, TGFβ1 is upregulated following carbon tetrachloride (CCl_4) or acetaminophen-induced liver damage(82). In addition to this, TGFβ1 mRNA and protein have been found to be expressed in normal, cirrhotic, and neoplastic human livers(83). A majority of research involving TGFβ1 in the liver is in regard to fibrosis, as TGFβ1 plays a critical role in liver fibrosis initiation(84). However, more recent studies have found that antifibrotic treatments can generate their effects with essentially no effect on TGFβ1(85). Also, it has been shown that following 90% hepatectomy subsequent treatment with antibodies against TGFβ1 was able to protect LPS-treated rats compared to rats treated with LPS alone(86). Interestingly, hepatic stellate cells but not hepatocytes were found to express TGFβ1, while the TGFβ1 receptor, TGFβ

receptor 2 (TGFβR2), was found to be expressed in hepatocytes(83). This supports the involvement of paracrine signaling in the liver following damage and may indicate that TGFβ1 has the ability to signal at distant sites similar to Shh. In support of this, TGFβ1 has been found to be elevated in the circulation of patients with bile duct injury(87). Interestingly, TGFβ1 has been shown to suppress the systemic immune response(88). Also, there is support in the brain that TGFβ1 reduces microglia activation and downregulates inflammatory factors(89). Thus, there is support for TGFβ1 upregulation in the liver following liver damage and TGFβ1 in the circulation could be suppressing the systemic, and potentially central, immune response.

Due to the fact that liver damage upregulates both hedgehog and TGFβ1 signaling, the current study was aimed at assessing whether following liver failure hedgehog and TGFβ1 are released from the liver into the circulation and can influence cell-signaling pathways at distant sites. The overall hypothesis for this study is that hedgehog and TGFβ1 are released from the liver following damage and these signaling proteins then suppress neuroinflammation during HE.

2. GLI1 ACTIVATION AND PROTECTION AGAINST HEPATIC ENCEPHALOPATHY IS SUPPRESSED BY CIRCULATING TRANSFORMING GROWTH FACTOR β1 IN MICE

2.1. Overview

The transcription factor Gli1, which can be modulated by hedgehog or TGFβ1 signaling, has been shown to be protective in various neuropathies. We measured levels of Gli1 in brain tissues from mice, rats, and patients with HE, and evaluated how circulating TGFβ1 and hedgehog signaling regulate its activation. Mice were injected with AOM to induce HE, in the presence of Gli1 hedgehog, or TGFβ1-modulating treatments. Gli1 was increased in brains of AOM mice and in patients with HE compared to controls. Intra-cortical infusion of Gli1 Vivo morpholinos exacerbated the neurologic deficits of AOM mice. Modulation of hedgehog signaling had no effect on HE neurological decline. Levels of TGFβ1 increased in liver and serum of mice following AOM administration. TGFβ neutralizing antibodies slowed neurologic decline following AOM administration without affecting liver damage. TGFβ1 inhibited Gli1 via a SMAD3-dependent mechanism. Overall, cortical activation of Gli1 protects mice from HE and TGFβ1 suppresses neural Gli1 via SMAD3 and promotes neurologic decline. Strategies to activate Gli1 or inhibit TGFβ1 might be developed to treat patients with HE.

2.2. Introduction

HE is a neurological complication that can arise following acute or chronic liver damage and is a metabolically-induced, functional disturbance of the brain(90). The most severe form of HE occurs following ALF, which can be caused by drug-related liver damage, hyperthermic injury, and toxin exposure(5). The neurological decline observed in HE is caused by toxin accumulation in the blood. These toxins have the ability to cross the BBB and generate neurotoxic effects in the brain, including swelling of astrocytes, cerebral edema, and dysregulation of water balance(91). Associated with impairment of astrocyte function is a decrease in neuronal function, which leads to progressive cognitive deficits, motor deficits, and eventually coma(92).

Glioma-associated oncogene homolog 1 (Gli1), a member of the Gli family of transcription factors, has previously been shown to be protective in neurological conditions such as ischemic injury, stroke, and Parkinson's disease(93-95). Activation of Gli1 is traditionally a downstream consequence of the hedgehog pathway, via the activation of smoothened (96). However, signaling outside of the canonical hedgehog pathway can also regulate Gli activity, such as TGFβ1 signaling(97-99). The signaling ligand TGFβ1 binds a receptor complex containing TGFβR2 leading to the phosphorylation/activation of SMAD3, which translocates to the nucleus and regulates transcription(100). Therefore, understanding both canonical hedgehog signaling and non-canonical

pathways, such as TGFβ1, is required to elucidate the regulation of Gli transcription factors during disease states.

Currently, studies have not addressed circulating factors released during liver failure and their influence on HE brain pathology. Recent data suggest that hedgehog signaling is involved in expansion of liver progenitor cells after injury, and thus can play a protective role in the liver itself(101). The hedgehog ligands Shh and Ihh are released from hepatocytes in various models of liver damage, where they act on liver myofibroblasts and activate endothelial cells(76, 102). Conversely, the TGFβ1 pathway has been assessed in chronic liver disease and fibrosis models where it facilitates fibrogenesis while also having anti-inflammatory effects(103). Necrotic hepatocytes release TGFβ1 into the local microenvironment where it is able to initiate the activation of nearby hepatic stellate cells(104). Furthermore, studies have found that rats with hepatic failure have elevated levels of serum TGFβ1(105). Currently little information exists concerning the roles of either cortical hedgehog or TGFβ1 signaling during HE pathogenesis.

Due to the lack of understanding of neural hedgehog pathway activation during HE, as well as the signaling that occurs between the circulation and brain in this disorder, this study was aimed at assessing the regulation and effects of neural Gli1 activation during HE and to determine how circulating Shh and TGFβ1 can influence its activation.

2.3. Materials and Methods

Materials

Antibodies against Shh were purchased from Santa Cruz Biotechnology (Santa Cruz, CA). Antibodies against TGFβ1, SMAD3, Gli1, Gli2, and Gli3 were purchased from Genetex (Irvine, CA). Antibodies for albumin were bought from Bethyl Laboratories (Montgomery, TX). NeuN antibodies were ordered from Millipore (Billerica, MA). Phosphorylated SMAD3 (pSMAD3) and TGFβR2 antibodies were ordered from Cell Signaling Technology (Danvers, MA). Neutralizing antibodies for TGFβ (anti TGFβ) and recombinant TGFβ1 protein (rTGFβ1) were purchased from R&D systems (Minneapolis, MN). All primers were purchased from SA Biosciences (Frederick, MD). The Gli1 Vivo-morpholino (5'- GTGGAGTCATTGGATTGAACATGGC-3') and mismatched Vivo-morpholino (5'- GTGCACTCATTGCATTCAACATCGC-3') were purchased from Gene Tools (Philomath, OR). Smoothened Vivo-morpholino (5'-GCCAAACAGCCAACTCAGCAAAAGC-3') and mismatched Vivo-morpholino (5'-GCGAAAGAGGCAACTGACCAAAAGC-3') were also purchased from Gene Tools. Smoothened agonist (SAG) was purchased from Millipore. All chemicals were purchased from Sigma-Aldrich (St. Louis, MO) unless otherwise noted, and were of the highest grade available.

Mouse azoxymethane model of hepatic encephalopathy

Mouse *in vivo* experiments were performed using male C57Bl/6 mice (25-30 g; Charles River Laboratories, Wilmington, MA). Mice were allowed free access to drinking water and standard mouse chow and were housed in constant temperature, humidity, and 12 hour light-dark cycling. Mice received a single intraperitoneal injection of 100 mg/kg AOM to induce ALF and HE. Control animals were injected with an equal amount of saline. After injection, mice were placed on heating pads set to 37°C and under heating lamps to ensure they maintained normal body temperature. Also, mice were supplied with hydrogel and rodent chow on their cage floor to ensure they had easy access to food and hydration. After 12 hours and every 4 hours following, mice were injected subcutaneously with 5% dextrose in 250 µL of saline to ensure that they did not become hypoglycemic. Mice were removed from the study if they exhibited a 20% weight loss.

Following injection, mice were monitored every two hours (starting at eight hours post AOM injection) for body temperature, weight, and neurological decline. Neurological decline was assessed by measuring the pinna reflex, corneal reflex, tail flexion, escape response, righting reflex, and ataxia, and with each given a score of 0 (no reflex evident), 1 (weak or delayed reflex), or 2 (intact reflex). Touching the external auditory meatus with a cotton applicator and observing ear retraction or head movement assessed the pinna reflex. The corneal reflex was measured by touching the cornea with a cotton applicator and

measuring the blink response. Tail flexion was measured via tail pinch with forceps and assessing tail flexion. Escape response was measured by tail pinch by forceps and a subsequent movement of mice away from stimuli. Placing the mice on their back and measuring the time for them to right themselves represented the righting reflex. Ataxia assessment was performed by observing movement activity when the mice were placed on the cage wire bar lid. The data were expressed as numerical values calculated from the summation of these six reflexes to give scores between 0 and 12. Tissue was collected at time points prior to onset of neurological symptoms (pre neurological), when minor neurological deficits were present (minor neurological) as determined by presence of ataxia and weakened reflexes, or at coma, which was defined as a loss of the righting and corneal reflexes.

Pharmacological treatment strategies in AOM mice

Systemic inhibition of the hedgehog pathway in mice was performed through the use of the smoothened inhibitor cyclopamine. Cyclopamine was dissolved in 45% (2-hydropropyl)-β-cyclodextrin (HBC) and intraperitoneal injections were given for 3 sequential days at 10 mg/kg culminating with injection of AOM on the third day. Control animals were injected with 10 mg/kg 45% HBC as vehicle. In order to suppress the activity of circulating TGFβ, injection of TGFβ neutralizing antibodies was performed. This required a single intraperitoneal injection at 1 mg/kg 2 hours prior to AOM injection. Lastly, *in vivo*

genetic Gli1 expression involved implanting mice with minipumps (Alzet, Cupertino, CA) that infused Gli1-Vivo morpholinos directly into frontal cortex at a dose of 1 mg/kg/day for 3 days prior to the injection of AOM or vehicle at coordinates AP +2.0, ML -2.0, DV -2.5. For controls, a mismatched Vivo-morpholino was directly infused into the cortex at 1 mg/kg/day for 3 days prior to vehicle or AOM intraperitoneal injection at the same coordinates as the Gli1 Vivo-morpholinos. Smoothened Vivo-morpholinos were infused in the same manner as the Gli1 Vivo-morpholinos with appropriate mismatched controls. SAG intracortical infusion was performed at 10 ng/g/day for 3 days prior to the injection of AOM or vehicle at coordinates AP +2.0, ML -2.0, DV -2.5.

In vivo *model of chronic liver cirrhosis and minimal hepatic encephalopathy in the rat*

In vivo experiments were performed using the BDL model of chronic biliary cirrhosis and subsequent HE using 250g male Sprague Dawley rats. This model is the only validated model for chronic cirrhosis with development of HE(26). For this study, rats were anesthetized and their peritoneal cavity was surgically opened. The common bile duct was isolated and subsequently ligated. Following BDL surgery, the rats were given appropriate postoperative monitoring and care and were given normal access to chow and water for 4 weeks. At this time point we observed reduced activity levels compared to sham-operated controls, but no overt signs of neurological decline were present,

which is similar to what has been previously reported(106). Rats were euthanized and liver, cortex, cerebellum, and blood were collected for further analysis.

Human samples

Brain tissues from patients who had HE following liver cirrhosis, cirrhotic patients without HE or aged-matched controls without liver disease were supplied through either the autopsy service from Scott & White Memorial Hospital Department of Pathology (Temple, TX) or the New South Wales Tissue Resource Centre at the University of Sydney. Physiological details and cause of death of these patients can be found below in Table 1. Immunohistochemistry or real-time PCR were performed on these tissues as described below.

Table 1 Summary of patient treatment groups

	Control (n=7)	Cirrhotic with HE (n=8)	Cirrhotic w/o HE (n=10)
Male/Female ratio	6/1	6/2	7/3
Age (avg ± SEM)	51.1 ± 2.52	59.6 ± 3.93	51.7 ± 2.92
Median age (range)	50 (37-61 yr)	58 (40-75 yr)	56 (40-75 yr)
Cause of death	Cardiac (n=7)	HE (n=8)	Cardiac (n=4) Respiratory/Toxicity (n=3) Blood Loss (n=2) Trauma (n=1)

Neuron isolation

Primary neurons were isolated from P1 rat pups. Rats were decapitated and whole brains were removed. Cortex was isolated and meninges and dura were surgically removed. Cortical tissue was mechanically and chemically disrupted in a 50% TrypLE and Hank's buffered salt solution (HBSS) solution and filtered through a 100-µm filter. Neurons were suspended in HBSS containing 10% heat-inactivated fetal bovine serum (HIFBS) and pelleted by centrifugation at 1400 *g*. Neurons were resuspended in Modified Eagle's Medium/Ham's Nutrient Mixture F12 (DMEM/F12) containing 10% heat-inactivated fetal bovine serum, 50 U/mL penicillin/streptomycin, and 10 µg/ml gentamicin. Cells were then plated on a 12-well plate with a seeding density of 750,000 cells per well. After 24 hours, cells were washed with phosphate buffered saline (PBS) and placed into MEM/F12 growth media containing 10% HIFBS, 2% B27 growth supplement, 50 U/mL pen/strep, and 10 µg/ml gentamycin. Cells were allowed to grow processes and after 10-14 days were treated. Neuronal treatments include varying doses of rTGFβ1, specific inhibitor of SMAD3 (SIS3), and TGFβ neutralizing antibodies. Cells were lysed and RNA or protein was isolated as required.

Liver biochemistry

Plasma alanine aminotransferasase and bilirubin were assessed using commercially available kits. Alanine aminotransferase (ALT) measurement was

performed using a fluoremetric activity assay (Sigma). Total bilirubin was assayed using a total bilirubin ELISA (CusaBio, Wuha, China). All assays and subsequent analyses were performed according to manufacturers' instructions.

Real-time PCR

RNA was extracted from tissue or cells and real-time PCR (RTPCR) was performed as previously described(107) using commercially available primers designed against mouse Gli1, Gli2, Gli3, Shh, TGFβ1, and GAPDH as well as rat Gli1 and GAPDH (SA Bioscience, Frederick, MD). A ΔΔCT analysis was performed using vehicle-treated tissue or untreated primary neurons as controls for subsequent experiments(108, 109). Data for all experiments are expressed as mean relative mRNA levels ± SEM (n=4).

Immunoblotting

For serum immunoblots, 10% serum samples were diluted in Laemmli buffer and loaded in 10% sodium dodecyl sulfate-polyacrylamide gel electrophoresis (SDS-PAGE) gels. For tissue western blots 10% SDS-PAGE gels were loaded with 10-20 μg of protein diluted in Laemmli buffer. Specific primary antibodies against Shh, TGFβ1, SMAD3, pSMAD3, albumin, and β-actin were used along with appropriate fluorescent secondary antibodies (LI-COR, Lincoln, NE). All imaging was performed on an Odyssey 9120 Infrared Imaging System (LI-COR). Data are expressed as fold change in fluorescent band

intensity of target antibody divided by β-actin, which was used as a loading control. The values of vehicle or control groups were used as a baseline and set to a relative protein expression value of 1. All treatment groups were represented as changes of fluorescent band intensity of target antibody to β-actin relative to vehicle or control groups. All band intensity quantifications were performed using ImageJ software (National Institutes of Health, Bethesda, MD). Data for all experiments were expressed as mean relative protein ± SEM (n=4).

Histology, immunohistochemistry, and immunofluorescence

Paraffin-embedded livers were cut into 3 μm sections and mounted onto glass slides where they were used for hemotoxylin and eosin (H&E) stains or immunohistochemistry as described(110). For brain immunohistochemistry and immunofluorescence, free-floating 30 μm sections were prepared. Immunohistochemistry for both liver and brain was performed using specific antibodies for Gli1, Gli2, Gli3, Shh, and TGFβ1. The sections were viewed using an Olympus BX40 microscope with an Olympus DP25 imaging system (Olympus, Center Valley, PA). Quantification of immunohistochemistry was performed by analysis of 4 or more fields per sample with a minimum of 3 samples per experiment. Mean staining density was calculated using ImagePro software (MediaCybernetics, Rockville, MD) while nuclear translocation was manually counted in the same fields. Immunofluorescence of the brain was performed using specific antibodies against Gli1, pSMAD3, TGFβR2 and NeuN.

Immunoreactivity was visualized using Dylight 488- or Cy3-conjugated secondary antibodies and counterstained with 4',6-diamidino-2-phenylindole (DAPI). Slides were viewed and imaged using a Leica TCS SP5-X inverted confocal microscope (Leica Microsystems, Buffalo Grove, IL).

Statistical analysis

All statistical analyses were performed using Graphpad Prism software (Graphpad Software, La Jolla, CA). Results were expressed as mean ± SEM. For data that passed normality tests, significance was established using the Student t test when differences between two groups were analyzed, and analysis of variance when differences between three or more groups were compared followed by the appropriate post hoc test. If tests for normality failed, two groups were compared with a Mann-Whitney U test or a Kruskal-Wallis ranked analysis when more than two groups were analyzed. Differences were considered significant when the p value was less than 0.05.

2.4. Results

Gli1 is activated in mouse brain during HE

The AOM model of HE is characterized by consistent neurological decline towards coma. Therefore, to better understand disease progression, we performed molecular analyses at times prior to neurological symptom onset (reduced activity but no decline in measured reflexes), where minor neurological deficits were evident (deficits in one or more reflexes with ataxia present); and once coma was reached (loss of corneal and righting reflexes). These stages of neurological decline are shown (figure 1A). In order to validate that AOM injections were generating liver damage, H&E stains and liver biochemistry were assessed at various stages in AOM-treated and vehicle-treated mice. The livers from AOM-treated mice displayed progressive liver damage with mice at coma having severe parenchymal damage including diffuse necrosis of hepatocytes, steatosis of surviving hepatocytes and hemorrhage (figure 1B). The observed histopathological changes were consistent with what has been previously shown using this model(28). Serum enzyme assays for bilirubin and ALT supported these liver damage assessments (Table 2).

The expression of Gli transcription factors was assessed at various time points after AOM injection. Cortical Gli1 mRNA was significantly upregulated in AOM mice after development of neurological symptoms and showed greatest elevation at coma (figure 1C).

Table 2 Serum liver enzymes for treated mice

Treatment	Bilirubin (nmol/ml)	ALT (U/L)
Vehicle	4.60 ± 0.42	10.09 ± 3.82
AOM	68.39 ± 5.29 *	108.62 ± 20.51 *
AOM + Cyclopamine	53.01 ± 1.20 *	107.45 ± 16.45 *
Cyclopamine	4.93 ± 0.10 #	16.75 ± 6.30 #
AOM + anti TGFβ	79.95 ± 12.33 *	139.07 ± 6.30 *
anti TGFβ	5.02 ± 0.13 #	9.84 ± 1.31 #
Mismatched-VM Vehicle	1.56 ± 0.32 #	10.41 + 1.43 #
Mismatched-VM AOM	57.27 ± 3.22 *	144.24 + 4.11 *
Gli1-VM Vehicle	1.82 ± 0.19 #	9.03 + 2.50 #
Gli1-VM AOM	55.59 ± 4.65 *	151.22 + 10.73 *

* = $p<0.05$ compared to vehicle, # = $p<0.05$ compared to AOM

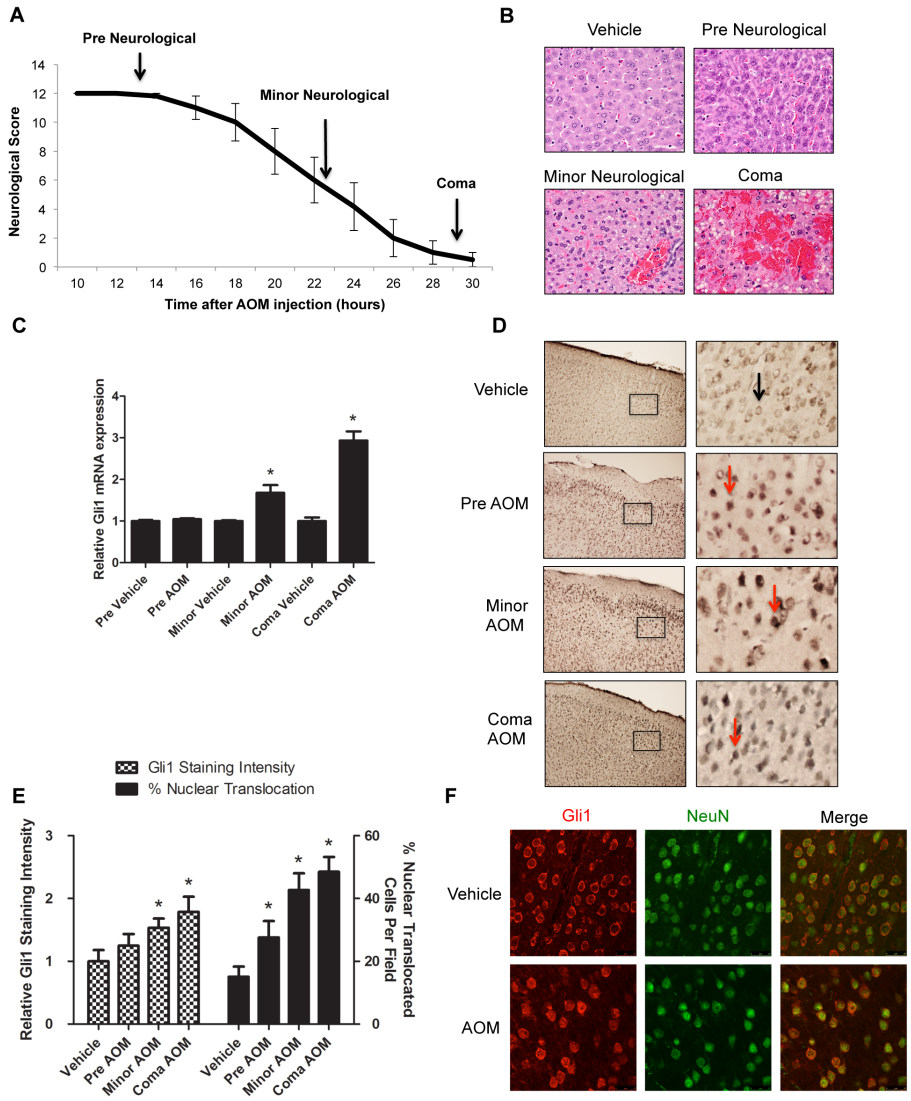

Fig. 1. Acute liver insult led to Gli1 activation in the cortex. (A) Time course of neurological decline present in the AOM model. Neurological score is a measure of 6 reflexes scored between 0 and 2, with a lower score indicating greater neurological decline. Stages of neurological decline are identified on the graph. (B) Liver damage was assessed using H&E histochemistry in AOM- and vehicle-treated mice. (C) Cortical Gli1 mRNA expression was assessed after AOM treatment. (D) Gli1 immunoreactivity was assayed after AOM injection. Subcellular location of immunoreactivity is indicated by a black arrow (cytoplasmic staining) or a red arrow (nuclear staining). (E) Quantitation of Gli1 immunohistochemistry from indicated stages of neurological decline. Quantifications include relative staining intensity per field (left axis) and percentage of Gli1 cells that undergo nuclear translocation (right axis). (F) Neuronal expression of Gli1 in vehicle and AOM cortex was assessed by immunofluorescence and counterstained with the neuron marker NeuN. For mRNA analyses and quantitative IHC, data are reported as mean ± SEM (n=4). *p<0.05 compared to vehicle cortex.

In addition, there was increased Gli1 immunoreactivity and nuclear translocation in the cortex as an early event after AOM injection that was significantly elevated in the later stages of neurological decline (figure 1D and 1E). Moreover, Gli1 expression was found to co-localize with the neuronal marker NeuN in vehicle- and AOM-treated mice, suggesting that Gli1 upregulation occurs primarily in neurons (figure 1F). This elevation was not observed in the cerebellum of AOM mice (figure 2A). There were no significant changes in cortical Gli2 and Gli3 mRNA expression (figure 2B and 2C), immunoreactivity, or subcellular localization (figure 2D and 2E) after AOM injection. Together, these results suggest that Gli1 was the primary Gli transcription factor that responded to the neural changes that take place during HE.

Gli1 is activated in the cortex during HE due to liver cirrhosis

To assess whether cortical Gli1 activation also occurs in HE as a result of chronic liver failure, we employed a rat model of BDL. Four weeks after BDL surgery, rats have mild cognitive deficits as well as elevated levels of ammonia(106), indicative of early HE. Consistent with the early time points of AOM-treated mice, Gli1 mRNA expression and immunoreactivity were relatively unchanged after BDL (figure 3A and 3B). However there was increased Gli1 nuclear translocation after BDL surgery, indicating an increase in Gli1 activity (figure 3B and 3C).

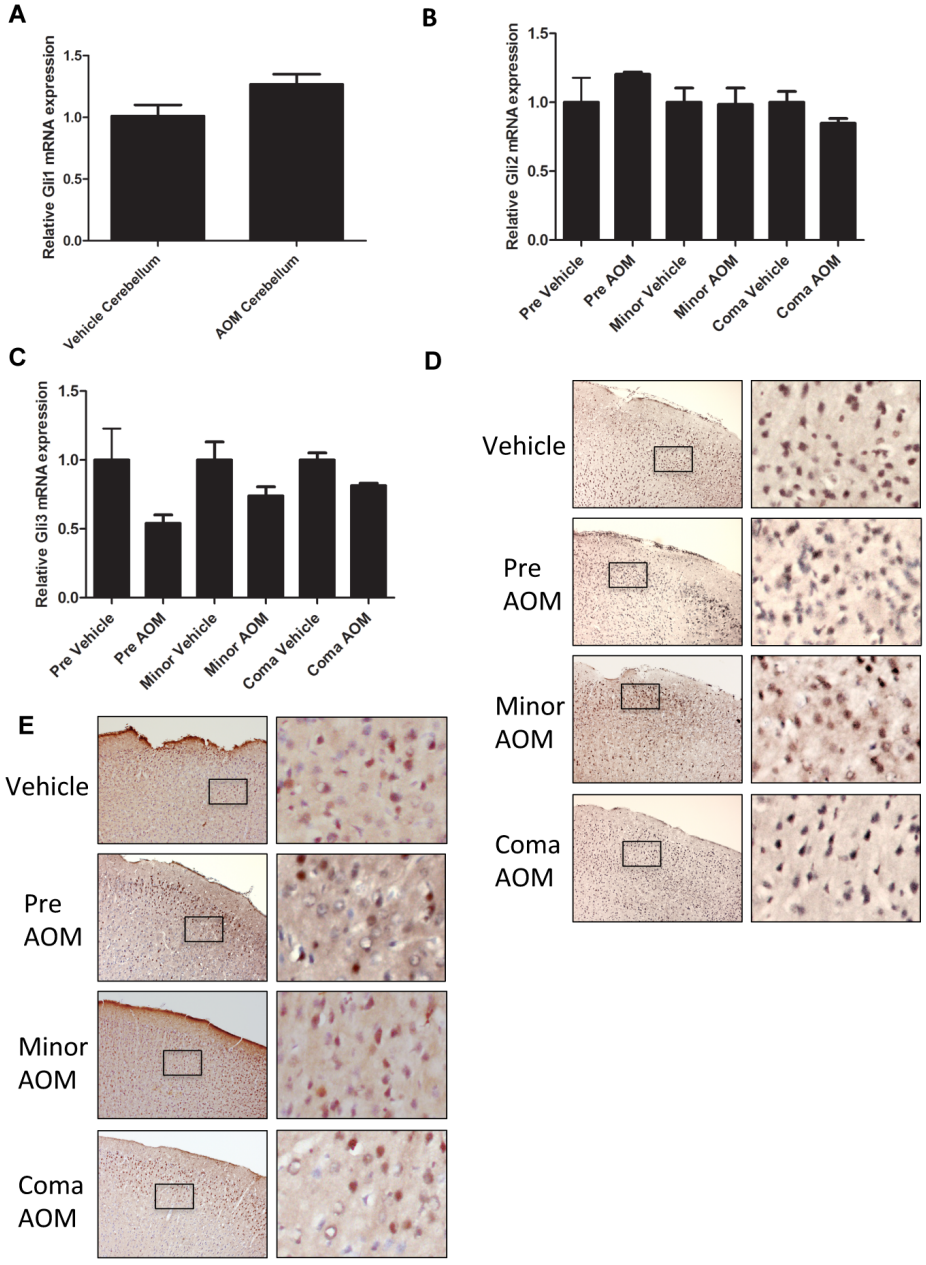

Fig. 2. Gli1, Gli2, and Gli3 mRNA expression and nuclear translocation. (A) RTPCR analysis for Gli1 mRNA expression in the cerebellum. (B) Timecourse cortex analysis for Gli2 mRNA expression as assessed via RTPCR. (C) RTPCR analysis of Gli3 mRNA expression in timecourse cortex. (D) Gli2 protein localization in timecourse cortex using immunohistochemistry with inset displayed in right panel. (E) Immunohistochemistry for Gli3 protein localization in both vehicle and timecourse AOM cortex. For mRNA analyses, data was reported as mean ± SEM (n=4).

To ensure that these findings were also present in clinical cases of HE, Gli1 expression was assessed in the cortex and cerebellum of cirrhotic patients with HE, cirrhotic patients without evidence of HE, and patients without any sign of liver failure. Cortical Gli1 mRNA was only upregulated in cirrhotic patients with HE (figure 3D), suggesting that neurological symptom onset was the primary factor involved in Gli1 mRNA expression upregulation. Furthermore, Gli1 immunoreactivity was evident predominantly in the cytoplasm of control patients, in HE patients there was significantly increased nuclear localization and immunoreactivity of Gli1 suggesting greater Gli1 activation in HE patients (figure 3E and 3F). Gli2 and Gli3 were assessed in both BDL rats and cirrhotic patients with no significant change in gene regulation or nuclear translocation (data not shown). Taken together, these data demonstrate that following liver cirrhosis and subsequent HE that there was increased cortical Gli1 activity.

Gli1 inhibition in the cortex aggravated HE neurological decline

In an effort to identify if cortical Gli1 is involved in HE pathogenesis, Gli1 protein expression was reduced by intracortical infusion of Gli1 Vivo-Morpholino (VM) sequences. Gli1 protein expression was knocked down adjacent to the infusion site in the cortex (figure 4A). Furthermore, intracortical Gli1-VM infusion significantly exacerbated neurological decline observed after AOM injection (figure 4B) and shortened the time to coma (figure 4C) compared to mice pretreated with mismatched-VM. Interestingly, there were no observable

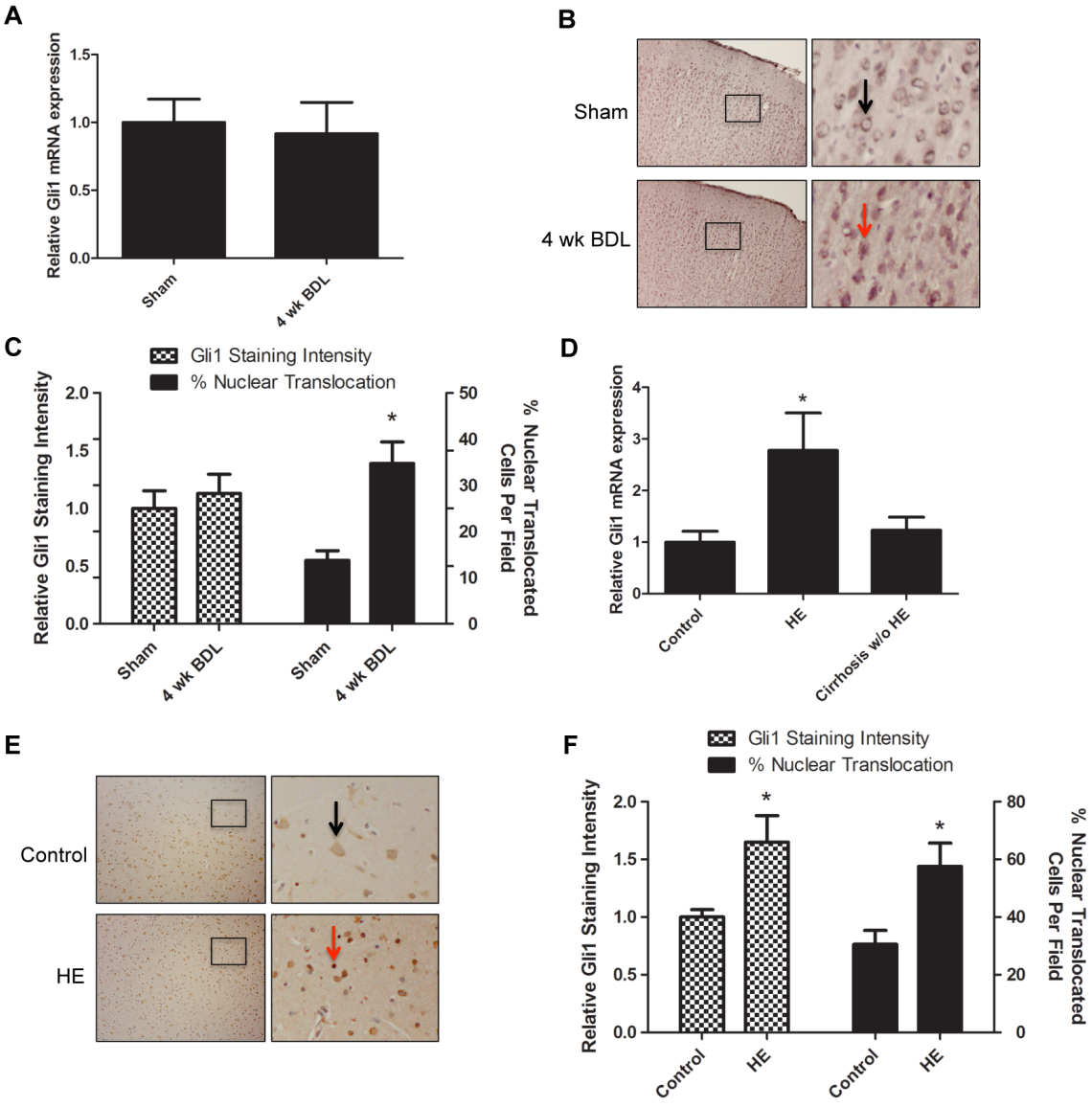

Fig. 3. Cortical Gli1 was activated during HE due to liver cirrhosis. (A) Cortical Gli1 mRNA expression in sham and 4-week BDL rats. (B) Cortical Gli1 immunoreactivity in sham and 4-week BDL rats. Subcellular localization is demonstrated by a black arrow (cytoplasmic staining) or red arrow (nuclear staining). (C) Quantitation of Gli1 immunohistochemistry from sham and 4 week BDL cortex. (D) Cortical Gli1 expression was assessed in control patients (n=7), cirrhotic patients without HE (n=10), and cirrhotic patients with HE (n=8). Data is expressed as mean ± SEM. *$p<0.05$ compared to control cortex. (E) Cortical Gli1 immunoreactivity in clinical HE patients and controls. Subcellular location is indicated by black arrow (cytoplasmic staining) or red arrow (nuclear staining). (F) Quantitation of Gli1 immunohistochemistry from control cortex and HE cortex from patient tissue. For mRNA analyses, data are reported as mean ± SEM (n=4). For quantitative IHC analyses, data are reported as mean ± SEM (n=3). *$p<0.05$ compared to sham cortex or control cortex.

differences in liver damage between these treatment groups as demonstrated by H&E staining (figure 4D) and biochemical analyses (Table 2). Together, these data support Gli1 to be a neuroprotective protein that is upregulated as a protective mechanism during HE.

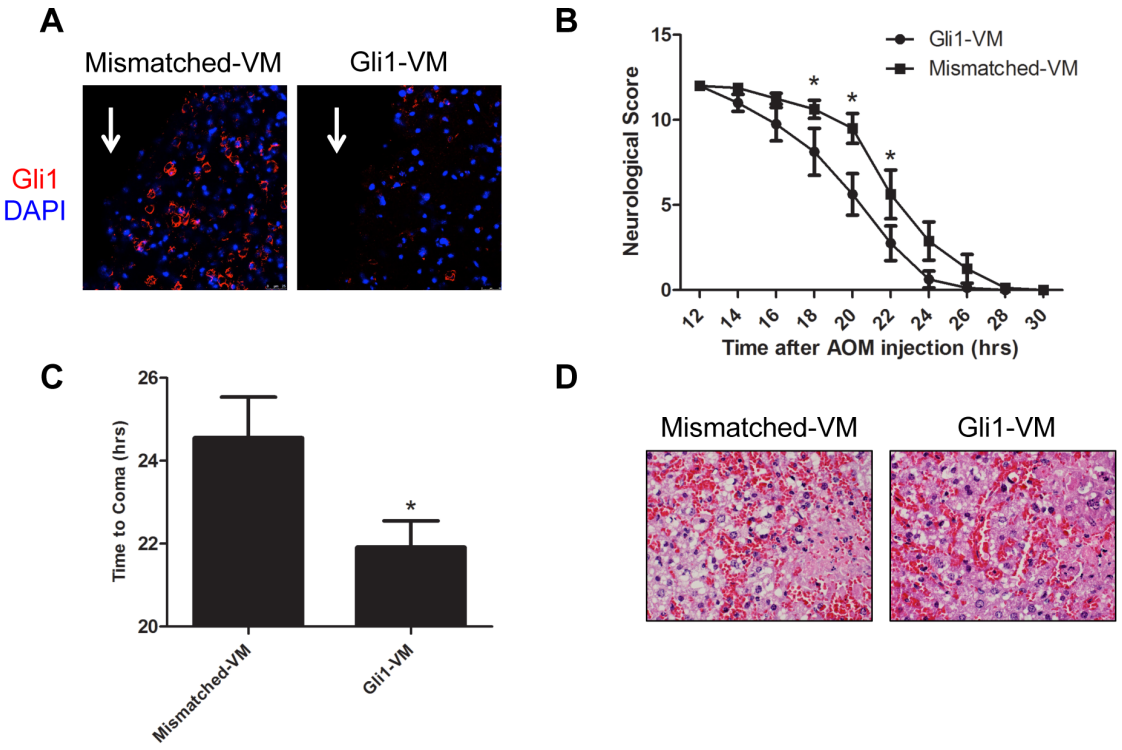

Fig. 4. Suppression of Gli1 expression exacerbated neurological decline. Mice were infused with Gli1-VM or mismatched-VM into the cortex 3 days prior to AOM injection. (A) Cortical Gli1 knockdown was validated by Gli1 immunofluorescence (red) near the infusion site (white arrow) with DAPI (blue) used as a counterstain. (B) Neurological decline was assessed using neurological score as previously described. Gli1-VM treatment significantly worsened neurological decline in AOM mice compared to mismatched-VM mice (p=.0435). (C) Time to coma in hours of Gli1-VM infused AOM-treated mice and mismatched-VM infused, AOM-treated mice. (D) Liver damage was assessed in Gli1-VM and mismatched-VM mice by H&E histochemistry. Data are reported as mean ± SEM (n=8). *p<0.05 compared to mismatch morpholino cortex.

Circulating TGFβ1, but not Shh, may be involved in the neurological decline during HE

In order to determine if neural Gli1 was elevated as a downstream consequence of hedgehog signaling, Shh expression was assessed. Following AOM treatment, Shh mRNA and protein were elevated in the liver (figure 5A and 5B), present in the serum (figure 5C), though unchanged in the brain (figure 5D). Pretreatment with cyclopamine, a smoothened antagonist, prior to AOM

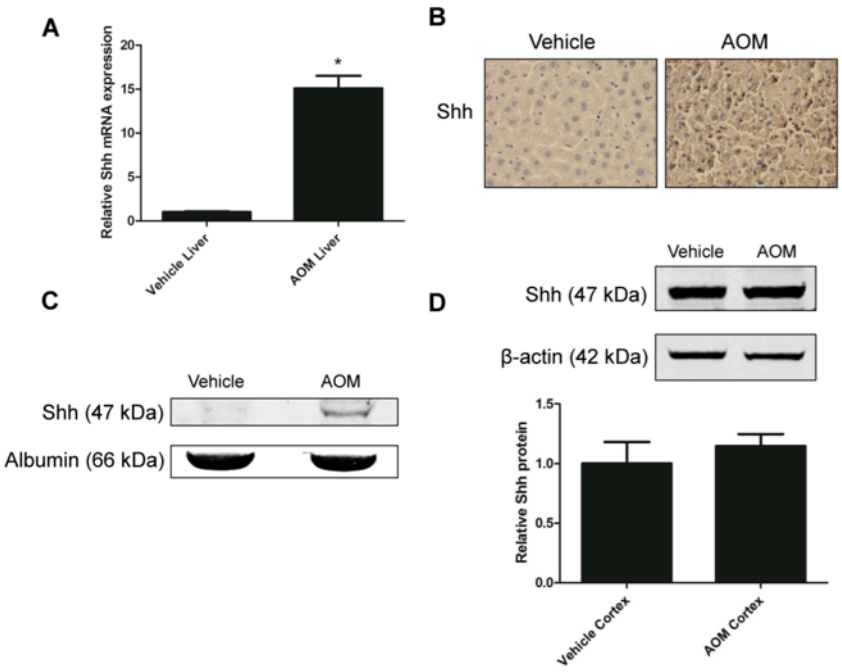

Fig. 5. Shh expression was elevated in the liver but not the brain following AOM treatment. (A) Liver Shh mRNA expression was assessed in vehicle and AOM-treated mice by RTPCR. (B) Immunohistochemistry for Shh in vehicle and AOM livers. (C) Immunoblots were performed to assess the presence of Shh protein in the serum of vehicle and AOM-treated mice. Albumin was used as a loading control. (D) Cortical Shh protein expression was measured in AOM-treated mice compared to controls with β-actin used as a loading control. For protein and mRNA analyses, data was reported as mean ± SEM (n=4). * $p<0.05$ compared to vehicle liver.

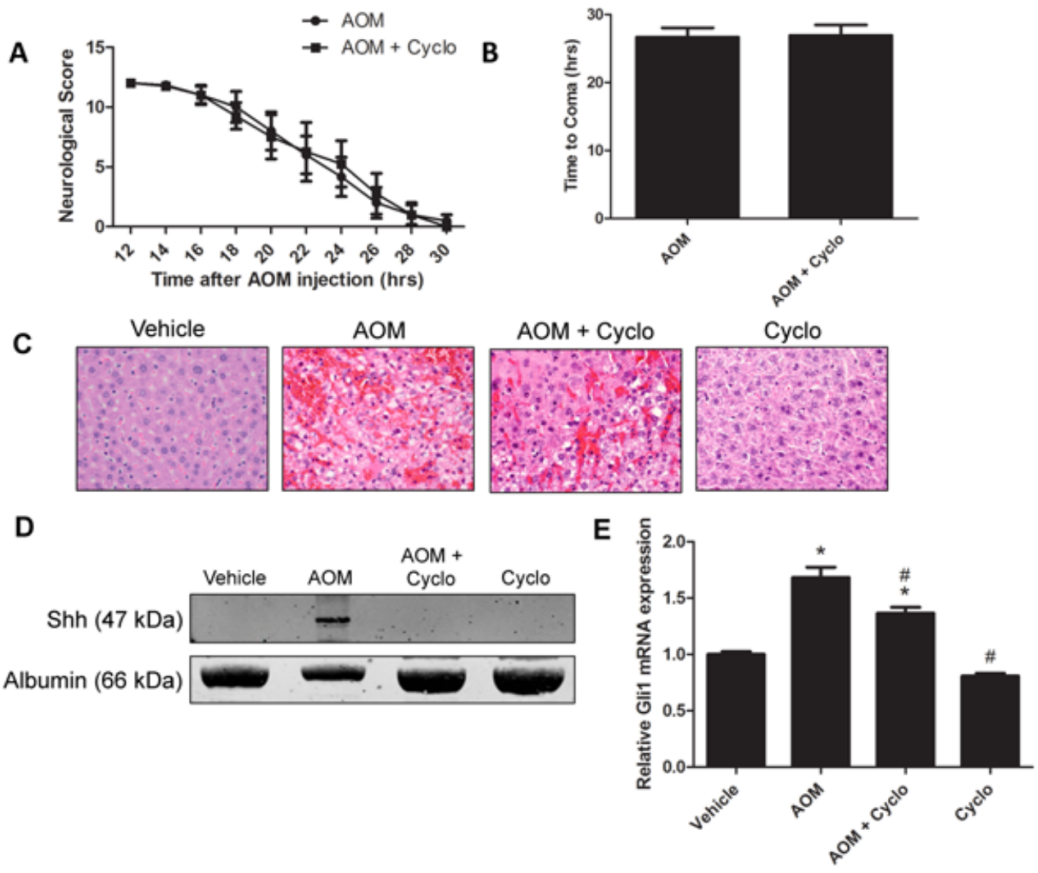

Fig. 6. Cyclopamine treatment had no significant effect on HE progression. (A) The neurological decline of AOM mice and AOM mice treated with cyclopamine (Cyclo). Neurological decline was assessed using the neurological score as previously described. (B) Time to coma in hours was assessed in AOM and AOM + Cyclo mice. (C) Liver damage was assessed by H&E histochemistry in mice were treated with vehicle, AOM, AOM + Cyclo, and Cyclo. No significant differences between AOM mice and AOM mice injected with Cyclo were observed. (D) Serum immunoblots were performed for Shh in mice treated with vehicle, AOM, AOM + Cyclo, and Cyclo. (E) Cortical Gli1 mRNA expression in mice treated with vehicle, AOM, AOM + Cyclo, and Cyclo. For mRNA analyses, data were reported as mean ± SEM (n=4). * $p<0.05$ compared to vehicle cortex. # $p<0.05$ compared to AOM cortex.

did not significantly affect neurological decline (figure 6A), time to coma (figure 6B), or liver damage (Table 2 and figure 6C). However, cyclopamine was able to reduce circulating Shh (figure 6D) and slightly dampen cortical Gli1 mRNA expression although it is still elevated above vehicle (figure 6E). This gives support that cyclopamine inhibited the hedgehog pathway but had no effects on

HE pathogenesis. To ensure that direct neural modulation of hedgehog signaling does not effect HE, smoothened agonist (SAG) or smoothened-VM were infused intracortically. Treatment with smoothened-VM generated no effect on time to coma and Gli1 immunoreactivity was still upregulated in the cortex of AOM mice (figure 7A and 7B). Also, SAG treatment had no effect on time to coma but did increase Gli1 immunoreactivity (figure 7C and 7D).

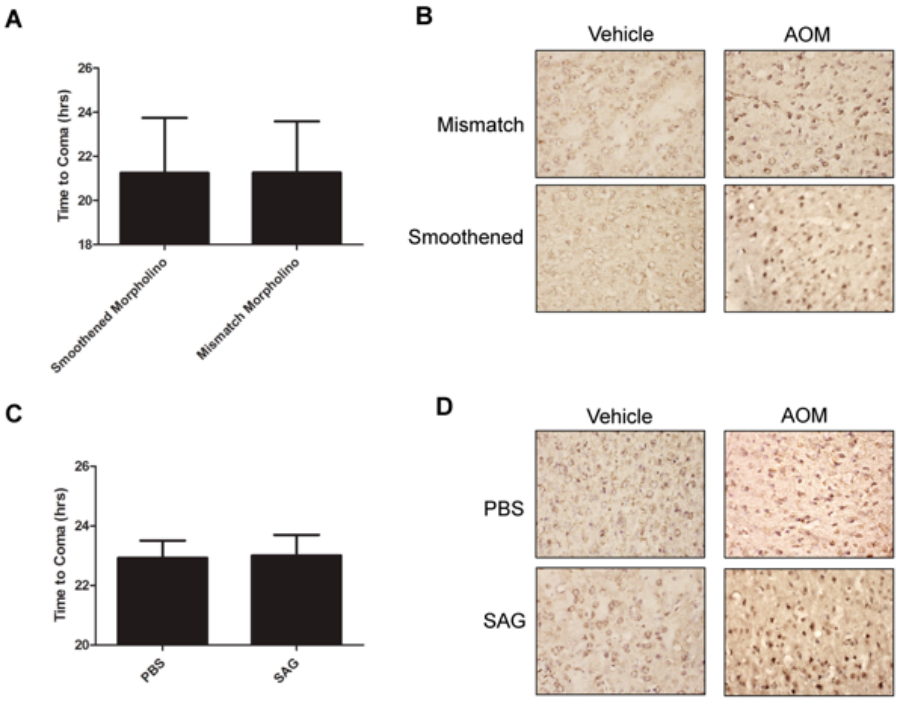

Fig. 7. Smoothened Vivo-morpholino and SAG treatment did not significantly affect HE neurological decline. (A) Time to coma in hours of mice cortically infused with smoothened-VM or mismatch-VM (n=4 per group). (B) Gli1 immunohistochemisty in vehicle- and AOM-treated mismatch-VM and Smo-VM. (C) Time to coma in hours for mice with cortical infusions of SAG or PBS (n=4 per group). (D) Gli1 immunohistochemisty in vehicle- and AOM-treated PBS and SAG mice.

Due to the fact that systemic and central modulation of smoothened had no effect on HE pathogenesis, we assessed the effects of TGFβ1 signaling on Gli1 activation and neurological decline. Liver TGFβ1 mRNA expression was significantly elevated following AOM injection compared to controls (figure 8A). Furthermore, increased TGFβ1 immunoreactivity was found in the livers of AOM-treated mice versus controls (figure 8B). TGFβ1 immunoreactivity occurred predominantly in albumin-positive cells in AOM mice, giving support that this upregulation is hepatocyte derived (figure 8C). In addition to this, TGFβ1 was present in serum of AOM-injected mice, but at undetectable levels in control serum (figure 8D). Due to the fact that TGFβ1 was upregulated in the liver and increased in the circulation, we wanted to determine if TGFβ1 was elevated in the brain. Cortical TGFβ1 protein expression was significantly elevated in AOM-injected mice compared to controls (figure 8E). This increase in protein did not coincide with increased cortical TGFβ1 mRNA expression (figure 8F), suggesting that increased cortical TGFβ1 protein may not be derived from local increases in TGFβ1 gene expression but rather systemic increases in TGFβ1.

TGFβ1 modulation in primary neuronal cultures directly affected Gli1 expression via a SMAD3-dependent mechanism

In order to investigate the interaction between TGFβ1 and Gli1, *in vitro*

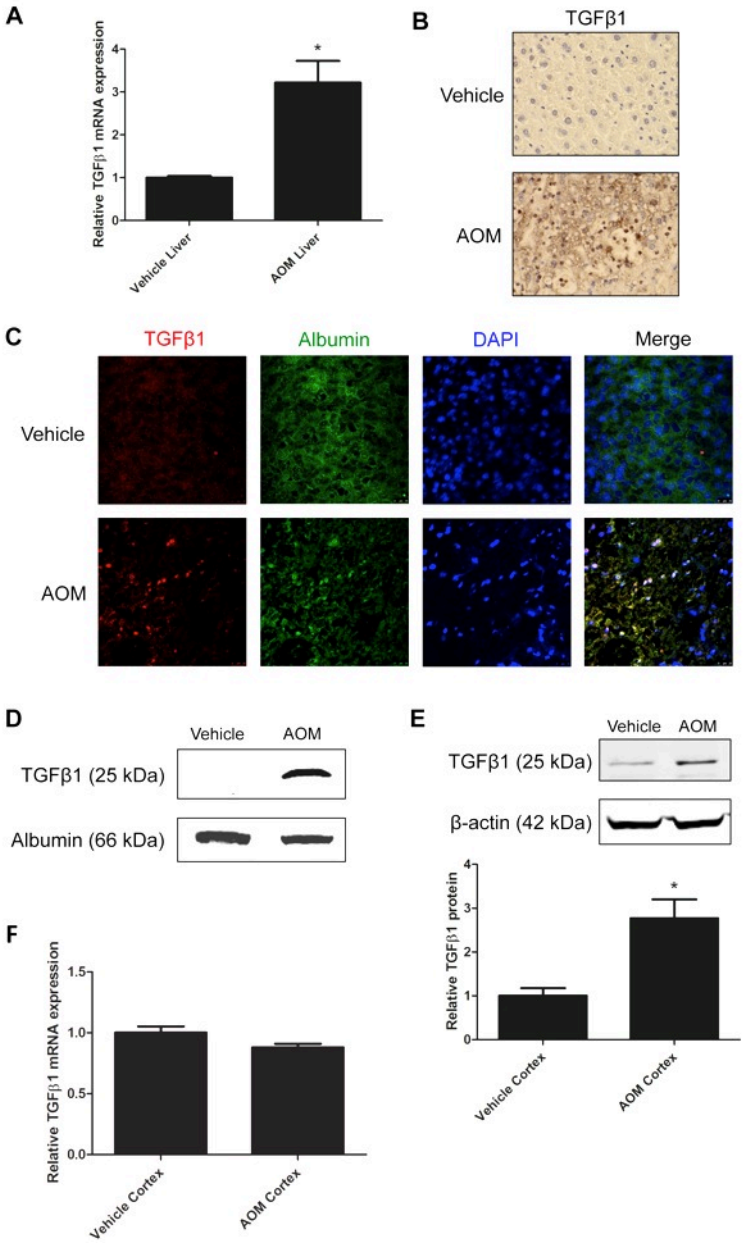

Fig. 8. TGFβ1 expression was upregulated in the liver and increased in the brain following HE. (A) Liver TGFβ1 expression was assessed in vehicle and AOM-treated mice by RTPCR (B) and immunohistochemistry. (C) TGFβ1 and albumin colocalization in vehicle and AOM livers using immunofluorescence. DAPI was used as a nuclear stain. (D) Serum TGFβ1 in vehicle and AOM-treated mice by immunoblotting with albumin used as a loading control. (E) Cortical TGFβ1 protein expression in vehicle and AOM-treated mice. (F) Cortical TGFβ1 mRNA expression in vehicle and AOM-treated mice. For protein and mRNA analyses, data are reported as mean ± SEM (n=4).

studies using primary cells were employed. Because TGFβR2 expression was found to colocalize with the neuron marker NeuN in the cortex of vehicle and AOM mice (figure 9A), we limited our *in vitro* studies to primary neuronal cultures. Treatment of neurons with rTGFβ1 for 24 hours suppressed Gli1 mRNA expression in a dose-dependent manner (figure 9B). Furthermore, treatment of neurons with rTGFβ1 (0.5 ng/ml) suppressed Gli1 mRNA from 3 hours to 24 hours (figure 9C). This demonstrates that low concentrations of rTGFβ1 can generate substantial effects on Gli1 mRNA expression. Conversely, treatment of neurons with neutralizing antibodies against TGFβ upregulated Gli1 mRNA expression at the 24-hour time point (figure 9D). Finally, treatment of neurons with SIS3 was able to reverse Gli1 suppression by rTGFβ1 demonstrating that SMAD3 is required to propagate the suppressive effect of TGFβ1 on Gli1 expression (figure 9E).

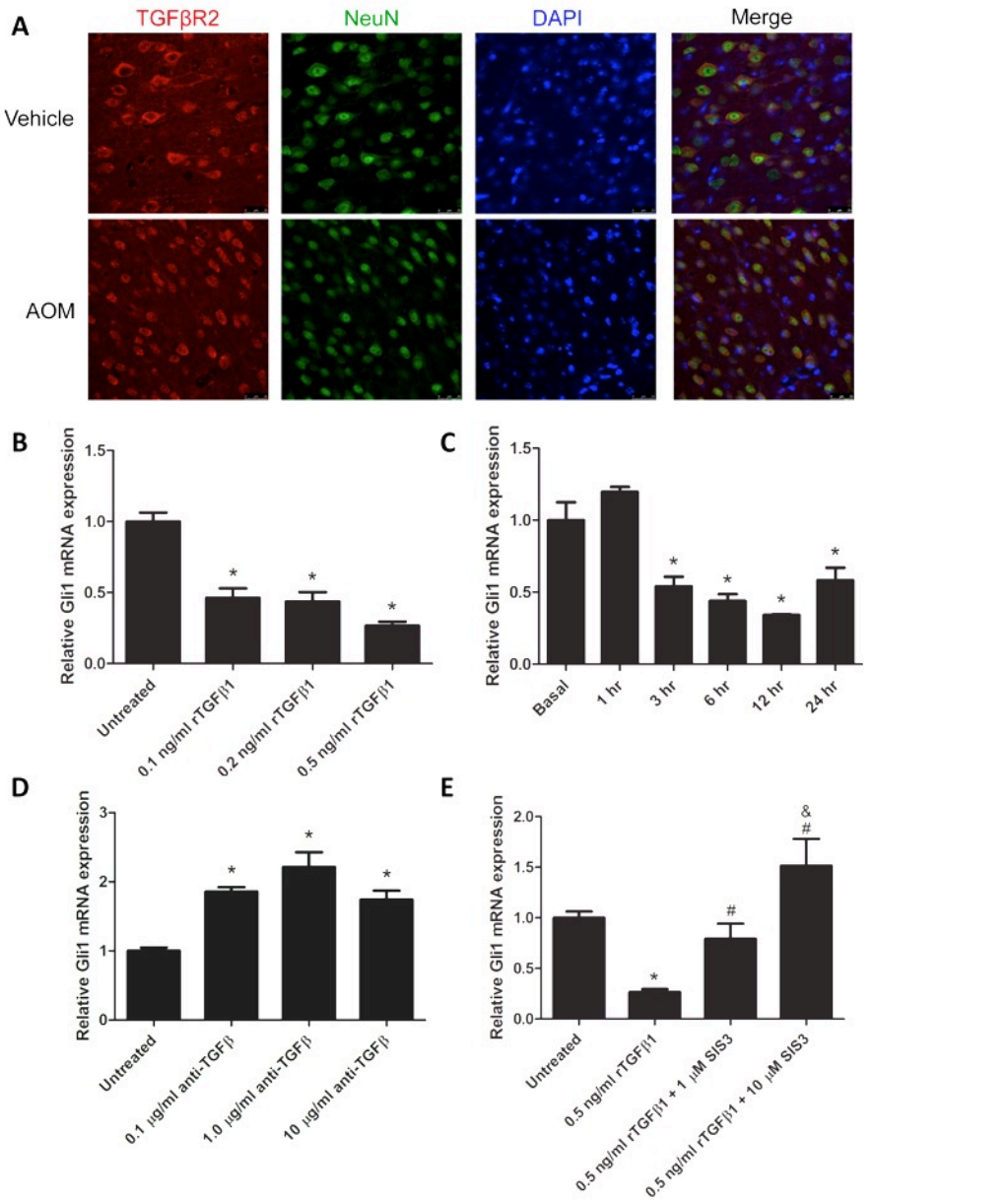

Fig. 9. TGFβ1 suppressed cortical Gli1 through a SMAD3-dependent mechanism. (A) TGFβR2 immunofluorescence in vehicle and AOM cortex costained with NeuN and the nuclear stain DAPI. (B) Gli1 mRNA expression in neurons treated with various concentrations of rTGFβ1 for 24 hours. (C) Neurons were treated with 0.5 ng/ml of rTGFβ1 for 1, 3, 6, 12, or 24 hours and assessed for Gli1 mRNA expression. (D) Neurons were treated with TGFβ neutralizing antibodies (anti-TGFβ) and Gli1 mRNA expression was measured. (E) Neurons co-treated with rTGFβ1 and the SMAD3 inhibitor SIS3 and Gli1 mRNA expression was assessed. *p<0.05 compared to untreated neurons. #p<0.05 compared to 0.5 ng/ml rTGFβ1. &p<0.05 compared to 0.5 ng/ml rTGFβ1 + 1 μM SIS3. For mRNA analyses, data are reported as mean ± SEM (n=4).

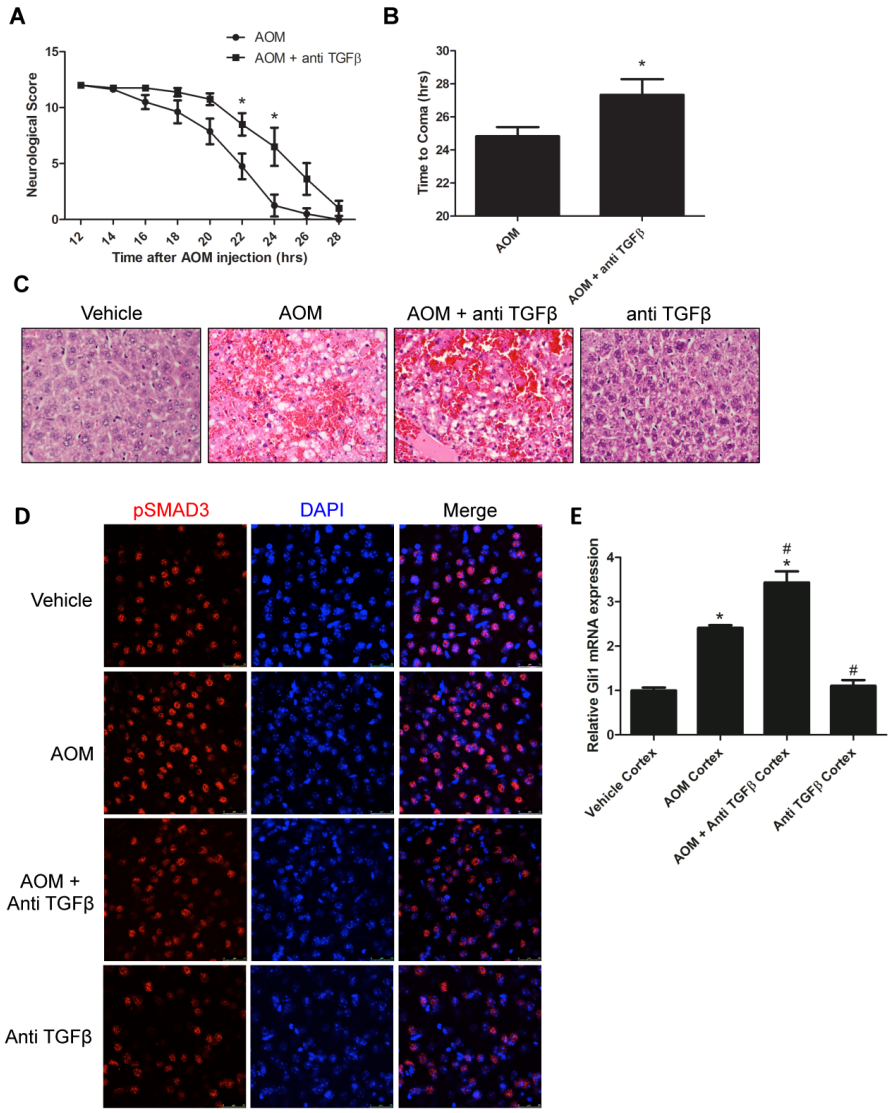

Fig. 10. Treatment of AOM mice with TGFβ neutralizing antibodies was neuroprotective. A) Mice pretreated with TGFβ neutralizing antibodies (anti TGFβ) prior to AOM injection had significantly lessened neurological decline (p=.0140). Neurological decline was assessed using the neurological score as previously described. (B) Time to coma for vehicle, AOM, AOM + anti-TGFβ, or anti-TGFβ mice. (C) H&E stains for livers from vehicle, AOM, AOM + anti-TGFβ, or anti-TGFβ mice. (D) Positive immunoreactivity of cortical phospho-SMAD3 in vehicle, AOM, AOM + anti-TGFβ, or anti-TGFβ mice. (E) Cortical Gli1 mRNA expression in vehicle, AOM, AOM + anti-TGFβ, or anti-TGFβ mice. For protein and mRNA analyses, data are reported as mean ± SEM (n=4). For time to coma and neurological decline analyses, data are reported as mean ± SEM (n=12). *p<0.05 compared to vehicle liver or vehicle cortex. #p<0.05 compare to AOM cortex.

TGFβ1 modulates the neurological decline in AOM-treated mice

In order to assess if inhibiting TGFβ1 *in vivo* could alleviate the symptoms of HE*,* mice were treated with TGFβ neutralizing antibodies prior to the injection of AOM. This treatment significantly delayed neurological decline (figure 10A) and increased the time taken to reach coma (figure 10B) compared to mice treated with AOM alone. H&E stains and liver biochemistry analyses found no definitive differences in damage between the livers of AOM-treated mice and those pretreated with TGFβ neutralizing antibodies (figure 10C and Table 2). AOM-treated mice had increased phosphorylated SMAD3 expression compared to mice pretreated with TGFβ neutralizing antibodies or vehicle controls (figure 10D)**.** Furthermore, pretreatment with TGFβ neutralizing antibodies prior to AOM injection increased Gli1 mRNA expression to a greater degree than mice treated with AOM alone (figure 10E).

2.5. Discussion

HE is a serious neurological complication that arises following liver disease(90). Currently, HE has few effective treatments and thus the need to identify targets for potential therapeutics is very important. Here we demonstrate that i) Gli1 is upregulated in the neocortex in rodent models of HE and in human autopsy samples from patients with HE, and is neuroprotective and ii) circulating TGFβ1 exacerbates HE neurological decline via suppression of Gli1 expression through a SMAD3-dependent pathway. Taken together, our data suggest that strategies to increase cortical Gli1 expression and/or inhibit TGFβ1 signaling may prove beneficial for the treatment of HE.

The data presented demonstrate that cortical Gli1 was activated in rodents and patients with HE. Furthermore, inhibiting Gli1 expression using VM technology exacerbated neurological decline, suggesting that Gli1 is exerting a neuroprotective effect during HE. Similar upregulation of Gli1 has been observed in other pathological brain states. For example, following cortical freeze injury or intracortical lipopolysaccharide injection, Gli1 induction was present and dependent on the inflammatory process generated by the injury(111). In addition, inhibition of Gli1 expression led to significant increases in infarct volume following ischemia(94). The use of polydatin, an anti-inflammatory agent, to treat experimentally induced stroke stimulated Gli1 expression and was able to reduce acute brain injury damage(95). These

studies demonstrate that Gli1 was upregulated during brain pathologies and was neuroprotective, which supports the findings of the current study on HE.

Canonical hedgehog signaling has been shown to be upregulated during liver injury, liver regeneration and in a number of liver diseases(112). Following liver damage, there is increased production of growth factors such as epidermal growth factor, platelet-derived growth factor and TGFβ1, which induce liver cells to produce hedgehog ligands(113-115). This leads to increased paracrine hedgehog signaling in the liver, which has been shown to be protective in cholestatic liver injury and facilitate liver regeneration after partial hepatectomy(113, 116). Indeed, inhibiting hedgehog signaling in the liver with cyclopamine disrupts liver regeneration, causes apoptosis of myofibroblasts and decreases cell survival of hepatic stellate cells(116-118). The data presented here demonstrated that while Shh expression was increased in the liver and bloodstream following injection of AOM, inhibiting canonical hedgehog signaling did not significantly affect liver damage across all metrics measured. This may be due to the acute and severe nature of the AOM model. Furthermore, inhibition of hedgehog signaling with cyclopamine had no effect on neurological decline even though the route and dose of cyclopamine treatment had previously been shown to inhibit brain hedgehog signaling(119). Treatment of AOM mice with SAG or with smoothened-VM validated the results from cyclopamine-treated mice. Together, these findings indicate that the increased cortical Gli1 expression during HE, and subsequent neuroprotection, may be

due to other unidentified signaling factors, rather than canonical hedgehog signaling. Understanding of the mechanisms by which Gli1 is activated in the brain is currently lacking and warrants further investigation.

Another interesting finding was that TGFβ1 was upregulated in hepatocytes and was present in the serum following liver damage. Interestingly, inhibition of circulating TGFβ1 via TGFβ-specific neutralizing antibodies delayed neurological decline in AOM mice. The deleterious effect of TGFβ1 in the brain of AOM-treated mice might be related to its role of promoting inflammation(120). In support of this concept, the pathogenic inflammation present in a mouse model of multiple sclerosis was dependent on TGFβ1 production in the CNS(121). It is becoming evident that HE is dependent on a neuroinflammatory response. Recent studies have demonstrated that microglia become activated in experimental hyperammonemia in rats and in patients who have HE(57). Furthermore, it has been shown that liver failure due to hepatic devascularization leads to an increase of proinflammatory cytokines that correlates to microglia activation(53). Additionally, mice that have an interleukin-1β or tumor necrosis factor alpha gene deletion have slower HE progression compared to wild-type mice(55). Since TGFβ1 can regulate neuroinflammation seen in other neurological disorders, TGFβ1 may play a role in neuroinflammation observed following ALF.

Here we demonstrated that TGFβ1 had an inhibitory effect on cortical Gli1 expression via a SMAD3-dependent mechanism. In contrast, previous studies

showed that TGFβ1 positively regulates Gli1 in pancreatic adenocarcinoma cells(97, 98). The differences in response of Gli1 expression to TGFβ1 may lie in the cell type (i.e. neuronal versus pancreas) and/or the transformation status (i.e. non-malignant versus cancerous) of the cell. For example, Gli1 regulates the cell cycle through cyclin D2 expression, which is more evident in cancer cells than in mature neurons that do not proliferate(122). Also, the finding that neurons elevated Gli1 mRNA expression when treated with neutralizing antibodies against TGFβ suggests that TGFβ1 is expressed endogenously in neurons. However, the findings that cortical TGFβ1 mRNA expression was not significantly changed in AOM mice provide evidence that circulating TGFβ1 played a more prominent role in Gli1 suppression. That being said, our data does not rule out a role for posttranslational mechanisms in the expression of TGFβ1 in the cortex and thus, studies to answer this definitively are warranted.

One of the clinical features of ALF may be a loss of BBB integrity(123), which can increase toxin entry into the brain(124). Since our data indicate that there is increased cortical TGFβ1 protein after AOM injection, without a concomitant increase in TGFβ1 transcriptional activity, it is reasonable to assume that the cortical TGFβ1 observed is peripherally derived. In addition, systemic treatment of mice with TGFβ neutralizing antibodies, which should not penetrate the BBB due to their high molecular weight(125), inhibited TGFβ1 activity in the circulation and protected against neurological decline.

Furthermore, TGFβ1 itself has been shown to inhibit proliferation of brain endothelial cells, which can disrupt BBB repair(126). Taken together, we propose that circulating TGFβ1 can induce TGFβ1 signaling in the brain and this may influence the BBB during HE.

In conclusion, the data presented demonstrate that Gli1 upregulation in cortical neurons occurs during HE and is protective against neurological decline seen during HE. In addition, there is release of hedgehog and TGFβ1 ligands from the liver, with TGFβ1 contributing to an increase of HE pathogenesis through neuronal suppression of Gli1. A working model of the liver-brain signaling axis as determined in this study is displayed in figure 11. This study demonstrated that suppressing circulating TGFβ1, or increasing cortical Gli1 activation, could serve as a potential therapeutic strategy for HE treatment. Furthermore, our findings suggest that targeting of the TGFβ1/Gli1 signaling axis could lend itself as a treatment strategy for other neurological disorders where inflammation and metabolic disturbances contribute to pathology.

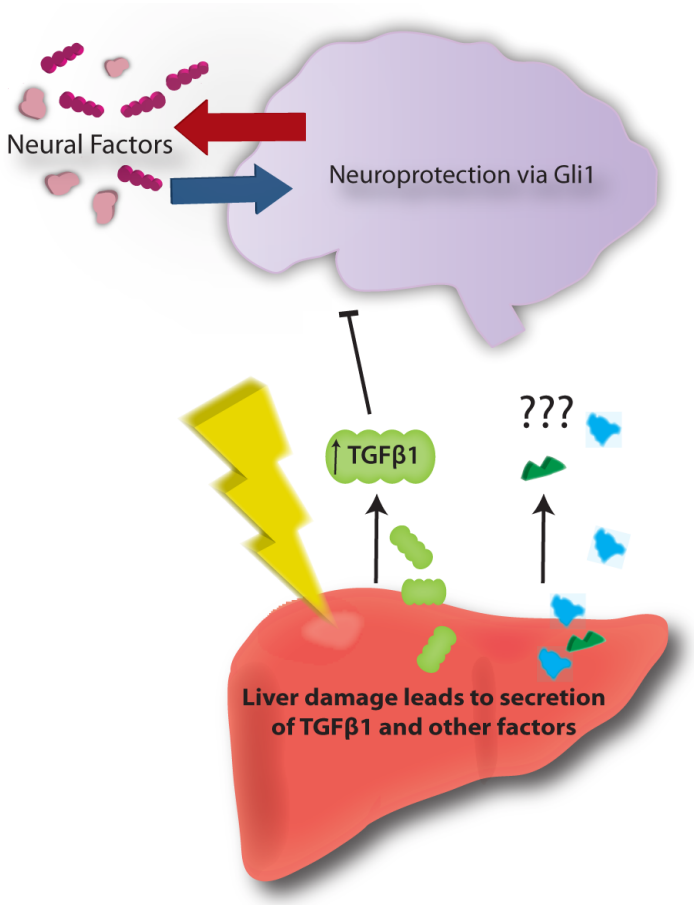

Fig. 11. Proposed working model of liver-brain signaling axis following liver damage. AOM is metabolized by the hepatocytes in the liver, which leads to their damage and death and eventual hepatic failure. This causes the release TGFβ1 and possibly other factors from the liver into the bloodstream. TGFβ1 plays a deleterious role by suppressing Gli1 mRNA in the cortex and exacerbating neurological decline. Other factors must lead to increases of cortical Gli1 activity, as hedgehog signaling cannot account for its upregulation and activation. These signaling factors that activate Gli1 may be either liver-derived or could be the result of neural signaling cascades. Treatments designed to reduce TGFβ1 activity or increase neural Gli1 could be efficacious in the treatment of HE.

3. TGFβ1 EXACERBATES BLOOD-BRAIN BARRIER PERMEABILITY IN A MOUSE MODEL OF HEPATIC ENCEPHALOPATHY VIA DOWNREGULATION OF CLAUDIN-5 AND UPREGULATION OF MMP9

3.1. Overview

Recent studies have found vasogenic brain edema to be present following ALF and that edema is dependent upon increased MMP9 activity and tight junction downregulation. Thus, the objective of this study was to assess if circulating TGFβ1 is driving changes in tight junction expression and MMP9 activity following ALF. BBB permeability was assessed via Evan's blue extravasation. Monolayers of bEnd.3 cells were treated with rTGFβ1 and permeability was assessed via FITC-dextran diffusion. BBB permeability was increased in ALF mice at 18 hours following AOM injection. Treatment of bEnd.3 cells with rTGFβ1 led to a decrease in Claudin-5 expression as well as elevation of MMP9 expression. Both the downregulation of Claudin-5 and upregulation of MMP9 were attenuated following co-treatment with a SMAD3 inhibitor. AOM-treated mice injected with neutralizing antibodies against TGFβ demonstrated significantly reduced BBB permeability. BBB permeability is induced in mice that undergo AOM-induced liver failure and this can be ameliorated by reducing circulating TGFβ1, which leads to increased Claudin-5 and downregulated MMP9 in brain endothelial cells.

3.2. Introduction

ALF can lead to many detrimental effects outside the liver, which can include a systemic inflammatory response, increased energy expenditure and catabolism, multiorgan failure and HE(5, 14, 15). HE is associated with cerebral accumulation of ammonia, which leads to the development of cytotoxic brain edema in astrocytes. This cytotoxic edema leads to the generation of Alzheimer's Type II astrocytes in the basal ganglia of patients which is a clinical marker of this disease(91, 127). However, for metabolites and ammonia to readily enter the brain and generate these effects, the BBB, which is not permeable in normal physiological conditions, must be disrupted(123).

Microvascular endothelial cells that line the vasculature of the BBB are significantly different from other endothelial cells as they lack fenestrations, have more extensive tight junctions, and have reduced pinocytic vesicular transport(128). Tight junctions, which are functional barriers created by joining together endothelial cells, are made up of cytoplasmic accessory proteins (zona occludens-1, -2, and -3) which anchor the actin cytoskeleton to transmembrane proteins (Claudins, and occludin)(129). While direct dysregulation of tight junctions can cause vasogenic edema, matrix metalloproteinases (MMP) have also been demonstrated to digest tight junction proteins, which allows for multiple levels of BBB dysregulation(130). During ALF, decreased zona occludens-2 protein expression has been shown to precede increased BBB

permeability(131). Furthermore, Claudin-5 and occludin have been shown to be decreased in the brains of mice with HE(124). MMP9 upregulation has been identified as having a causative role in the subsequent permeabilization of the BBB at later stages of HE(132). This gives strong support that BBB permeability does occur during HE, however, the specific signaling pathways influencing the BBB during HE are not well classified at this time and warrant investigation.

TGFβ1 is a signaling protein involved in many processes, including immune system modulation, cell proliferation, cell differentiation, and apoptosis(77, 78). In HE it has been demonstrated that TGFβ1 is found in the circulation of rats with fulminant hepatic failure(105) and we have found it present as well in a mouse model of liver toxin injury. In regards to the BBB, evidence exists to suggest that TGFβ1 can directly affect endothelial cell permeability. Lung endothelial cells grown in monolayers treated with TGFβ1 demonstrated significantly increased permeability(133) following treatment. Also, retinal endothelial cells treated with TGFβ1 were found to increase MMP9 expression, which subsequently increased permeability of these endothelial cells(134).

The hypothesis of the current study is that the BBB is disrupted during HE and that circulating TGFβ1 contributes to increased vascular permeability of the BBB via disruption of tight junctions and upregulation of MMP9. These combined mechanisms would allow a greater degree of toxin entry into the brain and exacerbate the pathogenesis of HE.

3.3. Materials and Methods

Materials

Immortalized mouse brain endothelial cells (bEnd.3 cells) were purchased from American Type Culture Collection (Manassas, VA). 24 well transwell inserts were purchased from Corning (Tewksbury, MA). Antibodies against MMP9 were purchased from Santa Cruz Biotechnology (Santa Cruz, CA) Antibodies against Claudin-5 were purchased from Invitrogen (Grand Island, NY). Antibodies against albumin used for immunocytochemistry were purchased from Genetex (Irvine, CA). Antibodies for tissue immunohistochemistry against albumin were bought from Bethyl Laboratories (Montgomery, TX). Neutralizing antibodies for TGFβ (anti TGFβ) and recombinant TGFβ1 protein (rTGFβ1) were purchased from R&D systems (Minneapolis, MN). SMI71 antibodies were purchased from Covance (Princeton, NJ). All primers were purchased from SA Biosciences (Frederick, MD). GW788388 was purchased from Tocris Bioscience (Minneapolis, MN). All other chemicals were purchased from Sigma-Aldrich (St. Louis MO) unless otherwise noted, and were of the highest grade available.

Experimental animals and hepatic encephalopathy model

Mouse *in vivo* experiments were performed using male C57Bl/6 mice (25-30 g; Charles River Laboratories, Wilmington, MA). Mice were allowed free

access to drinking water and standard mouse chow and were housed in constant temperature, humidity, and 12 hour light-dark cycling. Mice received a single intraperitoneal injection of 100 mg/kg AOM to induce ALF and HE. Control animals were injected with an equal volume of saline. After injection, mice were placed on heating pads set to 37°C and under heating lamps to ensure they maintained normal body temperature. Also, mice were supplied with hydrogel and rodent chow on their cage floor to ensure they have easy access to food and hydration. After 12 hours and every 4 hours following, mice were injected subcutaneously with 500µl of a 5% dextrose solution to ensure that they did not become hypoglycemic. Mice were removed from the study if they underwent a 20% weight loss.

In order to suppress the activity of circulating TGFβ, injection of TGFβ neutralizing antibodies (R&D Systems, Minneapolis, MN) was performed. This required a single intraperitoneal injection at 1 mg/kg 2 hours prior to AOM injection. Mice in all groups were euthanized at indicated timepoints or were allowed to progress to coma (loss of both righting and corneal reflexes).

In vivo *BBB permeability measurements*

To assess *in vivo* permeabilization of the BBB in the AOM HE mouse model a modified Evan's blue dye assay was performed in vehicle and AOM mice(135). Briefly, mice were anesthetized with isoflurane inhalation and an incision was made in the neck to expose the carotid artery. Evan's blue dye was

injected (5mg/ml; 500µl) and allowed to circulate for 20 minutes at which time mice were euthanized. Mice were then perfused transcardially with 50ml ice cold PBS, the meninges were removed and the brain was blotted dry. The brain stem and cerebellum were removed and the two remaining hemispheres were homogenized with 1.5 ml ice-cold trichloroacetic acid (50% v/v) in a glass homogenizer. The resulting homogenates were centrifuged for 10 minutes at 10,000 g and absorbance of the supernatant was read at 620nm. *In vivo* permeabilization was measured in mice treated with neutralizing antibodies against TGFβ as well.

In vitro *permeability assessments*

In order to assess endothelial cell permeabilization *in vitro*, monolayers of bEnd.3 cells were seeded at a density of 5.0 x 10^4 cells/cm^2 onto 24 well Transwell™ inserts with a 0.4µm pore. After cells grew into a confluent monolayer (48-72 hours), cells were treated with rTGFβ1, GW788388, SIS3, or dimethyl sulfoxide (DMSO) for 24 hours. Following treatment, inserts and chambers were washed with PBS and medium was replaced with phenol-red free media. 10kDa FITC-dextran (10 mg/ml; 10µl) was added to the upper well for one hour. Fluorescence (excitation 494nm; emission 520nm) was read in the upper and lower well and the permeability co-efficient determined using the following formula(136): $P_{dextran} = (RFU^{lower}/RFU^{upper})(V)(1/t)(1/A)$, where RFU is the relative fluorescent units in the upper and lower wells, V is the volume of the

bottom well, t is the time that the FITC-dextran was allowed to diffuse and A is the total surface area of the monolayer (cm^2). Permeability coefficients were normalized by setting basal cell monolayers to a value of 1 to minimize variability between trials.

Immunofluorescence and immunohistochemistry

For brain immunohistochemistry free-floating 30 μm sections were sectioned and put into 12-well plates containing PBS. Sections were put in 0.5% hydrogen peroxide to quench endogenous peroxidase activity. Brain sections were blocked in 5% goat serum prior to overnight incubation with specific antibodies against albumin. Secondary antibodies and DAB peroxidase substrate were supplied from Vector Labs (Burlingame, CA). Incubations and staining development were performed according to manufacturers protocols. The sections were viewed using an Olympus BX40 microscope with an Olympus DP25 imaging system (Olympus, Center Valley, PA).

Free-floating immunofluorescence of the brain was performed on 30 μm sections. Brains were initially blocked in 5% goat serum prior to overnight incubation with specific antibodies against albumin and SMI71. Immunocytochemistry in bEnd.3 cells was performed using the same methods with antibodies against MMP9 and Claudin-5. Immunoreactivity was visualized using Dylight 488- or Cy3-conjugated secondary antibodies and counterstained

with DAPI. Slides were viewed and imaged using a Leica TCS SP5-X inverted confocal microscope (Leica Microsystems, Buffalo Grove, IL).

Real-time PCR

RNA was extracted from bEnd.3 cells using the RNeasy mini kit from Qiagen (Valencia, CA) as per manufacturer's protocols. RNA content of isolated samples was calculated using a Thermo Scientific Nanodrop 2000 (Rockford, IL). An iScript™ cDNA synthesis kit (Bio-Rad, Hercules, CA) was used to amplify 1 µg of RNA per reaction in a MyCycler™ thermal cycler (Bio-Rad). cDNA was loaded onto 96-well plates with iTaq universal SYBR green supermix (Bio-Rad) along with commercially available primers designed against mouse Claudin-5, MMP9, and GAPDH. qPCR was performed using a Strategene Mx3005P qPCR system (Santa Clara, CA) and a ΔΔCT analysis was performed using basal bEnd.3 cells as controls(108, 109). Data for all experiments are expressed as mean relative mRNA levels ± SEM (n=4).

Immunoblotting

Homogenization of bEnd.3 cells was accomplished by scraping cells in lysis buffer supplemented with 1% protease inhibitor cocktail. Protein content in cell lysates from bEnd.3 cells was quantified using a BCA protein assay from Thermo Scientific. SDS-PAGE gels were loaded with 10-20 µg of protein diluted in Laemmli buffer per lane. Specific antibodies against Claudin-5, MMP9, and β-

actin were used. All imaging was performed on an Odyssey 9120 Infrared Imaging System (LI-COR, Lincoln, NE). Data are expressed as fold change in fluorescent band intensity of target antibody divided by β-actin, which is used as a loading control. The values of basal bEnd.3 cells were used as a baseline and set to a relative protein expression value of 1. All treatment groups were changes of fluorescent band intensity of target antibody to β-actin relative to basal. All band intensity quantifications were performed using ImageJ software (National Institutes of Health, Bethesda, MD). Data for all experiments are expressed as mean relative protein ± SEM (n=4).

Statistical analysis

All statistical analyses were performed using Graphpad Prism software (Graphpad Software, La Jolla, CA). Results were expressed as mean ± SEM. For data that passed normality tests, significance was established using the Student t test when differences between two groups were analyzed, and analysis of variance when differences between three or more groups were compared followed by the appropriate post hoc test. If tests for normality failed, two groups were compared with a Mann-Whitney U test or a Kruskal-Wallis ranked analysis when more than two groups were analyzed. Differences were considered significant when the p value was less than 0.05.

3.4. Results

The BBB is disrupted following AOM-induced liver failure

C57Bl/6 mice were treated with the hepatotoxin AOM for 6, 12, or 18 hours prior to assessing Evan's blue extravasation. Mice that were treated for 18 hours had significantly increased Evan's blue dye present in their brains compared to those only perfused with the dye (figure 12A). Interestingly, mice that underwent Evan's blue extravasation assays at 6 and 12 hours post AOM injection had essentially no difference of Evan's blue dye in the brain compared to untreated mice. As Evan's blue binds albumin, this gives support that the BBB is being disrupted in the later stages of ALF to a large enough degree to allow the passage of larger proteins through the barrier. Representative pictures of untreated, 0-12 hours, and 18-hour brains support the findings from our absorbance measures (figure 12B). Albumin immunofluorescence was performed in the cortex of vehicle mice and AOM mice and demonstrated that in vehicle mice there was only slight residual albumin staining in cerebral microvessels while in AOM mice albumin immunoreactivity is found diffusely spread throughout the tissue (figure 12C). Together, these findings demonstrated that treatment with AOM, which induced liver failure, also caused disruption of the BBB at later stages that is demonstrated by increased albumin entry into the brain.

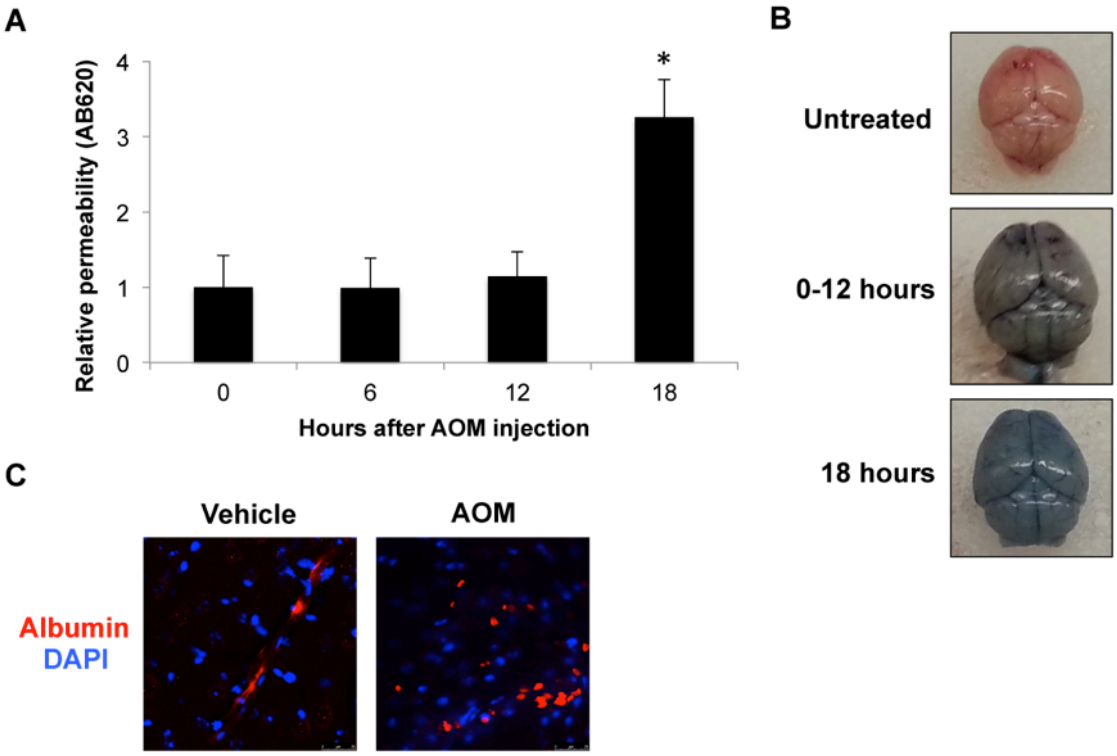

Fig. 12. The BBB was disrupted in the later stages of HE. (A) Evan's blue permeability assay of AOM mice at indicated timepoints following AOM injection (n=4). Permeability was measured by measuring absorbance of Evan's blue dye (620 nM). (B) Representative pictures of brains from mice that had no Evan's blue extravasation (untreated), mice infused with Evan's blue dye after AOM treatment from 0-12 hours, and mice infused with Evan's blue dye 18 hours after AOM injection. (C) Immunofluorescence in vehicle and AOM cortex for albumin (red) and DAPI (blue). Data in the permeability assay is reported as mean ± SEM. *=p<0.05 compared to 0 hour mice.

Circulating TGFβ1 can disrupt the BBB

In an effort to understand the specific molecular effects of TGFβ1 on brain endothelial cells, confluent bEnd.3 monolayers were used as an *in vitro* model of the BBB. Monolayers were treated with increasing doses of rTGFβ1 to determine if TGFβ1 could induce permeability of the monolayers. At doses of 1.0 ng/ml and 5.0 ng/ml of rTGFβ1 monolayers showed a significant increase in

permeability to 10 kDa FITC-dextran (figure 13A). To ensure that the effects being generated that lead to this permeabilization were entirely due to TGFβ1 signal transduction, monolayers were treated with rTGFβ1 in combination with a TGFβRII antagonist, GW788388. Treatment of bEnd.3 monolayers with 1.0 ng/ml rTGFβ1 permeabilized the monolayers, but this effect was significantly reduced following treatment with 1 μM GW78838 (figure 13B). This demonstrates that TGFβ1 is able to permeabilize monolayers of brain endothelial cells.

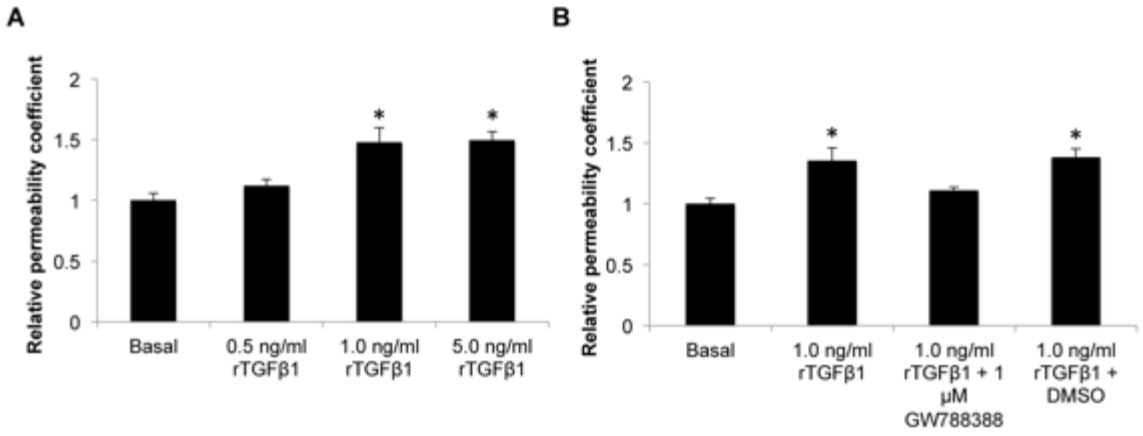

Fig. 13. Monolayers of brain endothelial cells were permeabilized by treatment with rTGFβ1. (A) Monolayers of bEnd.3 cells plated on transwells were treated with indicated doses of rTGFβ1 for 24 hours. Permeability was assessed by 10-kDa FITC-dextran diffusion from the top chamber to the bottom chamber and subsequent reading of fluorescence from both top and bottom chamber (Excitation 494/Emission 520). (B) Monolayers of brain endothelial cells were treated with rTGFβ1, the TGFβRII antagonist GW788388, or DMSO (vehicle for GW788388) for 24 hours. Permeability was assessed by 10-kDa FITC-dextran diffusion from the top chamber to the bottom chamber and subsequent reading of fluorescence from both top and bottom chamber (Excitation 494/Emission 520). Data in the monolayer assays are reported as mean ± SEM. *=$p<0.05$ compared to basal bEnd.3 cells.

Claudin-5 was downregulated by TGFβ1 in bEnd.3 cells

Due to the fact that TGFβ1 was able to permeabilize monolayers, the mechanism that generated this effect was investigated. Assessment of the tight junction proteins Claudin-5, occludin, ZO-1, and ZO-2 was assessed following rTGFβ1 treatment. There were no changes in occludin, ZO-1, and ZO-2 expression when assessed by western blotting, RTPCR, or immunofluorescence (data not shown). However, there were changes observed in Claudin-5. Treatment of bEnd.3 cells with rTGFβ1 above 1.0 ng/ml led to a significant suppression of Claudin-5 mRNA expression (figure 14A). This effect translated into a reduction of Claudin-5 protein with significant suppression at doses of 0.5 ng/ml rTGFβ1 and greater (figure 14B). In order to determine if this translated to a functional disruption of the tight junction, immunofluorescence against Claudin-5 was performed and demonstrated staining in the cell membrane of basal cells. However, when bEnd.3 cells were treated with rTGFβ1, Claudin-5 immunostaining became increasingly cytoplasmic as doses increased, indicating a disruption of tight junctions (figure 14C). These data demonstrated that TGFβ1 is able to both downregulate Claudin-5 and disrupt its localization to tight junctions in brain endothelial cells.

MMP9 was also upregulated by TGFβ1

In order to determine if the TGFβ1-induced disruption of brain endothelial cell permeability is also due to increased MMP9 activity, bEnd.3 cells were

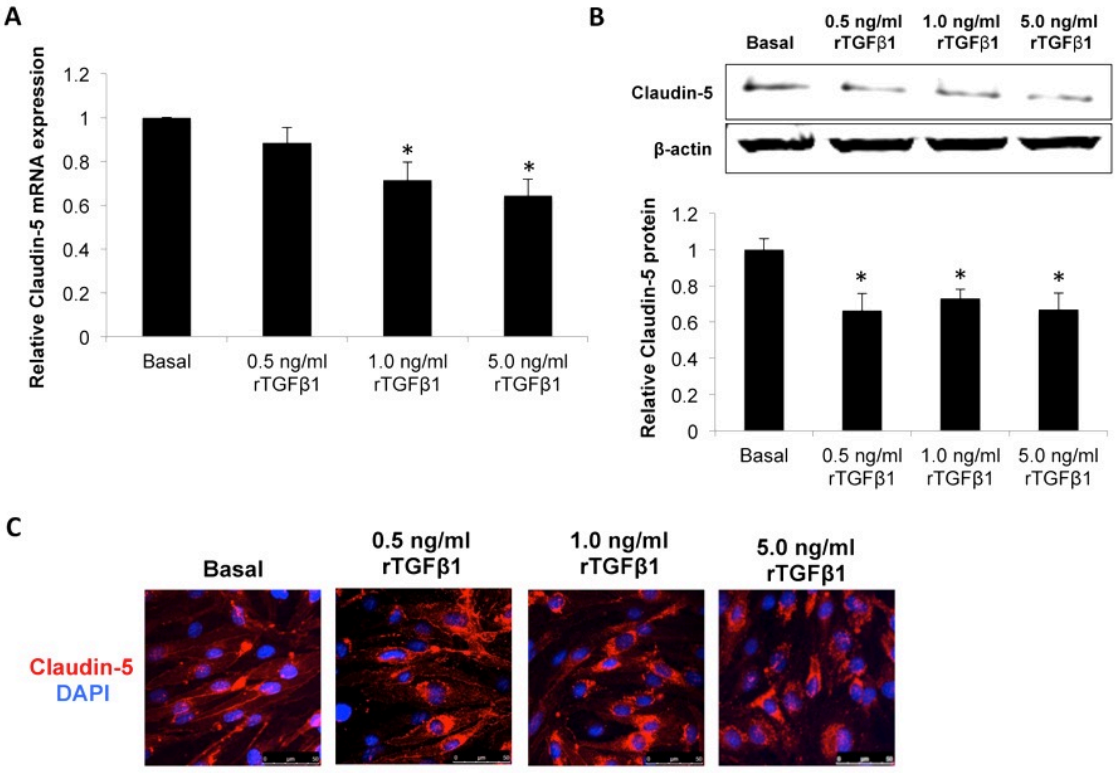

Fig. 14. Claudin-5 expression was downregulated in bEnd.3 cells by TGFβ1. (A) Claudin-5 mRNA expression in bEnd.3 treated with increasing concentrations of rTGFβ1 as assessed by RTPCR. (B) Claudin-5 protein expression in bEnd.3 cells treated with increasing concentrations of rTGFβ1 assessed by immunoblotting. β-actin was used as a loading control and quantifications are normalized to basal bEnd.3 cells. (C) Immunofluorescence investigating Claudin-5 (red) staining along tight junctions with DAPI (blue) used to stain nuclei. The data from mRNA and protein analyses are reported as mean ± SEM. *=p<0.05 compared to basal bEnd.3 cells.

treated with rTGFβ1 and assessed for MMP9 expression. Treatment with rTGFβ1 led to a dose-dependent increase of MMP9 mRNA expression with treatments of 0.5 ng/ml rTGFβ1 and higher generating a significant increase (figure 15A). To determine if this treatment led to increased protein levels of MMP9, immunofluorescence was performed and demonstrated a dose-dependent increase in MMP9 immunostaining (figure 15B). Quantification of

this immunofluorescence determined that doses of 1.0 ng/ml and 5.0 ng/ml of rTGFβ1 led to a significant increase of MMP9 immunoreactivity (figure 15C). These data demonstrate that TGFβ1 may generate its effects on permeability through upregulation of MMP9.

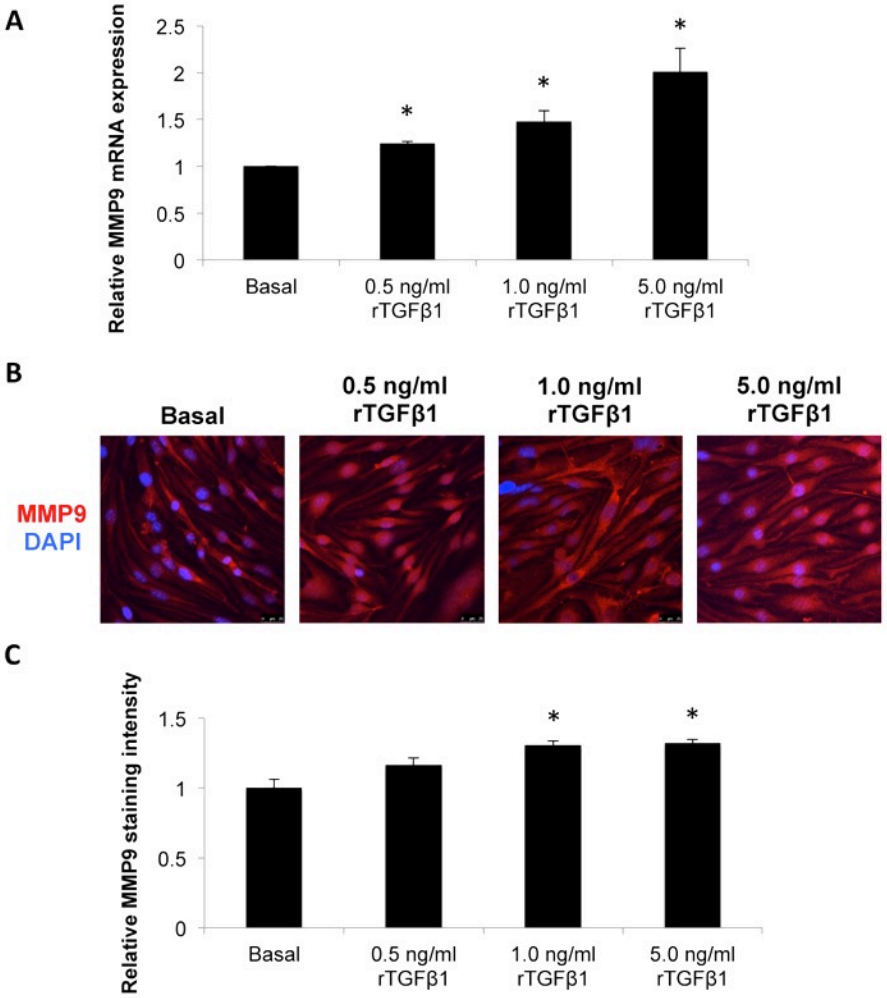

Fig. 15. MMP9 was upregulated by TGFβ1 in bEnd.3 cells. (A) MMP9 mRNA expression in bEnd.3 cells following treatment with rTGFβ1 as assessed by RTPCR. (B) Coverslips of bEnd.3 cells were stained for MMP9 (red) and DAPI (blue) as a nuclear stain following treatment with increasing doses of rTGFβ1. (C) Quantification of MMP9 immunofluorescence for bEnd.3 cells grown on coverslips following treatment with rTGFβ1. The data from mRNA and immunofluorescence quantification analyses are reported as mean ± SEM. *=$p<0.05$ compared to basal bEnd.3 cells.

Modulations of Claudin5 and MMP9 via TGFβ1 were dependent on SMAD3

To determine if TGFβ1 was exerting its effects through a SMAD3-dependent mechanism, bEnd.3 cells were treated with rTGFβ1 and the SMAD3 antagonist SIS3. Treatment of monolayers with TGFβ1 and SIS3 was able to alleviate the permeability caused by TGFβ1 (figure 16A). Associated with this, treatment with both TGFβ1 and SIS3 was also able to rescue the downregulation of Claudin-5 mRNA (figure 16B) and protein (figure 16C) compared to TGFβ1 treatment by itself. In order to determine if disruption of cellular localization of Claudin-5 was dependent upon SMAD3, coverslips of bEnd.3 cells were treated with rTGFβ1 and SIS3. Treatment of bEnd.3 cells with SIS3 was able to somewhat restore the localization of Claudin-5 to the cell membrane (figure 16D).

A SMAD3-dependent mechanism could potentially play a role in the upregulation of MMP9 by TGFβ1 as well. Treatment of bEnd.3 cells with TGFβ1 and SIS3 significantly reduced MMP9 mRNA expression back to near the levels of basal cells (figure 17A). Associated with this, SIS3 treatment of TGFβ1 treated bEnd.3 coverslips was able to reduce MMP9 immunofluorescence to near basal levels (figure 17B). Quantification of MMP9 immunofluorescence determined that treatment with SIS3 was able to significantly reduce MMP9 immunoreactivity in bEnd.3 cells to near basal levels (figure 17C). Together, these findings demonstrate that downregulation of Claudin-5 and upregulation of MMP9 via TGFβ1 in brain endothelial cells is dependent upon SMAD3.

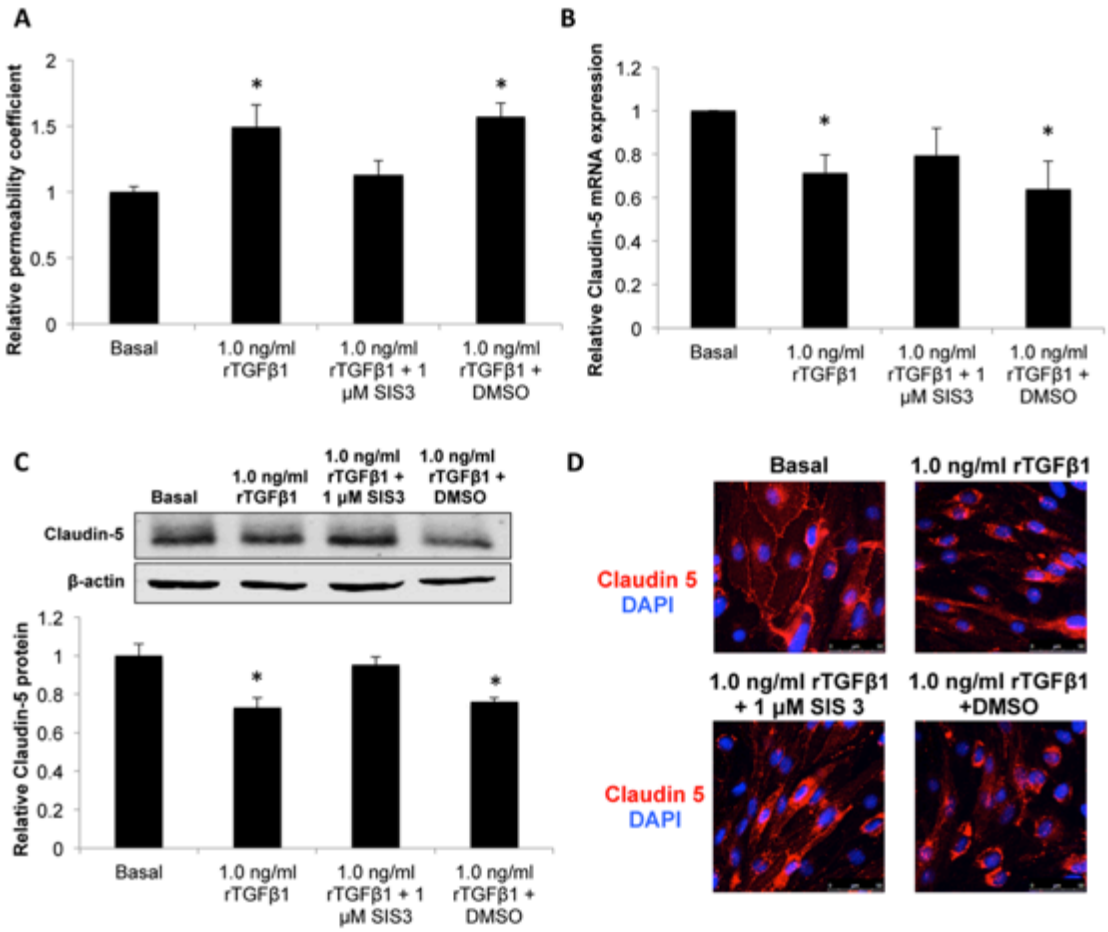

Fig. 16. Claudin-5 downregulation via TGFβ1 occured through a SMAD3-dependent mechanism. (A) Monolayers of bEnd.3 cells were treated with rTGFβ1, the SMAD3 inhibitor SIS3, or SIS3 vehicle (DMSO) for 24 hours. Permeability was assessed by 10-kDa FITC-dextran diffusion from the top chamber to the bottom chamber and subsequent reading of fluorescence from both top and bottom chamber (Excitation 494/Emission 520). (B) Claudin-5 mRNA expression in bEnd.3 cells treated with rTGFβ1, the SMAD3 inhibitor SIS3, or SIS3 vehicle (DMSO) for 24 hours. (C) Claudin-5 protein in bEnd.3 cells treated with rTGFβ1, the SMAD3 inhibitor SIS3, or SIS3 vehicle (DMSO) for 24 hours as assessed by immunoblotting. β-actin is used as a loading control and quantifications are normalized to basal bEnd.3 cells. (D) Claudin-5 (red) immunofluorescence in bEnd.3 cells treated with rTGFβ1, the SMAD3 inhibitor SIS3, or SIS3 vehicle (DMSO) for 24 hours. DAPI (blue) was used as a nuclear stain. The data from mRNA and immunoblot analyses are reported as mean ± SEM. *=p<0.05 compared to basal bEnd.3 cells.

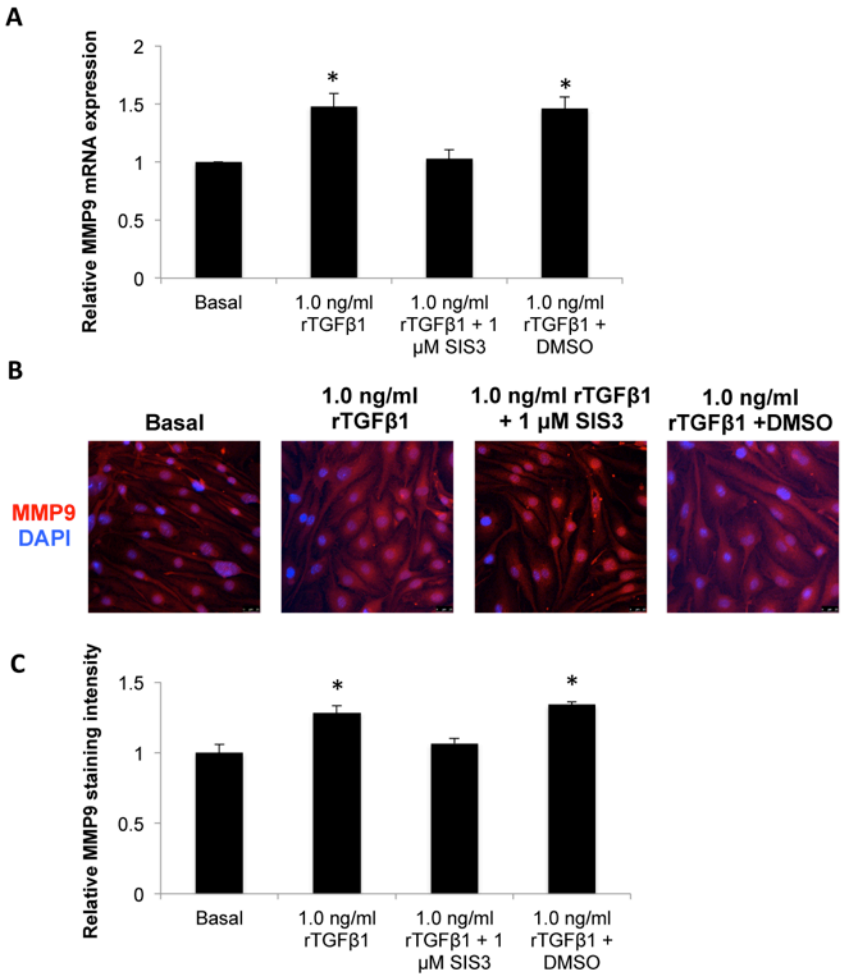

Fig. 17. SMAD3 was required for upregulation of MMP9 by TGFβ1. (A) Relative MMP9 mRNA expression in bEnd.3 cells treated with rTGFβ1, the SMAD3 inhibitor SIS3, or SIS3 vehicle (DMSO) for 24 hours. (B) bEnd.3 cells were grown on coverslips and treated with rTGFβ1, the SMAD3 inhibitor SIS3, or SIS3 vehicle (DMSO) for 24 hours. Immunofluorescence against MMP9 (red) and DAPI (blue) were performed. (C) Quantification of MMP9 immunofluorescence in bEnd.3 cells following treatment with rTGFβ1. The data from mRNA and immunofluorescence quantification analyses are reported as mean ± SEM. *=$p<0.05$ compared to basal bEnd.3 cells.

In vivo *neutralization of TGFβ1 reduced BBB permeability following liver failure*

Evan's blue extravasation assay was performed in mice treated with AOM and/or neutralizing antibodies against TGFβ for 18 hours. Mice injected with AOM demonstrated a significant increase in Evan's blue dye in their brain and this increase was significantly reduced if the mice were pretreated with neutralizing antibodies against TGFβ (figure 18A). Representative pictures of the brains of mice treated with AOM and/or neutralizing antibodies against TGFβ support these results (figure 18B). To show this effect to a greater degree, immunohistochemistry was performed against albumin in the brains of mice treated with AOM and neutralizing antibodies against TGFβ. This immunohistochemistry displayed a significant elevation of albumin in the cortex of AOM mice that was reduced in mice treated with neutralizing antibodies against TGFβ (figure 18C). In order to visualize the brain microvascular endothelial cells, immunofluorescence staining was performed for the endothelial cell marker SMI71. AOM-treated mice showed discontinuous staining for SMI71 while mice pretreated with neutralizing antibodies against TGFβ displayed continuous staining which is similar to vehicle-treated mice (figure 18D). These data demonstrated that inhibiting circulating TGFβ1 activity *in vivo* was able to restore BBB function following ALF.

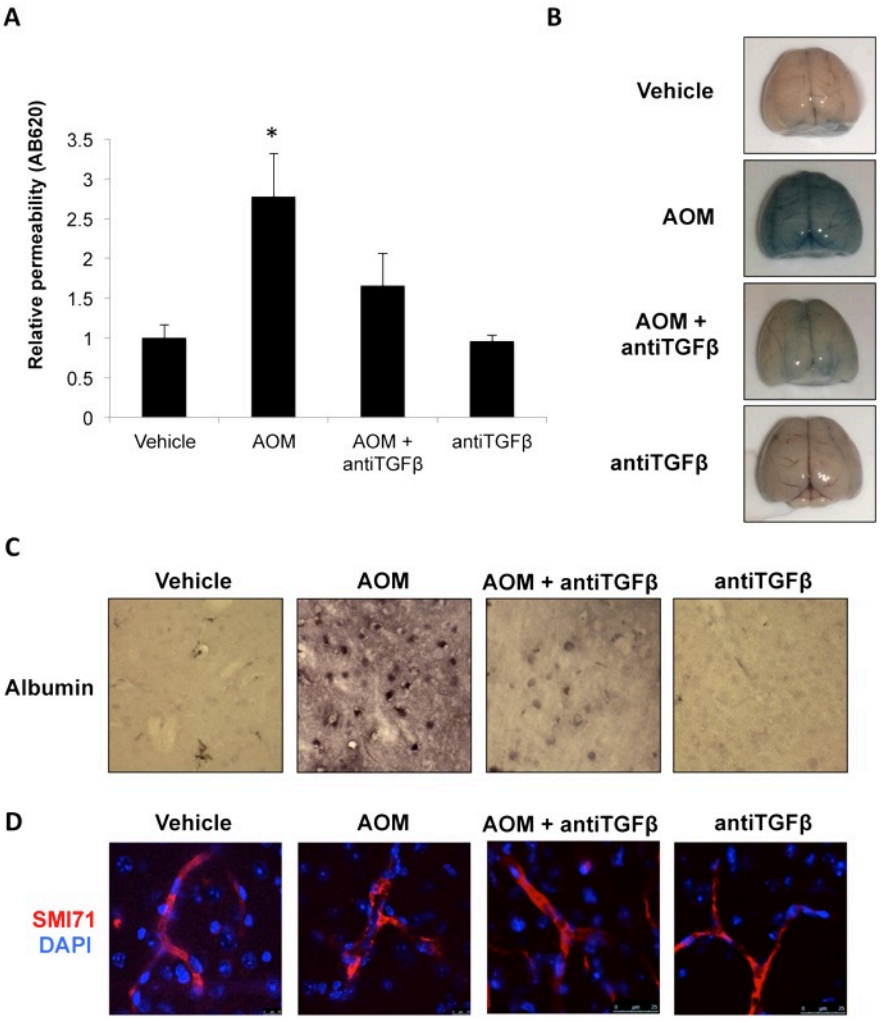

Fig. 18. Treatment of AOM mice with neutralizing antibodies against TGFβ reduced BBB dysfunction. (A) Evan's blue permeability assay of mice treated with AOM or with neutralizing antibodies against TGFβ for 18 hours (n=4). Permeability was measured by measuring absorbance of Evan's blue dye (620 nM). (B) Representative images of Evan's blue extravasation in vehicle, AOM, AOM + antiTGFβ, and antiTGFβ mice. (C) Immunohistochemistry against albumin in the cortex of vehicle, AOM, AOM + antiTGFβ, and antiTGFβ mice. (D) Immunofluorescence staining for the endothelial cell marker SMI71 (red) with DAPI (blue) used as a nuclear stain in the cortex of vehicle, AOM, AOM + antiTGFβ, and antiTGFβ mice. Data in the permeability assay are reported as mean ± SEM. *=$p<0.05$ compared to vehicle treated mice.

3.5. Discussion

This manuscript reports the findings that 18 hours following AOM injection the BBB is significantly disrupted as measured by Evan's blue extravasation. Investigation into the molecular mechanisms that drive this effect determined that brain endothelial cells have reduced Claudin-5 expression and increased MMP9 expression following treatment with rTGFβ1. The suppression of Claudin-5 and increased MMP9 expression was found to be dependent upon SMAD3 signaling as treatment with the SMAD3 inhibitor SIS3 was able to reverse the effects of rTGFβ1 treatment. Finally, inhibition of circulating TGFβ1 in AOM-treated mice by injection of neutralizing antibodies was able to reduce albumin infiltration in the brain, reduce microvessel disruption and significantly reduce BBB permeability compared to mice treated with AOM alone. A working model of our findings is presented in figure 19.

This study demonstrates that the AOM model of HE generates a significant disruption of the BBB as measured by the presence of Evan's blue dye in the cerebral cortices of AOM-treated mice. Interestingly, this only occured at later stages of HE when severe neurological decline was present (ataxia and minor reflex deficits are typically observed around twelve hours in this model). Other researchers have performed Evan's blue extravasation using a lower dose of AOM (50 mg/kg) and have shown similar findings(132).

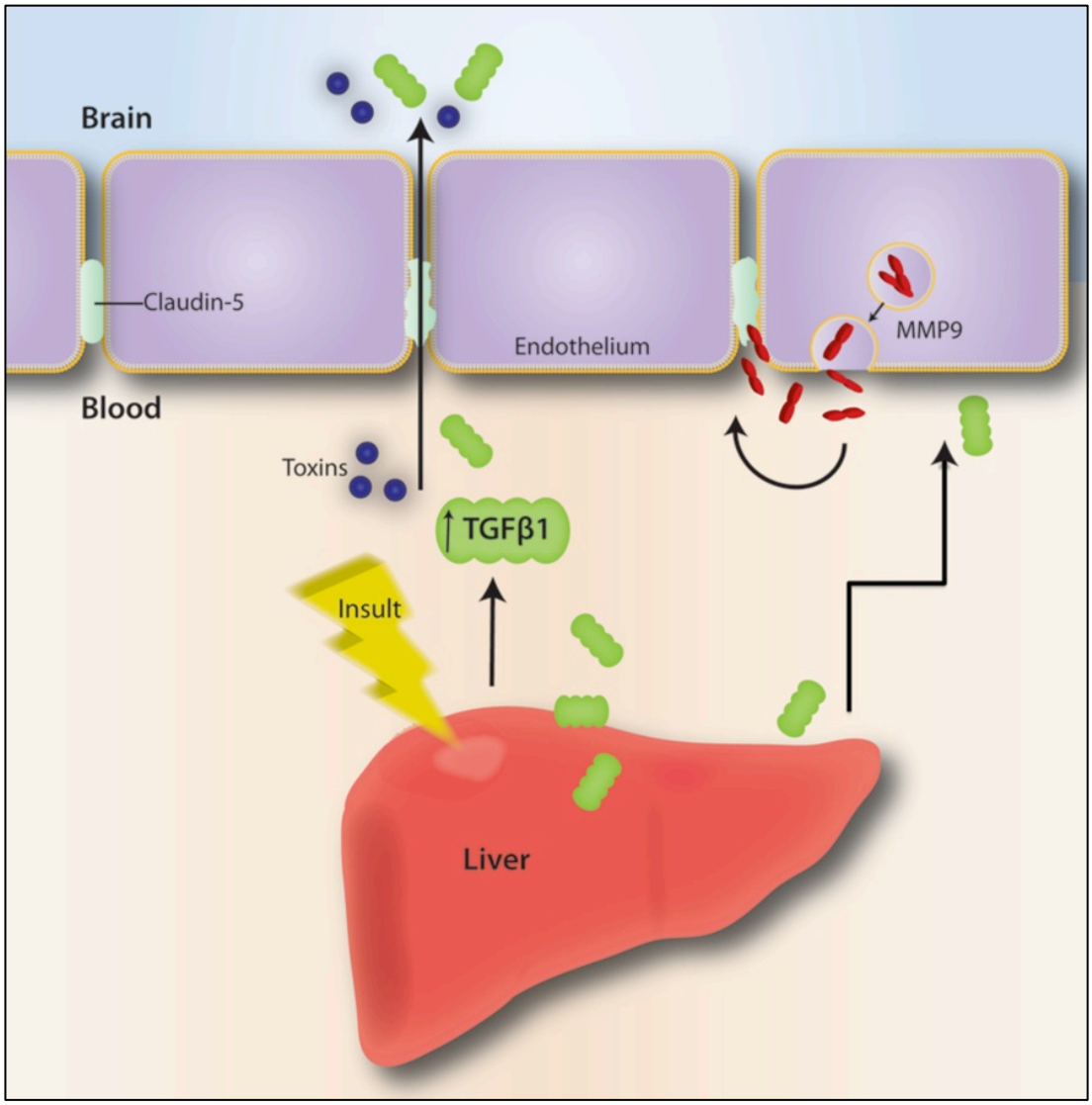

Fig. 19. Working model of TGFβ-induced permeability of BBB. Following liver insult, TGFβ1 is released from the liver into the circulation. This generates two separate effects. One is a direct effect on endothelial cells by downregulating Claudin-5 and subsequent disruption of tight junctions. The other effect of TGFβ1 is the upregulation of MMP9 in endothelial cells with subsequent release into the circulation and digestion of Claudin-5. Together these effects allow signaling proteins like TGFβ1 and toxins to pass through the BBB and enter into the brain to exacerbate HE pathology.

Furthermore, rats treated with D-galactosamine to induce ALF show significant increase of Evan's blue extravasation at coma(137). These findings mirror the more recent reports of vasogenic edema that have been reported in clinical studies in both acute and chronic liver failure(138, 139). That being said, the findings from our current study do support the finding that BBB permeability is only seen in later stages of HE. This in itself does not answer what pathological processes could be involved in the earlier stages of HE progression and remain an area that needs to be further studied to better understand this disease.

Previous research into the effects of tight junction proteins following ALF has been conflicting. One group of researchers found that AOM-treated mice have a disruption of occludin, Claudin-5, zona occludens-1, and zona occludens-2 as assessed by western blot(124). However, other researchers have used the AOM model and observed no changes in immunoblot tight junction protein expression(140). Our findings in the treatment of bEnd.3 cells with rTGFβ1 demonstrated a downregulation of the tight junction protein Claudin-5 as well as translocation of the protein from the cell membrane to the cytosol. Claudin-5 downregulation has been shown to lead to increased BBB permeability following hypoxia(141), focal cerebral cooling(142), and ischemia reperfusion injury(143). Also, other studies have found that TGFβ1 can lead to the direct downregulation of Claudin-5(144). Interestingly, we found that rTGFβ1 treatment led to no significant changes in occludin, zona occludens-1, or zona occuldens-2. Thus, our findings support the concept that circulating TGFβ1 could be driving the BBB

permeability that we observed *in vivo* through downregulation of Claudin-5. This does not discount involvement of occludin or zona occuldens in BBB permeability following ALF and studies investigating these signaling proteins and the signaling factors that interact with them are still necessary.

This study also found that MMP9 expression was increased in bEnd.3 cells following treatment with rTGFβ1. TGFβ1 has been shown to lead to increased expression of MMP9 in corneal epithelial cells(145) and in podocytes (146). MMP9 plays many roles in dysregulation of the BBB as it has the capability to degrade Claudin-5, occludin, ZO-1, and ZO-2(130). In models of AOM-induced ALF, MMP9 has been demonstrated to be upregulated in the serum while its physiological inhibitor TIMP1 is downregulated(132, 137). This upregulation of MMP9 has been shown to disrupt tight junctions and inhibiting MMP9 can reduce BBB permeability(124). Interestingly, it has also been shown that ammonia treatment of rat brain microvascular endothelial cells by itself is able to induce MMP9 expression(147). Thus, it is conceivable that TGFβ1 could potentially be acting synergistically with ammonia to induce MMP9 expression and further drive BBB permeability.

TGFβ1 is able to transduce its signaling via activation of its receptor and subsequent phosphorylation of SMAD proteins. TGFβ1 signaling can be transduced via SMAD2 or through SMAD3(148). We determined that SMAD3 was generating the majority of the effects that we were seeing both *in vivo* and *in vitro* due to the fact that treatment with SIS3 was able to reverse most of the

effects of TGFβ1. Interestingly, other studies have inhibited TGFβ receptor kinase activity, which reduced SMAD3 activity and was able to elevate Claudin-5 expression(149). In addition, human meningeal cells treated with a SMAD3 inhibitor were able to attenuate TGFβ1-dependent MMP9 upregulation(150). Thus, there is strong evidence that supports dysregulation of both Claudin-5 and MMP9 by TGFβ1 via a SMAD3-dependent mechanism and these effects could be driving some of the effects on BBB permeability observed here. However, this does not exclude the possibility that TGFβ1/SMAD3 signaling could be having other effects on these cells as well, such as affecting junctional adhesion molecules or proteins of the adherens junction, which could also disrupt permeability of the BBB. Also of note is that our studies specifically investigated only the effects of SMAD3 activity modulation, and due to this, we cannot discount that there might be some involvement of SMAD2 in the effects that were observed.

BBB manipulations *in vivo* via sequestration of circulating TGFβ1 demonstrated that TGFβ1 plays a significant role in promoting permeability of the BBB in this model of ALF. It is possible that some of these effects could be due to downstream TGFβ1 signaling in brain endothelial cells. One of TGFβ1 downstream targets is the activation of PI3K/Akt signaling(151) which has been demonstrated to promote vascular permeability in cancer models(152, 153). Also, this pathway has been shown to induce BBB permeability following focal cerebral ischemia(154), HIV-induced BBB disruption(155), and traumatic brain

injury(156). Outside of this pathway, hedgehog signaling has been shown to be protective in experimental autoimmune encephalomyelitis, a mouse model of multiple sclerosis, by promoting BBB integrity(66). Also, treatment of mice with polydatin, which elevates Gli1, has been shown to restore BBB function following ischemic insult(95). These findings support that inhibiting TGFβ1 could promote BBB integrity via suppression of vascular permeability pathway signaling as well as inducing factors to promote BBB vascular integrity. However, research into the specific signaling pathways that are dysregulated by TGFβ1 specifically in brain endothelial cells are still warranted and are currently ongoing in the laboratory.

Together, our findings support that TGFβ1 is driving BBB permeability via downregulation of Claudin-5 and upregulation of MMP9 and that these effects are dependent upon SMAD3. These results support that manipulations of TGFβ1 or therapies to target SMAD3 may be potential therapeutic targets to treat patients with ALF who have the potential to develop HE.

4. TGFβ1 ACTIVATES MICROGLIA DURING HEPATIC ENCEPHALOPATHY

4.1. Overview

HE that arises following liver failure has been associated with increases in neuroinflammation. CCL3 is a proinflammatory chemokine that leads to activation of microglia through activation of CCR1-mediated signaling. The aims of this study were to assess CCL3/CCR1 signaling during HE and if TGFβ1 is a primary inducer of this signaling. Microglia depletion was accomplished through ICV injection of clodronate liposomes. Treatment with neutralizing antibodies against TGFβ was used to inhibit circulating TGFβ1. CCL3 knockout mice were employed to determine its role in HE pathogenesis. Neural expression of CCL3, CCR1, NF-κB, and ERK1/2 were assessed. CCL3 and CCR1 protein expression was assessed in patients with HE, in cirrhotic patients w/o HE, or age-matched controls. Microglia were activated during HE and their depletion via clodronate liposomes reduced neurological decline. CCR1 activity was found to be elevated without increased CCR1 expression in HE mice. Systemic reduction of TGFβ1 reduced CCL3/CCR1 signaling in AOM mice. CCL3 knockout did not affect neurological decline associated with HE. Microglia activation was pathological during HE and was dependent on circulating TGFβ1. However, the CCL3/CCR1 signaling axis may not be the primary signaling pathway that activates microglia during HE.

4.2. Introduction

Chemokines are chemoattractant cytokines that facilitate immune cell differentiation, regulate inflammation, and promote leukocyte trafficking(157). Besides these functions, chemokines have the ability to regulate free radicals, nitric oxide, cytokines, and matrix metalloproteinases as well as control apoptosis, cell cycle regulation and angiogenesis(158). In the brain, chemokines facilitate the recruitment and activation of microglia(159). In regards to HE, it has been demonstrated that microglia are activated in a model of ammonia neurotoxicity in rats treated with an intraperitoneal injection of ammonium acetate(57), during hepatic devascularization in rats(54), and in the AOM model of liver failure(160). However, there are few studies that have studied the influence of chemokines during HE with no reports investigating chemokines in toxin-induced liver failure with subsequent HE.

Chemokine ligand 3 (CCL3), or macrophage inflammatory protein-1α, is a proinflammatory chemokine that transduces its signaling via chemokine receptor 1 (CCR1)(161). In the liver, CCL3 expression, as well as other cytokines, have been found to be elevated following chronic injury using BDL or CCl_4 models of liver damage(162). In the brain, elevated CCL3 expression has been shown in a mouse model of the lysosomal storage disorder Goucher's disease, which has been classified with microgliosis(163). Also excitotoxic injury with kainic acid was found to lead to elevations of CCL3, which correlated with microglia

recruitment(164). As models of HE have portrayed microglia recruitment to be a part of the pathology present, it is conceivable that CCL3/CCR1 signaling may be playing a role in facilitating microglial activation during HE, although definitive evidence of this is lacking.

TGFβ1 is a signaling factor involved in many pathological inflammatory processes. However, its role in inflammation in the brain has not been fully elucidated. Previous research in our laboratory has demonstrated the inhibition of circulating TGFβ1 during HE reduced neurological decline associated with the disorder. Also, studies have found that during experimental autoimmune encephalomyelitis, a mouse model of multiple sclerosis, that TGFβ1 helps sustain neuroinflammation(120). This effect could be a result of TGFβ1 having the ability to upregulate chemokine receptor expression, in particular CCR1(165).

Thus, the overall hypothesis of this study is that microglia are activated during HE via CCL3/CCR1 signaling and that TGFβ1 is exacerbating neuroinflammation by enhancing the activity of this signaling pathway. Gaining understanding into the inflammatory processes that occurs during HE could eventually help lead to the development of therapeutics to help treat patients with this disease.

4.3. Materials and Methods

Materials

Antibodies against CCR1, CCL3, p84 and GAPDH were purchased from Genetex (Irvine, CA). Antibodies against NeuN were purchased from Millipore (Billerica, MA). Antibodies against NF-κB p65 were purchased from Santa Cruz Biotechnology (Santa Cruz, CA). Neutralizing antibodies against TGFβ (anti TGFβ) were purchased from R&D systems (Minneapolis, MN). All RTPCR primers were purchased from SA Biosciences (Frederick, MD). All other chemicals were purchased from Sigma-Aldrich (St. Louis MO) unless otherwise noted, and were of the highest grade available.

Experimental animals and hepatic encephalopathy model

Mouse *in vivo* experiments were performed using male C57Bl/6 mice (25-30 g; Charles River Laboratories, Wilmington, MA). Mice were allowed free access to drinking water and standard mouse chow and were housed in constant temperature, humidity, and 12 hour light-dark cycling. Mice received a single intraperitoneal injection of 100 mg/kg AOM to induce ALF and HE. Control animals were injected with an equal volume of saline. After injection, mice were placed on heating pads set to 37°C and under heating lamps to ensure they maintained normal body temperature. Also, mice were supplied with hydrogel and rodent chow on their cage floor to ensure they had easy

access to food and hydration. After 12 hours and every 4 hours following, mice were injected subcutaneously with 500 µl of a 5% dextrose solution to ensure that they did not become hypoglycemic. Mice were removed from the study if they underwent a 20% weight loss.

Following AOM injection, mice were monitored every two hours (starting at eight hours post AOM injection) for body temperature, weight, and neurological decline. Neurological decline was assessed by measuring the pinna reflex, corneal reflex, tail flexion, escape response, righting reflex, and ataxia. The pinna reflex was assessed by touching the external auditory meatus with a cotton applicator and observing ear retraction or head movement. The corneal reflex was measured by touching the cornea with a cotton applicator and measuring the blink response. Tail flexion was measured via tail pinch with forceps and assessing tail flexion. Escape response was measured by tail pinch by forceps and a subsequent movement of mice away from stimuli. The righting reflex was assessed by placing the mice on their back and measuring the time for them to right themselves. Assessment of ataxia was performed by observing movement activity when the mice were placed on the cage wire bar lid. Mice in all groups were euthanized at indicated timepoints or were allowed to progress to coma (loss of both righting and corneal reflexes).

Genetic and pharmacological manipulations

Suppression of circulating TGFβ1 activity was accomplished through injection of TGFβ neutralizing antibodies. This required a single intraperitoneal injection at 1 mg/kg 2 hours prior to AOM injection. Clodronate liposomes or control liposomes were intracerebroventricular (ICV) injected into the lateral ventricle (10 µl of a 100 µg/g solution) to deplete microglia in the brain. The liposomes were obtained from Dr. Nico van Rooijen (Harleem, The Netherlands). CCL3 gene expression was ablated in vehicle and AOM mice through the use of commercially available CCL3 knockout mice (The Jackson Laboratory, Stock # 002687, Bar Harbor, ME).

Human samples

Brain tissue from patients who had HE following liver cirrhosis, cirrhotic patients without HE or aged-matched controls without liver disease were supplied through the New South Wales Tissue Resource Centre at the University of Sydney. Immunohistochemistry was performed against human CCL3 or CCR1 on these tissues as described below.

Free floating immunofluorescence

Free-floating immunofluorescence of the brain was performed on 30 µm sections. Brains were initially blocked in 5% goat serum prior to overnight incubation with specific antibodies against CCR1, CCL3, IBA1 and/or NeuN.

Immunoreactivity was visualized using Dylight 488- or Cy3-conjugated secondary antibodies and counterstained with DAPI following mounting onto slides. Mounted brain sections were viewed and imaged using a Leica TCS SP5-X inverted confocal microscope (Leica Microsystems, Buffalo Grove, IL).

Real-time PCR

RNA was extracted from brain tissue using the RNeasy mini kit from Qiagen (Valencia, CA) as per manufacturer's protocols. RNA content of isolated samples was calculated using a Thermo Scientific Nanodrop 2000 (Rockford, IL). An iScript™ cDNA synthesis kit (Bio-Rad, Hercules, CA) was used to amplify 1 µg of RNA per reaction in a MyCycler™ thermal cycler (Bio-Rad). cDNA was loaded onto 96-well plates with iTaq universal SYBR green supermix (Bio-Rad) along with commercially available primers designed against mouse CCL3 and GAPDH. qPCR was performed using a Strategene Mx3005P qPCR system (Santa Clara, CA) and a ΔΔCT analysis was performed using vehicle tissue as controls(108, 109). Data for all experiments are expressed as mean relative mRNA levels ± SEM (n=4).

Immunoblotting

Homogenization of cortex and cerebellum was accomplished by mechanical disruption in cell lysis buffer supplemented with 1% protease inhibitor cocktail. Tissue fractionations were accomplished using a

ProteoExtract™ Subcellular Proteome Extraction Kit (Calbiochem, Billerica, MD). Protein content in lysates was quantified using a BCA protein assay from Thermo Scientific. SDS-PAGE gels were loaded with 10-20 µg of protein diluted in Laemlli buffer per lane. Specific antibodies against CCL3, CCR1, NF-κB, p84, pERK1/2, tERK1/2, GAPDH and β-actin were used. All imaging was performed on an Odyssey 9120 Infrared Imaging System (LI-COR, Lincoln, NE). Data are expressed as fold change in fluorescent band intensity of target antibody divided by β-actin, which was used as a loading control. The values of control cortex were used as a baseline and set to a relative protein expression value of 1. All treatment groups were plotted as changes of fluorescent band intensity of target antibody to β-actin relative to basal. All band intensity quantifications were performed using ImageJ software (National Institutes of Health, Bethesda, MD). Data for all experiments are expressed as mean relative protein ± SEM (n=4).

Genotyping

DNA was isolated from brain tissue from CCL3 knockout and wild-type mice using a Qiagen DNeasy Blood & Tissue Kit. DNA was quantified in the samples using a Thermo Scientific Nanodrop 2000. Standard PCR was performed using the protocol supplied from The Jackson Laboratory using 250 ng of DNA per sample and the reaction was run in a Bio-Rad MyCycler™ thermal cycler. Wild-type primers used 5' → 3' were ATG AAG GTC TCC ACC ACT GC and AGT CAA CGA TGA ATT GGC G. CCL3 knockout primers used

5’ → 3’ were CTT CGG TGG AGA GGC TAT TC and AGG TGA GAT GAC AGG AGA TC. Amplified DNA was loaded into a 2% agarose gel and electrophoresis was performed. Gels were stained for 10 minutes with ethidium bromide (Amresco, Solon, OH) and imaged in a FischerBiotech™ ultraviolet transilluminator (Fisher Scientific, Pittsburg, PA).

Statistical analysis

All statistical analyses were performed using Graphpad Prism software (Graphpad Software, La Jolla, CA). Results were expressed as mean ± SEM. For data that passed normality tests, significance was established using the Student t test when differences between two groups were analyzed, and analysis of variance when differences between three or more groups were compared followed by the appropriate post hoc test. If tests for normality failed, two groups were compared with a Mann-Whitney U test or a Kruskal-Wallis ranked analysis when more than two groups were analyzed. Differences were considered significant when the p value was less than 0.05.

4.4. Results

Microglia activation during HE contributed to pathology

Microglia, as imaged with IBA1 immunostaining, demonstrated a shift from a quiescent ramified morphology to a more amoeboid phenotype in the cortex of AOM mice (figure 20A). Representations of field IBA1 staining in the cortex of vehicle and AOM-treated mice demonstrated increased staining in AOM cortex compared to vehicle, which was indicative of microgliosis being present following the development of HE (figure 20B). Quantification of this staining demonstrated that there was a significant increase in IBA1 staining in the cortex and cerebellum of AOM mice, demonstrating that microgliosis was present in the brain following development of HE (figure 20C). In order to see if this microglia activation was driving the pathogenesis of HE, clodronate liposomes were injected ICV into the lateral ventricle. This depletion of microglia was found to be protective as animals injected with clodronate liposomes took significantly longer to reach coma than mice injected with PBS liposomes (figure 20D).

CCL3 was upregulated in cortical neurons following development of HE

The cortex of AOM mice displayed a significant elevation of CCL3 mRNA compared to vehicle-treated mice (figure 21A). Investigation into whether this change in gene expression translated to a subsequent increase of CCL3 protein

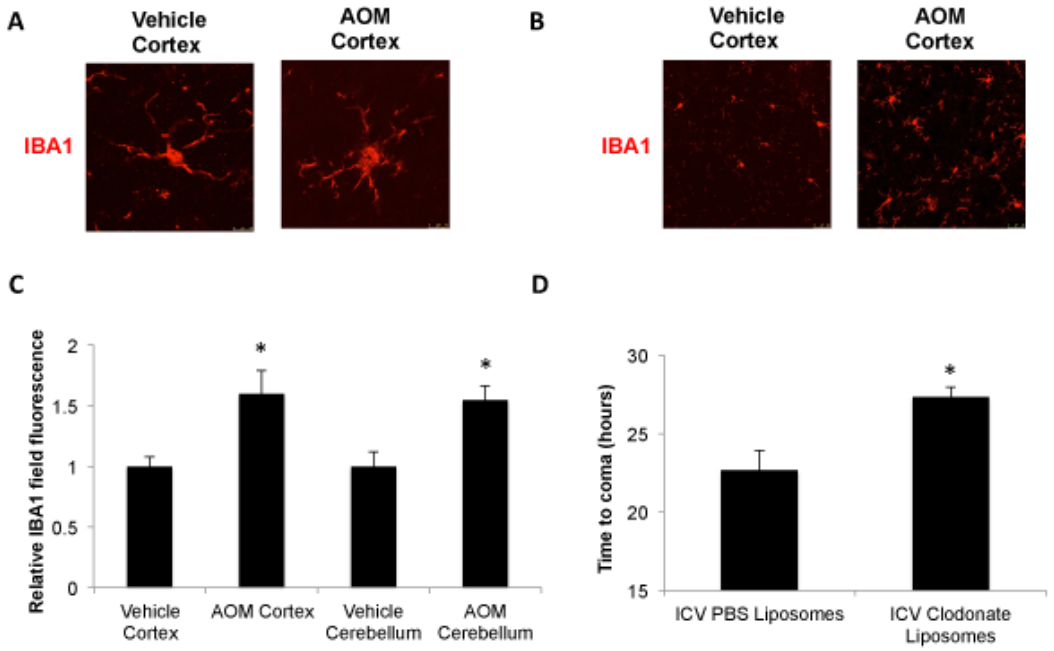

Fig. 20. Microglia activation during HE exacerbated pathology. (A) Immunofluorescence for IBA1 in the cortex of mice treated with AOM or vehicle. (B) Representative field views of IBA1 immunofluorescence in AOM or vehicle-injected cortices. (C) Quantifications of IBA1 field fluorescence in both the cortex and cerebellum of vehicle and AOM mice. (D) Time to coma in hours for AOM mice following ICV injection of PBS or clodronate liposomes. The data from immunofluorescence quantification and time to coma analyses are reported as mean ± SEM. *=$p<0.05$ compared to vehicle or PBS liposomes.

found that AOM mice demonstrated a significant increase of cortical CCL3 protein compared to vehicle-treated mice (figure 21B). Cortical neurons were found to predominantly express CCL3 protein due to the co-localization of CCL3 with the neuronal marker NeuN (figure 21C). In order to ascertain whether these observations that were present in AOM mice are also found in cases of clinical HE, immunohistochemistry was performed against CCL3 in cortical tissue from

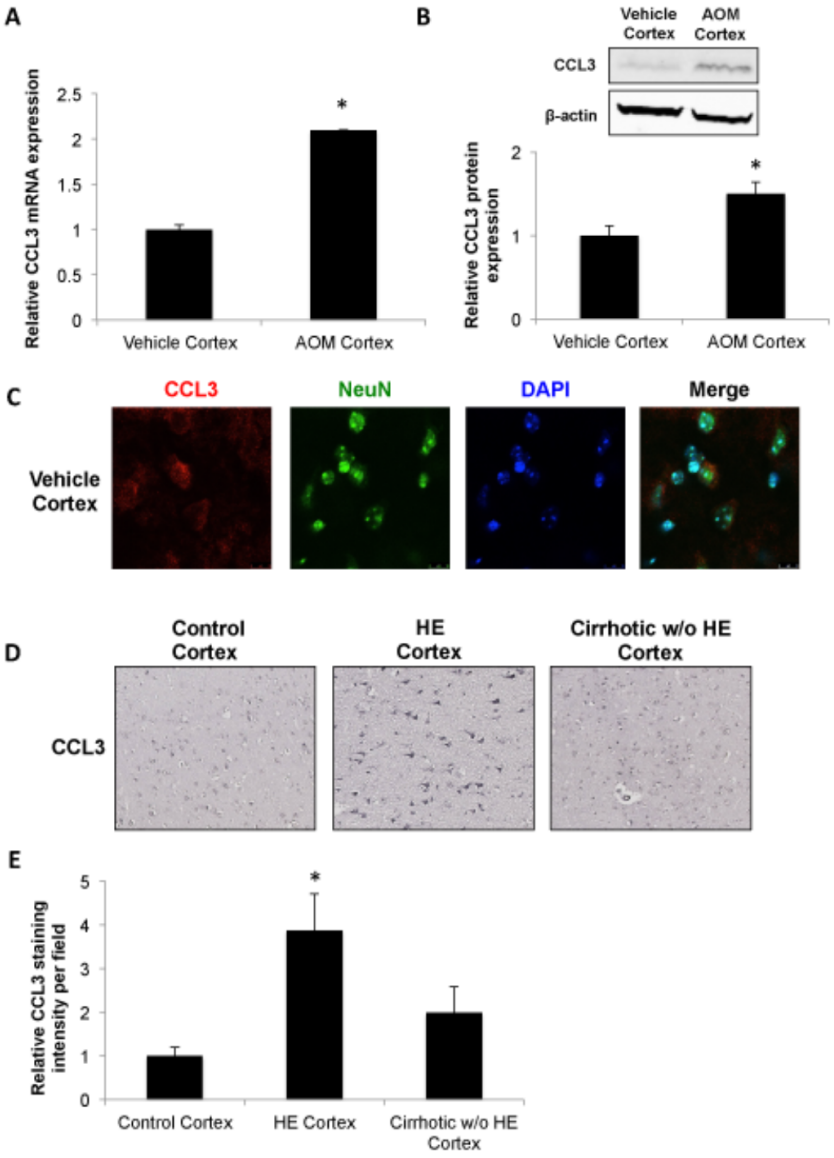

Fig. 21. CCL3 was upregulated during HE in both mice and patients. (A) Cortical CCL3 mRNA was assessed in vehicle and AOM-treated mice via RTPCR. (B) Immunoblots against CCL3 in the cortex of vehicle and AOM mice. (C) Immunofluorescence for CCL3 (red) and NeuN (green) in the cortex of vehicle mice. (D) Representative CCL3 immunohistochemistry in the cortex of patients with HE, cirrhotics w/o HE, or age-matched controls. (E) Quantification of CCL3 immunohistochemical staining in the cortex of patients with HE, cirrhotics w/o HE, or age-matched controls. The data from RTPCR, immunoblot, and immunostaining quantification analyses are reported as mean ± SEM. *=$p<0.05$ compared to vehicle or control patient cortex.

HE patients, cirrhotic patients without HE, and appropriate controls (figure 21D). Quantifications of these stains demonstrated that HE patients had significantly increased CCL3 protein compared to control patients or to cirrhotic patients without HE (figure 21E).

CCR1 activity, but not expression, was elevated during HE

Both vehicle and AOM mice had no significant differences in protein expression of CCR1 (figure 22A). However, there was evidence of increased CCR1 activity by measuring downstream signaling. Measurements of phosphorylated ERK1/2 in the cortex at various stages of neurological decline after AOM injection demonstrated increased phosphorylation with the greatest increase being early in disease progression (figure 22B). In addition to this, fractionated cortex homogenates demonstrated increased NF-κB in the nuclear fraction of AOM mice compared to vehicle-treated mice (figure 22C). Due to previous publications finding CCR1 expression in microglia(166-168), we wanted to validate that CCR1 was not present in cortical neurons or astrocytes. Immunofluorescence was performed and we found no colocalization of CCR1 expression with the neuronal marker NeuN or the astrocyte marker GFAP (figure 22D). To ensure that patients with HE had no significant changes in CCR1 expression, immunohistochemistry was performed in HE patients, cirrhotic patients without HE, and appropriate age-matched controls (figure 22E). Quantification of this data determined that there were no significant

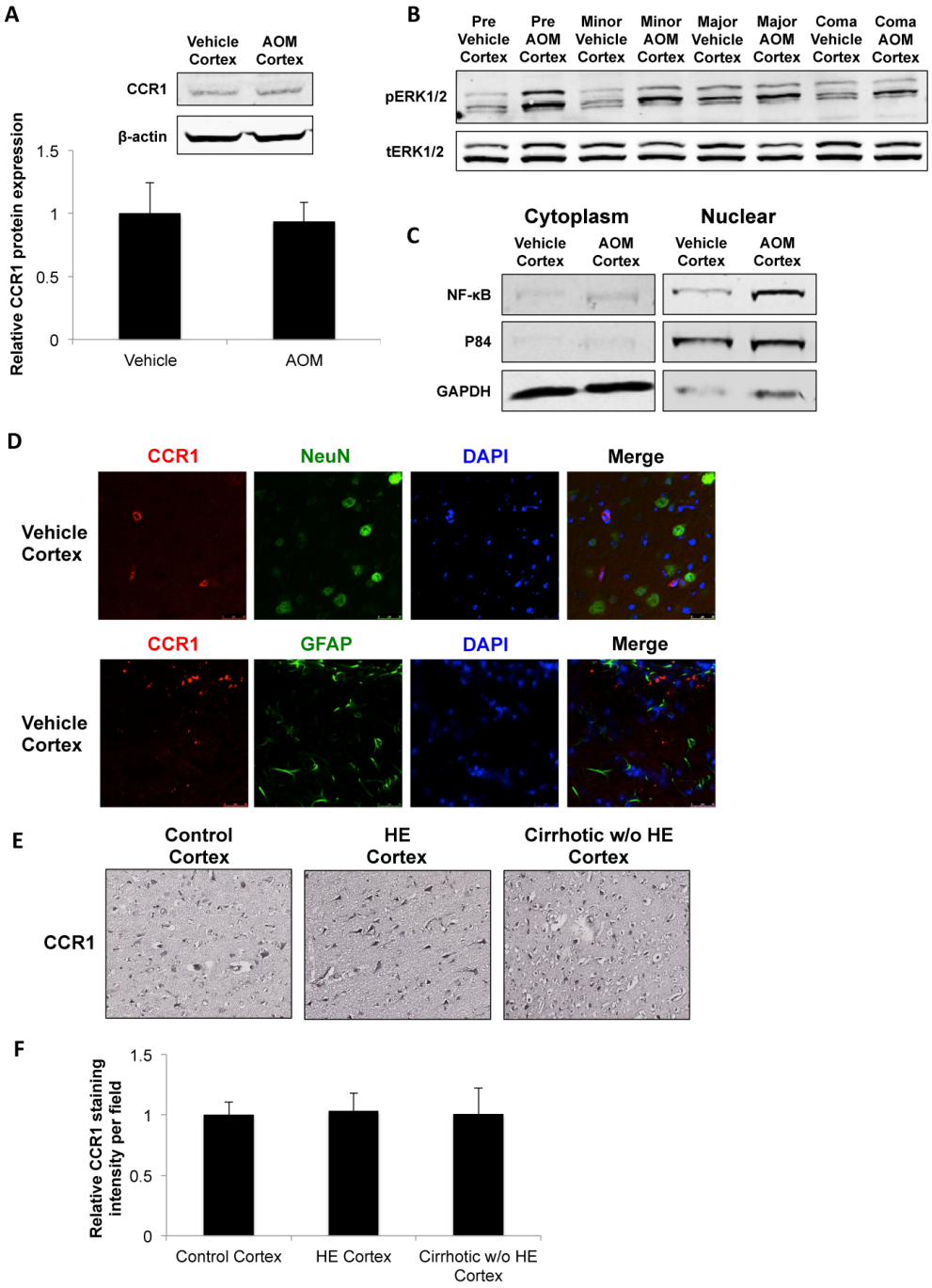

Fig. 22. CCR1 downstream activity was elevated during HE. (A) CCR1 protein expression in vehicle and AOM cortex. (B) Phosphorylation of ERK1/2 was assessed in vehicle and AOM cortex across all stages of neurological decline. (C) NF-κB immunoblots in cytoplasmic and nuclear fractions from vehicle and AOM cortex. (D) CCR1 (red), NeuN (green), or GFAP (green) immunofluorescence in the cortex of vehicle mice with DAPI (blue) used as a nuclear stain. (E) CCR1 immunohistochemistry in HE patients, cirrhotic patients w/o HE, or age-matched controls. (F) Relative CCR1 staining intensity of the three clinical groups. The data from immunostaining quantification analyses are reported as mean ± SEM.

differences in CCR1 protein in the cortex of these three clinical populations (figure 22F).

TGFβ1 drives CCL3 upregulation and CCR1 receptor activity

As we have previously demonstrated that TGFβ1 is upregulated following AOM administration both systemically and centrally, we wanted to see if this protein was driving some of the effects that we were observing with chemokines. The upregulation of CCL3 protein observed following AOM administration in the cortex was significantly reduced following treatment with neutralizing antibodies against TGFβ (figure 23A). Furthermore, the nuclear translocation of NF-κB that was present in the cortex of AOM mice was significantly reduced as well (figure 23B). To see if these signaling events had any effects on microglia activation and microgliosis, IBA1 staining was performed in the cortex and cerebellum. In the cortex of AOM mice, microglia adopted a more amoeboid shape, which was not observed as readily in mice treated with neutralizing antibodies against TGFβ (figure 23C). Quantification of IBA1 staining in the cortex of mice treated with AOM and/or neutralizing antibodies against TGFβ demonstrated that AOM mice had a significant increase of microgliosis and this effect was not found in mice co-treated with AOM and neutralizing antibodies against TGFβ (figure 23D). These same observations also held true in the cerebellum (figure 23E). Thus, there is evidence that TGFβ1 may be driving microglia activation through CCL3/CCR1 signaling.

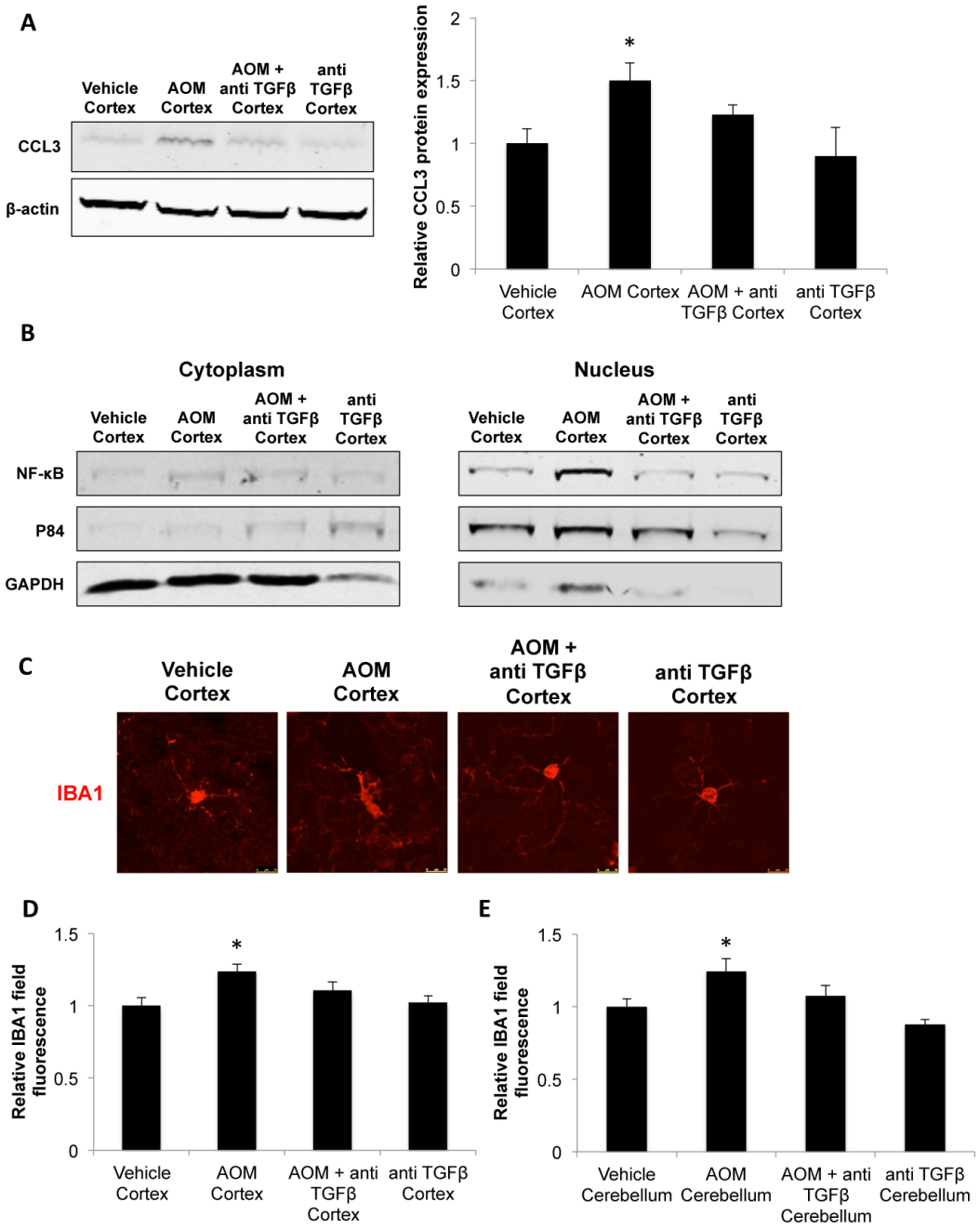

Fig. 23. Treatment with neutralizing antibodies against TGFβ reduced CCL3/CCR1 activity and microglia activity. (A) Western blots for CCL3 in vehicle, AOM, AOM + anti TGFβ, and anti TGFβ cortex. (B) NF-κB protein in fractionated cortex of vehicle, AOM, AOM + anti TGFβ, and anti TGFβ mice. (C) IBA1 immunofluorescence in vehicle, AOM, AOM + anti TGFβ, and anti TGFβ cortex. (D) Quantification of IBA1 immunofluorescence in vehicle, AOM, AOM + anti TGFβ, and anti TGFβ cortex. (E) Quantification of IBA1 immunofluorescence of vehicle, AOM, AOM + anti TGFβ, and anti TGFβ cerebellum. The data from immunoblot and immunofluorescence quantification analyses are reported as mean ± SEM. *=$p<0.05$ compared to vehicle cortex or cerebellum.

CCL3 knockout does not protect from neurological decline

The use of a commercially available knockout mouse for CCL3 was employed to investigate the contribution of this chemokine to the pathogenesis of HE. CCL3 knockout and wild-type mice were injected with AOM and there were no significant differences in time to coma between these two groups (figure 24A). As this effect was surprising, we validated that these mice did have a genetic manipulation that led to the functional suppression of CCL3 protein. CCL3 PCR was performed and demonstrated that the CCL3 knockout mice did in fact have a genetic manipulation as described by the manufacturer (figure 24B). We performed CCL3 immunofluorescence in the brain to validate that CCL3 protein expression was reduced in the knockouts. Vehicle and AOM-treated wild-type mice displayed CCL3 protein expression, but there was no expression in the CCL3 knockout mice (figure 24C).

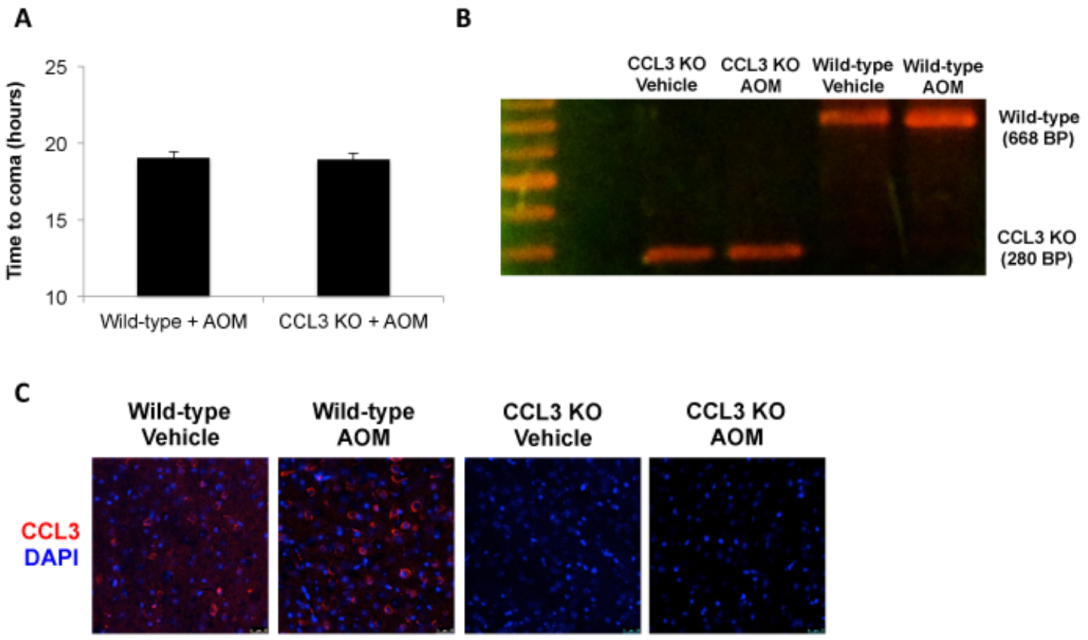

Fig. 24. Knockout of CCL3 did not reduce HE pathogenesis. (A) Time to coma in wild-type and CCL3 knock out (KO) mice. (B) Representative PCR gel for the CCL3 gene (668 base pairs for the normal gene compared to 280 base pairs in the mutant gene) in the knockout animals compared to wild-type. (C) Immunofluorescence for CCL3 (red) in the wild-type and knockouts of both vehicle and AOM mice with DAPI (blue) used as a nuclear stain. The data from the time to coma analysis is reported as mean ± SEM.

4.5. Discussion

The following study identified that microglia become activated, undergo microgliosis, and generate pathology in AOM-treated mice. Associated with this was an increase of CCL3 expression and CCR1 activity in the cortex of both AOM mice and patients who had HE. Therapeutic strategies to reduce circulating levels of TGFβ1 were demonstrated to reduce CCL3 expression and CCR1 activity in AOM mice. However, CCL3 knockout did not generate a significant change in pathology demonstrating that targeting of total CCL3 signaling may not be the appropriate therapeutic target for management of HE. A working model of our findings is displayed below (figure 25).

Our initial finding was that microglia were activated and microgliosis was occurring during AOM-induced HE. Inhibition of microglia activation using minocycline in rats whom had undergone hepatic devascularization to cause ALF was found to have reduced oxidative stress and a reduction in inflammatory cytokine expression(54, 58). Also, knockouts of the receptors for IL-1 or TNF were found to reduce the onset of encephalopathy and reduce brain edema in AOM-treated mice(55). The use of hypothermia, which reduces inflammation and oxidative stress, has been shown to be protective during HE in rats with ALF(169) and can be used to improve clinical patient outcomes until transplantation is available(20, 38). Due to the fact that others have identified microgliosis and microglia activation during HE and that

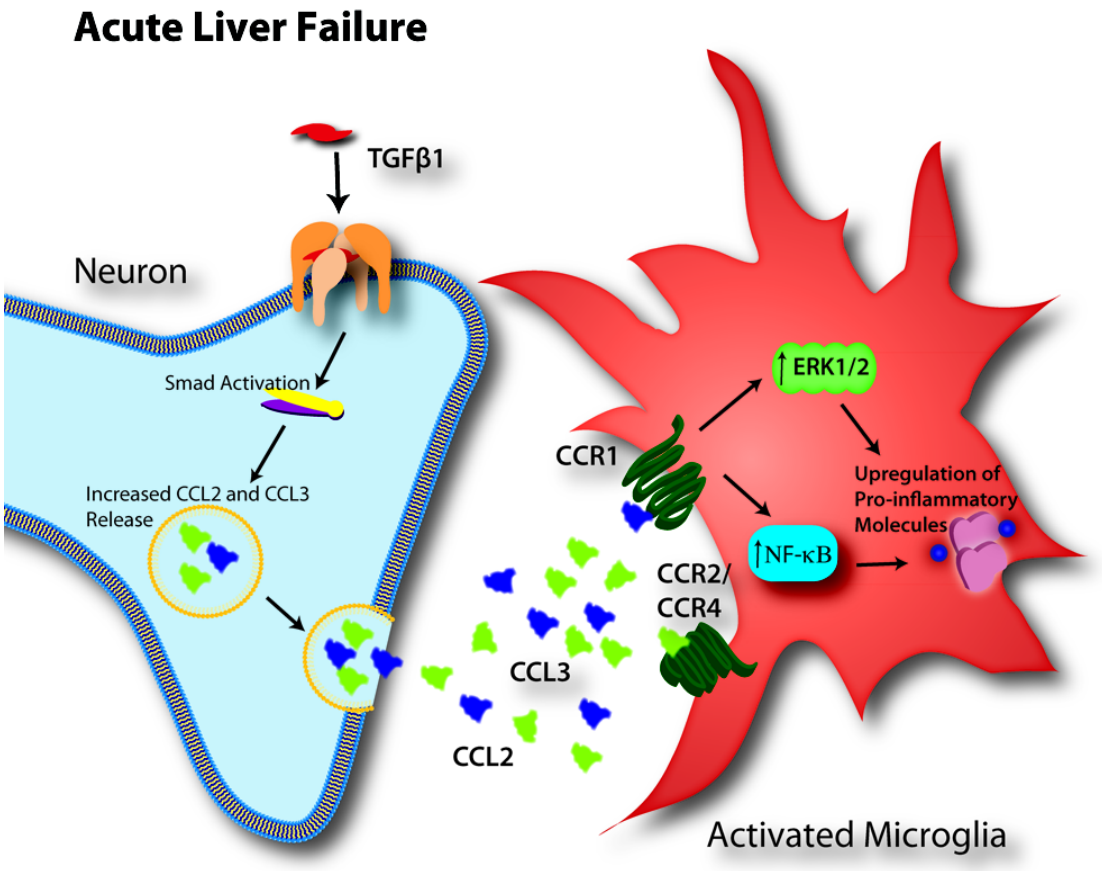

Fig. 25. Working model of TGFβ induced CCL3/CCR1 signaling following ALF. TGFβ1 is elevated in the brain following ALF with subsequent HE development. TGFβ1 binds its receptor on neurons leading to subsequent SMAD activation. This results in increased CCL3 protein expression and release, which binds CCR1 on microglia. Increased CCR1 activity was found to increase ERK1/2 and NF-κB activity. Both of these pathways have been shown to increase proinflammatory cytokine expression and release in microglia.

inflammation is highly correlated with HE pathogenesis, there is support that microglia were playing a prominent role in driving the pathology present during HE.

There have been a number of studies assessing the role of CCL3 in liver damage and fibrosis following injury. The use of a concanavalin A-induced hepatitis model of liver damage in mice demonstrates that CCL3 promotes

inflammation by recruitment of $CD4^+$ T cells to the liver, which was found to promote liver failure(170). This shift in immune cell populations in the liver following damage has also been observed in patients with liver failure who have suppressed circulating $CD3^+$ and $CD8^+$ T cells and increased monocyte populations(171). Also, CCL3 upregulation was found to occur in the liver following methionine and choline deficient diets, which has been demonstrated to promote liver damage with subsequent fibrosis(172). Interestingly, low concentrations of ammonia, similar to what would be found in the circulation during HE, are able to impair neutrophil chemotaxis, phagocytosis, and causes them to generate reactive oxygen species(173, 174). Also, CCL3 has been shown to promote the chemotaxis of monocytes and neutrophils(175). These findings, combined with BBB disruption during HE, give support that systemic inflammatory cells, such as neutrophils, could be recruited to the brain via CCL3 and this could worsen HE pathology.

Chemokine receptors are seven-transmembrane G-protein coupled receptors (GPCRs) that can transduce their signals through multiple ligands(176). CCR1-mediated signaling is transduced downstream via Gi/Go GPCR signal transduction leading to increased activity of NF-κB, ERK1/2, and other signaling proteins(177, 178). Microglial activation of the proinflammatory cytokine IL-6 has been demonstrated to be dependent upon ERK1/2 and NF-κB signaling(179). Our study found that CCR1 protein expression was not changed during HE, but that downstream CCR1 signaling mediators were activated.

These findings were not surprising as increased CCL3 ligand activity can promote increased receptor activity without an increase in the expression of the receptor itself. These findings do not rule out the role of other GPCR-mediated signaling pathways in generating HE pathology and is an area that warrants further investigation.

Previous studies in our laboratory have found that inhibition of circulating TGFβ1 is protective. The current study added one potential mechanism that allows TGFβ1 to drive HE pathology, which was the upregulation of CCL3 expression and increased CCR1 signaling activity. Interestingly, TGFβ1 is generally thought to be anti-inflammatory and has been shown to induce neuroprotective factors in the brain like BDNF(180). Also, knockout of TGFβ1 was found to increase neuronal cell death and increased microgliosis following excitotoxic injury(181). This anti-inflammatory effect of TGFβ1 has been observed in our lab when primary neurons, astrocytes, and microglia were treated with rTGFβ1 and we observed decreased cytokine/chemokine expression (unpublished observations). Thus, the effect of TGFβ1 observed in the AOM model may be reliant on effects on the liver-brain-inflammation signaling axes to generate its deleterious effects, which cannot be observed *in vitro*.

Systemic knockout of CCL3 gene expression demonstrated no significant change in HE pathology. This finding could be caused by multiple factors. Firstly, these mice have had CCL3 activity knocked out systemically from

conception, and as such it is conceivable that they have a compensatory upregulation in a number of other chemokines. In support of this, we have preliminary data to suggest that the CCL3 knockout mice have elevated expression of CCL2, a chemokine we have shown to be involved in the pathogenesis of HE (McMillin and DeMorrow, unpublished observation). Secondly, CCL3 is not the only chemokine that binds CCR1 as CCL5, CCL6, CCL9, CCL15, and CCL23 have also been shown to have affinity for CCR1 and could potentially be upregulated to rescue the effects of CCL3 knockout(182). Also, it is possible that the inflammatory processes that occur in the liver and in the brain during ALF are dependent upon divergent chemokine signaling and thus systemic knockout could be protective for one organ while being deleterious for the other. The final possibility is that a completely separate signal is leading to the activation and microgliosis that was observed following development of HE. Thus, there are multiple possibilities as to why systemic knockout of CCL3 did not generate effects in this model and continued studies in this area will be needed to fully identify the specific role of this chemokine during HE.

In conclusion, the following study found that CCL3/CCR1 signaling is activated during HE and that inhibition of TGFβ1 reduces activity of this signaling pathway, microglia activation, and microgliosis. Together, this identifies that TGFβ1 could be exerting its deleterious effect during HE through increasing CCL3/CCR1 signaling though more research in this area is needed to conclusively identify the role of CCL3 in HE.

5. CONCLUSIONS

Liver failure from both acute and chronic hepatic insults can lead to significant disruptions in metabolic homeostasis and subsequent pathology outside of the liver. One of the most difficult complications to address clinically is the development of HE. Multiple pathological mechanisms can lead to the initiation of HE to include increases in circulating ammonia and exacerbated systemic and central inflammation. One clinical challenge in this disease is that few treatment options are efficacious for patients who progress to grade 3 or grade 4 HE with liver transplantation being the only effective option available(183). However, liver transplantation comes with its own risks, as most clinical measures of neurological and hepatic function do not correlate well with patient outcomes(184). In addition liver transplantation costs are high with limited supplies, which causes many patients to succumb to the disease prior to transplantation. Thus, there is a great need to develop new therapeutics to subvert transplantation or slow disease progression so patients can remain eligible for transplantation for longer periods of time.

In order to identify novel therapeutic targets for the management of HE, studies are needed to investigate outside of the current treatment paradigms as this has led to few recent advances in therapeutic development. In fact, therapies aimed to reduce ammonia are still relatively unproven with some studies showing no benefit on HE(185). Studies into inflammation have been

slightly more fruitful with research into *N*-acetylcysteine being shown to improve survival of patients with HE grade 3-4(186). Also, hepatectomy with portacaval shunting has been used in specialized centers when patients will succumb to HE prior to transplantation with one study demonstrating that this allowed for 19 out of 32 patients to be successfully transplanted(187). This strategy has been found to reduce intracranial pressure and liver-derived proinflammatory cytokines giving support that liver-derived immune signaling plays a role in increasing brain pathology(188). However, inflammation is associated with many stimuli and cell signaling mediators, so the purpose of the current dissertation was to delineate the role of two signaling proteins released from the liver following damage, Shh and TGFβ1, and their effects on HE pathogenesis.

Initially, investigations into downstream hedgehog signaling began with experiments aimed to assess and manipulate the transcription factor Gli1. Gli1 was found to be upregulated in the cortex of AOM-treated mice, 4-week BDL rats, and cirrhotic patients with HE. Also, the use of Vivo-morpholinos against Gli1 was found to exacerbate pathology. This finding supports what has been previously demonstrated in other neuropathies with Gli1 being shown to be protective in Parkinson's disease and stroke(93, 94). One area that we did not pursue in these studies was the signaling pathway that contributed to the upregulation of Gli1. Due to the fact that hedgehog suppression only mildly reduced Gli1 activation and TGFβ1 was found to suppress Gli1, we did not identify other factors in these studies that contributed to Gli1 activation. Other

researchers have identified that Gli1 has the ability to be activated by PI3K/Akt signaling and can be downregulated by protein kinase A and Notch/HES/HEY signaling(97). This opens the possibility that upregulation and downregulation of these signaling pathways may be potential mechanisms driving the effects that we observed. Identifying the source of Gli1 upregulation is an area that needs to be further investigated during HE, as this could be a primary pathway that is leading to neuroprotection during this disease.

Interestingly, the rationale for pursuing this research on liver-brain axis signaling during HE was built upon multiple studies on hedgehog signaling, yet methods that we employed to suppress circulating and central Shh/smoothened axis signaling were found to have no effect during HE. These findings are very surprising, especially since Gli1 was determined to be neuroprotective. That being said, there are studies that have shown that there is increased regulation of Shh/smoothened outside of the traditional signaling pathway. Smoothened is currently thought to act in a similar manner to a G-protein coupled receptor and has the ability to activate G_{α} signaling(189). Also, smoothened activity may be repressed by increases in GTPase activity, which has been demonstrated to be caused by increased activity of regulator of G-protein signaling 5(190). Due to the fact that G-protein coupled receptor signaling pathways are modulated by a multitude of ligands and other factors, there is support that independent modulation of smoothened is not an effective approach to attempt to alleviate HE pathology. It is conceivable that G-protein coupled receptor-mediated

signaling plays a significant role during HE, but to identify the specific factors stimulating these signaling events *in vivo* is quite difficult. For this reason, we can state that Shh/smoothened axis signaling seems to play a minimal role in HE pathology when investigated as a stand-alone signaling pathway. Future studies will need to be performed to better understand this signaling axis and the factors that regulate this signaling pathway.

Due to the fact that Shh/smoothened signaling had essentially no effect on HE pathology, our focus shifted towards TGFβ1 as it has been demonstrated to activate Gli1 signaling(98). In addition to this, TGFβ1 is found to be have increased expression in the liver and is increased in the circulation following liver damage(82, 87). Our idea was that elevation of TGFβ1 was leading to increased paracrine signaling outside the liver and strategies to reduce circulating levels of TGFβ1 would help restore homeostasis and reduce HE pathology. There is some evidence that reducing TGFβ1 is protective in the liver, as systemic delivery of TGFβ siRNA has been found to reduce liver cirrhosis pathology(191). Initial assessments identified that TGFβ1 expression was increased in the liver, circulation, and brain following AOM injection. The use of neutralizing antibodies did not generate any significant effects on liver damage as measured by H&E stains or liver biochemistry, which was surprising and demonstrated that the protective effects of TGFβ1 suppression in the liver may not be observed in severe acute hepatotoxin models. That being said, neutralizing TGFβ actually led to increased Gli1 mRNA expression and nuclear

translocation, which correlated to reduced neurological decline. Thus, our findings indicated that TGFβ1 was neuroprotective as it reduced neurological decline with no apparent effects on liver damage or function.

In order to investigate how TGFβ1 could be directly influencing neuropathological processes during HE, it would first need to pass through the BBB in order to generate any effect. Research into BBB function following HE development has demonstrated that vasogenic brain edema is observed and has also been shown to be present in the AOM model(132). While there are some investigations into mechanisms that promote vasogenic edema in the brain during HE, none have investigated TGFβ1. Outside of the brain, TGFβ1 signaling has been shown to promote vascular permeability, so it is entirely feasible that increased BBB permeability during HE could be caused by this protein(192). Our findings identified that BBB is disrupted *in vivo* following 18 hours of AOM treatment and that inhibition of TGFβ1 via neutralizing antibodies was protective *in vivo* by reducing Evan's blue dye presence in the brain. In order to better identify the specific effects of TGFβ1 on BBB permeability we employed bEnd.3 cells to investigate monolayer permeability and cell signaling events that occur following treatment with recombinant protein. TGFβ1 was found to increase monolayer permeability, downregulate Claudin-5 expression and upregulate MMP9 and that these effects could be reversed via inhibition of SMAD3. These effects generated by TGFβ1 support that this protein has the ability to open pores in the BBB and could explain the *in vivo* effects of our AOM

model. Due to the fact that the treatment of AOM mice with neutralizing antibodies against TGFβ did not fully recover BBB permeability, there is evidence for TGFβ1 acting in synergism with other factors to exacerbate permeability of the BBB. There is extensive evidence that ammonia alters passage of amino acids and other proteins across the BBB but does not induce the formation of large pores(193). However, exacerbated inflammatory mediators such as TNFα have been demonstrated to open pores and potentiate BBB permeability during HE(194). Thus, it is entirely possible that interactions between TGFβ1 and other inflammatory mediators are the primary factors affecting BBB permeability during HE, but more studies in this area are still warranted.

Chemokines have not been identified to play a prominent role in inflammation during HE but have been demonstrated to be involved in liver injury. CCL2 has been demonstrated to recruit macrophages to the liver during CCl_4-induced chronic liver injury and following methionine-choline-deficient diet-induced liver injury(195). Also, hepatic CCL2 expression and plasma circulating levels are increased during alcoholic liver disease and this correlates with neutrophil infiltration(196). In regards to ALF, patients with liver failure have increased levels of multiple chemokines to include CCL2, CCL3, CCL4, and CCL5 in both the liver and serum(197). Initially, we began our studies investigating CCL3/CCR1 signaling in the brain as there are currently no manuscripts that have specifically investigated this signaling pathway following

HE development. The subsequent experiments identified that the chemokine CCL3 was upregulated during HE and that its receptor, CCR1, had increased activity. In addition to this it was determined that inhibition of TGFβ1 was able to inhibit the upregulation of CCL3 protein in the brain and reduce microglia activation. Interestingly, the genetic knockout of CCL3 was found to have no effect on HE pathology. While puzzling, a recent report found that both CCL2 and CCL3 are increased in the liver following acetaminophen-induced liver failure and help recruit monocytes to the liver(198). Also, CCL2 expression has been demonstrated to be increased in the brains of mice following peripheral organ inflammation caused by BDL-induced liver injury(199). These studies gave us the idea that systemic knockout of CCL3 may lead to compensatory recovery of function via upregulation of CCL2. We have generated preliminary data that demonstrates that following CCL3 knockout, cortical CCL2 mRNA expression is upregulated. Furthermore, mice that had systemic injections of antagonists against CCR2 of CCR4, the receptors for CCL2, prior to AOM injection had significantly improved neurological outcomes. The current effects of TGFβ1 and its interaction with CCL2, as well as how CCL2/CCL3 independently affect pathology during HE, are still being investigated and are an area of future studies in the lab.

In summary this body of work described novel findings in regards to cell signaling and HE pathology. First of all, it was found that circulating TGFβ1 suppressed the neuroprotective transcription factor Gli1 in the brain and

exacerbated HE. Secondly, TGFβ1 was able to permeabilize the BBB via upregulation of MMP9 and downregulation of Claudin-5 in brain endothelial cells. Finally, it was determined that TGFβ1 was able to activate microglia, generated microgliosis, and upregulated CCL3/CCR1 signaling following development of HE. Thus, these findings demonstrate that TGFβ1 is a pathological signaling protein with direct involvement in HE pathogenesis via downregulation of neuroprotective Gli1, exacerbating BBB permeability, and promoting microglial activation and microgliosis (a working model of these findings is presented below in figure 26). More importantly, however, is that this identifies that signaling proteins that are upregulated following liver damage have the potential to generate distant paracrine signaling that can contribute to HE pathology. This allows for a change in perspective in regards to research into HE, as previous studies have focused on toxic metabolites and inflammation without direct investigations into cell signaling pathways.

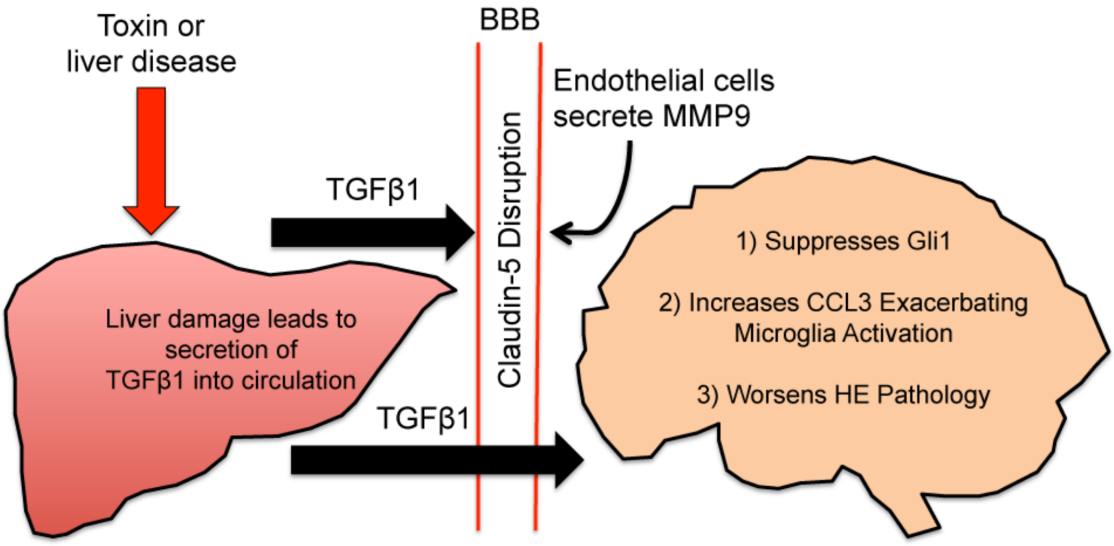

Fig. 26. Overall working model of TGFβ1 signaling. Toxin insult or liver disease leads to an upregulation of TGFβ1 in the liver and circulation. This leads to Claudin-5 disruption at the BBB and causes endothelial cells to secrete MMP9 exacerbating BBB permeability. This allows the entry of TGFβ1 into the brain where it suppresses the neuroprotective transcription factor Gli1, increases CCL3 expression, and activates microglia. Together, these processes lead to a significant increase of HE pathology.

REFERENCES

1. Abdel-Misih SR, Bloomston M. Liver anatomy. Surg Clin North Am 2010;90:643-653.

2. Protzer U, Maini MK, Knolle PA. Living in the liver: hepatic infections. Nat Rev Immunol 2012;12:201-213.

3. Pineiro-Carrero VM, Pineiro EO. Liver. Pediatrics 2004;113:1097-1106.

4. Jiang D. Care of chronic liver disease. Prim Care 2011;38:483-498; viii-ix.

5. Bernal W, Auzinger G, Dhawan A, Wendon J. Acute liver failure. Lancet 2010;376:190-201.

6. Acharya SK, Batra Y, Hazari S, Choudhury V, Panda SK, Dattagupta S. Etiopathogenesis of acute hepatic failure: Eastern versus Western countries. J Gastroenterol Hepatol 2002;17 Suppl 3:S268-273.

7. Nourjah P, Ahmad SR, Karwoski C, Willy M. Estimates of acetaminophen (Paracetomal)-associated overdoses in the United States. Pharmacoepidemiol Drug Saf 2006;15:398-405.

8. Larson AM, Polson J, Fontana RJ, Davern TJ, Lalani E, Hynan LS, Reisch JS, et al. Acetaminophen-induced acute liver failure: results of a United States multicenter, prospective study. Hepatology 2005;42:1364-1372.

9. Mindikoglu AL, Magder LS, Regev A. Outcome of liver transplantation for drug-induced acute liver failure in the United States: analysis of the United Network for Organ Sharing database. Liver Transpl 2009;15:719-729.

10. Ichai P, Samuel D. Etiology and prognosis of fulminant hepatitis in adults. Liver Transpl 2008;14 Suppl 2:S67-79.

11. Zischka H, Lichtmannegger J, Schmitt S, Jagemann N, Schulz S, Wartini D, Jennen L, et al. Liver mitochondrial membrane crosslinking and destruction in a rat model of Wilson disease. J Clin Invest 2011;121:1508-1518.

12. Zhang W, Kudo H, Kawai K, Fujisaka S, Usui I, Sugiyama T, Tsukada K, et al. Tumor necrosis factor-alpha accelerates apoptosis of steatotic hepatocytes from a murine model of non-alcoholic fatty liver disease. Biochem Biophys Res Commun 2010;391:1731-1736.

13. McGill MR, Sharpe MR, Williams CD, Taha M, Curry SC, Jaeschke H. The mechanism underlying acetaminophen-induced hepatotoxicity in humans and mice involves mitochondrial damage and nuclear DNA fragmentation. J Clin Invest 2012;122:1574-1583.

14. Rolando N, Wade J, Davalos M, Wendon J, Philpott-Howard J, Williams R. The systemic inflammatory response syndrome in acute liver failure. Hepatology 2000;32:734-739.

15. Walsh TS, Wigmore SJ, Hopton P, Richardson R, Lee A. Energy expenditure in acetaminophen-induced fulminant hepatic failure. Crit Care Med 2000;28:649-654.

16. Harry R, Auzinger G, Wendon J. The clinical importance of adrenal insufficiency in acute hepatic dysfunction. Hepatology 2002;36:395-402.

17. Parekh NK, Hynan LS, De Lemos J, Lee WM. Elevated troponin I levels in acute liver failure: is myocardial injury an integral part of acute liver failure? Hepatology 2007;45:1489-1495.

18. Cote GA, Gottstein JH, Daud A, Blei AT. The role of etiology in the hyperamylasemia of acute liver failure. Am J Gastroenterol 2009;104:592-597.

19. Antoniades CG, Berry PA, Wendon JA, Vergani D. The importance of immune dysfunction in determining outcome in acute liver failure. J Hepatol 2008;49:845-861.

20. Stravitz RT, Larsen FS. Therapeutic hypothermia for acute liver failure. Crit Care Med 2009;37:S258-264.

21. Ferenci P, Lockwood A, Mullen K, Tarter R, Weissenborn K, Blei AT. Hepatic encephalopathy--definition, nomenclature, diagnosis, and quantification: final report of the working party at the 11th World Congresses of Gastroenterology, Vienna, 1998. Hepatology 2002;35:716-721.

22. Traber P, DalCanto M, Ganger D, Blei AT. Effect of body temperature on brain edema and encephalopathy in the rat after hepatic devascularization. Gastroenterology 1989;96:885-891.

23. Potvin M, Finlayson MH, Hinchey EJ, Lough JO, Goresky CA. Cerebral abnormalities in hepatectomized rats with acute hepatic coma. Lab Invest 1984;50:560-564.

24. Chung C, Gottstein J, Blei AT. Indomethacin prevents the development of experimental ammonia-induced brain edema in rats after portacaval anastomosis. Hepatology 2001;34:249-254.

25. Dixit V, Chang TM. Brain edema and the blood brain barrier in galactosamine-induced fulminant hepatic failure rats. An animal model for evaluation of liver support systems. ASAIO Trans 1990;36:21-27.

26. Butterworth RF, Norenberg MD, Felipo V, Ferenci P, Albrecht J, Blei AT. Experimental models of hepatic encephalopathy: ISHEN guidelines. Liver Int 2009;29:783-788.

27. Matkowskyj KA, Marrero JA, Carroll RE, Danilkovich AV, Green RM, Benya RV. Azoxymethane-induced fulminant hepatic failure in C57BL/6J mice: characterization of a new animal model. Am J Physiol 1999;277:G455-462.

28. Belanger M, Cote J, Butterworth RF. Neurobiological characterization of an azoxymethane mouse model of acute liver failure. Neurochem Int 2006;48:434-440.

29. Butterworth RF, Girard G, Giguere JF. Regional differences in the capacity for ammonia removal by brain following portocaval anastomosis. J Neurochem 1988;51:486-490.

30. Rodrigo R, Jover R, Candela A, Compan A, Saez-Valero J, Erceg S, Felipo V. Bile duct ligation plus hyperammonemia in rats reproduces the alterations in the modulation of soluble guanylate cyclase by nitric oxide in brain of cirrhotic patients. Neuroscience 2005;130:435-443.

31. Chan CY, Huang SW, Wang TF, Lu RH, Lee FY, Chang FY, Chu CJ, et al. Lack of detrimental effects of nitric oxide inhibition in bile duct-ligated rats with hepatic encephalopathy. Eur J Clin Invest 2004;34:122-128.

32. Shawcross DL, Wright G, Olde Damink SW, Jalan R. Role of ammonia and inflammation in minimal hepatic encephalopathy. Metab Brain Dis 2007;22:125-138.

33. Prasad S, Dhiman RK, Duseja A, Chawla YK, Sharma A, Agarwal R. Lactulose improves cognitive functions and health-related quality of life in patients with cirrhosis who have minimal hepatic encephalopathy. Hepatology 2007;45:549-559.

34. Flamm SL. Rifaximin treatment for reduction of risk of overt hepatic encephalopathy recurrence. Therap Adv Gastroenterol 2011;4:199-206.

35. Jalan R, Olde Damink SW, Deutz NE, Hayes PC, Lee A. Restoration of cerebral blood flow autoregulation and reactivity to carbon dioxide in acute liver failure by moderate hypothermia. Hepatology 2001;34:50-54.

36. Jalan R, Olde Damink SW, Deutz NE, Hayes PC, Lee A. Moderate hypothermia in patients with acute liver failure and uncontrolled intracranial hypertension. Gastroenterology 2004;127:1338-1346.

37. Canalese J, Gimson AE, Davis C, Mellon PJ, Davis M, Williams R. Controlled trial of dexamethasone and mannitol for the cerebral oedema of fulminant hepatic failure. Gut 1982;23:625-629.

38. Jalan R, SW OD, Deutz NE, Lee A, Hayes PC. Moderate hypothermia for uncontrolled intracranial hypertension in acute liver failure. Lancet 1999;354:1164-1168.

39. Vaquero J, Belanger M, James L, Herrero R, Desjardins P, Cote J, Blei AT, et al. Mild hypothermia attenuates liver injury and improves survival in mice with acetaminophen toxicity. Gastroenterology 2007;132:372-383.

40. Lee WM, Hynan LS, Rossaro L, Fontana RJ, Stravitz RT, Larson AM, Davern TJ, 2nd, et al. Intravenous N-acetylcysteine improves transplant-free survival in early stage non-acetaminophen acute liver failure. Gastroenterology 2009;137:856-864, 864 e851.

41. Ostapowicz G, Fontana RJ, Schiodt FV, Larson A, Davern TJ, Han SH, McCashland TM, et al. Results of a prospective study of acute liver failure at 17 tertiary care centers in the United States. Ann Intern Med 2002;137:947-954.

42. Lee WM. Acute liver failure in the United States. Semin Liver Dis 2003;23:217-226.

43. Swain M, Butterworth RF, Blei AT. Ammonia and related amino acids in the pathogenesis of brain edema in acute ischemic liver failure in rats. Hepatology 1992;15:449-453.

44. Norenberg MD. Astrocyte responses to CNS injury. J Neuropathol Exp Neurol 1994;53:213-220.

45. Sanchez-Perez AM, Felipo V. Chronic exposure to ammonia alters basal and NMDA-induced phosphorylation of NMDA receptor-subunit NR1. Neuroscience 2006;140:1239-1244.

46. Basile AS. Direct and indirect enhancement of GABAergic neurotransmission by ammonia: implications for the pathogenesis of hyperammonemic syndromes. Neurochem Int 2002;41:115-122.

47. Shawcross DL, Sharifi Y, Canavan JB, Yeoman AD, Abeles RD, Taylor NJ, Auzinger G, et al. Infection and systemic inflammation, not ammonia, are associated with Grade 3/4 hepatic encephalopathy, but not mortality in cirrhosis. J Hepatol 2011;54:640-649.

48. Auron A, Brophy PD. Hyperammonemia in review: pathophysiology, diagnosis, and treatment. Pediatr Nephrol 2012;27:207-222.

49. Hung TY, Chen CC, Wang TL, Su CF, Wang RF. Transient hyperammonemia in seizures: a prospective study. Epilepsia 2011;52:2043-2049.

50. Shawcross DL, Davies NA, Williams R, Jalan R. Systemic inflammatory response exacerbates the neuropsychological effects of induced hyperammonemia in cirrhosis. J Hepatol 2004;40:247-254.

51. Bemeur C, Butterworth RF. Liver-brain proinflammatory signalling in acute liver failure: role in the pathogenesis of hepatic encephalopathy and brain edema. Metab Brain Dis 2013;28:145-150.

52. Vaquero J, Polson J, Chung C, Helenowski I, Schiodt FV, Reisch J, Lee WM, et al. Infection and the progression of hepatic encephalopathy in acute liver failure. Gastroenterology 2003;125:755-764.

53. Jiang W, Desjardins P, Butterworth RF. Direct evidence for central proinflammatory mechanisms in rats with experimental acute liver failure: protective effect of hypothermia. J Cereb Blood Flow Metab 2009;29:944-952.

54. Jiang W, Desjardins P, Butterworth RF. Cerebral inflammation contributes to encephalopathy and brain edema in acute liver failure: protective effect of minocycline. J Neurochem 2009;109:485-493.

55. Bemeur C, Qu H, Desjardins P, Butterworth RF. IL-1 or TNF receptor gene deletion delays onset of encephalopathy and attenuates brain edema in experimental acute liver failure. Neurochem Int 2010;56:213-215.

56. Butterworth RF. Hepatic encephalopathy: a central neuroinflammatory disorder? Hepatology 2011;53:1372-1376.

57. Zemtsova I, Gorg B, Keitel V, Bidmon HJ, Schror K, Haussinger D. Microglia activation in hepatic encephalopathy in rats and humans. Hepatology 2011;54:204-215.

58. Jiang W, Desjardins P, Butterworth RF. Minocycline attenuates oxidative/nitrosative stress and cerebral complications of acute liver failure in rats. Neurochem Int 2009;55:601-605.

59. Rodrigo R, Cauli O, Gomez-Pinedo U, Agusti A, Hernandez-Rabaza V, Garcia-Verdugo JM, Felipo V. Hyperammonemia induces neuroinflammation

that contributes to cognitive impairment in rats with hepatic encephalopathy. Gastroenterology 2010;139:675-684.

60. Andersson AK, Adermark L, Persson M, Westerlund A, Olsson T, Hansson E. Lactate contributes to ammonia-mediated astroglial dysfunction during hyperammonemia. Neurochem Res 2009;34:556-565.

61. Pomier-Layrargues G, Spahr L, Butterworth RF. Increased manganese concentrations in pallidum of cirrhotic patients. Lancet 1995;345:735.

62. Rose C, Butterworth RF, Zayed J, Normandin L, Todd K, Michalak A, Spahr L, et al. Manganese deposition in basal ganglia structures results from both portal-systemic shunting and liver dysfunction. Gastroenterology 1999;117:640-644.

63. Dodd CA, Filipov NM. Manganese potentiates LPS-induced heme-oxygenase 1 in microglia but not dopaminergic cells: role in controlling microglial hydrogen peroxide and inflammatory cytokine output. Neurotoxicology 2011;32:683-692.

64. Zhang P, Lokuta KM, Turner DE, Liu B. Synergistic dopaminergic neurotoxicity of manganese and lipopolysaccharide: differential involvement of microglia and astroglia. J Neurochem 2010;112:434-443.

65. Echelard Y, Epstein DJ, St-Jacques B, Shen L, Mohler J, McMahon JA, McMahon AP. Sonic hedgehog, a member of a family of putative signaling molecules, is implicated in the regulation of CNS polarity. Cell 1993;75:1417-1430.

66. Alvarez JI, Dodelet-Devillers A, Kebir H, Ifergan I, Fabre PJ, Terouz S, Sabbagh M, et al. The Hedgehog pathway promotes blood-brain barrier integrity and CNS immune quiescence. Science 2011;334:1727-1731.

67. Choi SS, Omenetti A, Syn WK, Diehl AM. The role of Hedgehog signaling in fibrogenic liver repair. Int J Biochem Cell Biol 2011;43:238-244.

68. Ingham PW, McMahon AP. Hedgehog signaling in animal development: paradigms and principles. Genes Dev 2001;15:3059-3087.

69. Taipale J, Beachy PA. The Hedgehog and Wnt signalling pathways in cancer. Nature 2001;411:349-354.

70. Goodrich LV, Scott MP. Hedgehog and patched in neural development and disease. Neuron 1998;21:1243-1257.

71. Ingham PW. Transducing Hedgehog: the story so far. EMBO J 1998;17:3505-3511.

72. Park HL, Bai C, Platt KA, Matise MP, Beeghly A, Hui CC, Nakashima M, et al. Mouse Gli1 mutants are viable but have defects in SHH signaling in combination with a Gli2 mutation. Development 2000;127:1593-1605.

73. Fleig SV, Choi SS, Yang L, Jung Y, Omenetti A, VanDongen HM, Huang J, et al. Hepatic accumulation of Hedgehog-reactive progenitors increases with severity of fatty liver damage in mice. Lab Invest 2007;87:1227-1239.

74. Jung Y, Witek RP, Syn WK, Choi SS, Omenetti A, Premont R, Guy CD, et al. Signals from dying hepatocytes trigger growth of liver progenitors. Gut 2010;59:655-665.

75. Sicklick JK, Li YX, Melhem A, Schmelzer E, Zdanowicz M, Huang J, Caballero M, et al. Hedgehog signaling maintains resident hepatic progenitors throughout life. Am J Physiol Gastrointest Liver Physiol 2006;290:G859-870.

76. Witek RP, Yang L, Liu R, Jung Y, Omenetti A, Syn WK, Choi SS, et al. Liver cell-derived microparticles activate hedgehog signaling and alter gene expression in hepatic endothelial cells. Gastroenterology 2009;136:320-330 e322.

77. Yoshimura A, Wakabayashi Y, Mori T. Cellular and molecular basis for the regulation of inflammation by TGF-beta. J Biochem 2010;147:781-792.

78. Shi Y, Massague J. Mechanisms of TGF-beta signaling from cell membrane to the nucleus. Cell 2003;113:685-700.

79. Verrecchia F, Mauviel A. Transforming growth factor-beta signaling through the Smad pathway: role in extracellular matrix gene expression and regulation. J Invest Dermatol 2002;118:211-215.

80. Massague J, Wotton D. Transcriptional control by the TGF-beta/Smad signaling system. EMBO J 2000;19:1745-1754.

81. Kurisaki A, Kose S, Yoneda Y, Heldin CH, Moustakas A. Transforming growth factor-beta induces nuclear import of Smad3 in an importin-beta1 and Ran-dependent manner. Mol Biol Cell 2001;12:1079-1091.

82. Jeon YJ, Han SH, Yang KH, Kaminski NE. Induction of liver-associated transforming growth factor beta 1 (TGF-beta 1) mRNA expression by carbon

tetrachloride leads to the inhibition of T helper 2 cell-associated lymphokines. Toxicol Appl Pharmacol 1997;144:27-35.

83. Bedossa P, Peltier E, Terris B, Franco D, Poynard T. Transforming growth factor-beta 1 (TGF-beta 1) and TGF-beta 1 receptors in normal, cirrhotic, and neoplastic human livers. Hepatology 1995;21:760-766.

84. Bedossa P, Paradis V. Transforming growth factor-beta (TGF-beta): a key-role in liver fibrogenesis. J Hepatol 1995;22:37-42.

85. Hou J, Tian J, Jiang W, Gao Y, Fu F. Therapeutic effects of SMND-309, a new metabolite of salvianolic acid B, on experimental liver fibrosis. Eur J Pharmacol 2011;650:390-395.

86. Yoshimoto N, Togo S, Kubota T, Kamimukai N, Saito S, Nagano Y, Endo I, et al. Role of transforming growth factor-beta1 (TGF-beta1) in endotoxin-induced hepatic failure after extensive hepatectomy in rats. J Endotoxin Res 2005;11:33-39.

87. del Pilar Alatorre-Carranza M, Miranda-Diaz A, Yanez-Sanchez I, Pizano-Martinez O, Hermosillo-Sandoval JM, Vazquez-Del Mercado M, Hernandez-Hoyos S, et al. Liver fibrosis secondary to bile duct injury: correlation of Smad7 with TGF-beta and extracellular matrix proteins. BMC Gastroenterol 2009;9:81.

88. Yang L, Pang Y, Moses HL. TGF-beta and immune cells: an important regulatory axis in the tumor microenvironment and progression. Trends Immunol 2010;31:220-227.

89. Huang WC, Yen FC, Shie FS, Pan CM, Shiao YJ, Yang CN, Huang FL, et al. TGF-beta1 blockade of microglial chemotaxis toward Abeta aggregates involves SMAD signaling and down-regulation of CCL5. J Neuroinflammation 2010;7:28.

90. Cash WJ, McConville P, McDermott E, McCormick PA, Callender ME, McDougall NI. Current concepts in the assessment and treatment of hepatic encephalopathy. QJM 2010;103:9-16.

91. Hazell AS, Butterworth RF. Hepatic encephalopathy: An update of pathophysiologic mechanisms. Proc Soc Exp Biol Med 1999;222:99-112.

92. Cauli O, Rodrigo R, Llansola M, Montoliu C, Monfort P, Piedrafita B, El Mlili N, et al. Glutamatergic and gabaergic neurotransmission and neuronal circuits in hepatic encephalopathy. Metab Brain Dis 2009;24:69-80.

93. Suwelack D, Hurtado-Lorenzo A, Millan E, Gonzalez-Nicolini V, Wawrowsky K, Lowenstein PR, Castro MG. Neuronal expression of the transcription factor Gli1 using the Talpha1 alpha-tubulin promoter is neuroprotective in an experimental model of Parkinson's disease. Gene Ther 2004;11:1742-1752.

94. Ji H, Miao J, Zhang X, Du Y, Liu H, Li S, Li L. Inhibition of sonic hedgehog signaling aggravates brain damage associated with the down-regulation of Gli1, Ptch1 and SOD1 expression in acute ischemic stroke. Neurosci Lett 2012;506:1-6.

95. Ji H, Zhang X, Du Y, Liu H, Li S, Li L. Polydatin modulates inflammation by decreasing NF-kappaB activation and oxidative stress by increasing Gli1, Ptch1, SOD1 expression and ameliorates blood-brain barrier permeability for its neuroprotective effect in pMCAO rat brain. Brain Res Bull 2012;87:50-59.

96. Matise MP, Joyner AL. Gli genes in development and cancer. Oncogene 1999;18:7852-7859.

97. Katoh Y, Katoh M. Integrative genomic analyses on GLI1: positive regulation of GLI1 by Hedgehog-GLI, TGFbeta-Smads, and RTK-PI3K-AKT signals, and negative regulation of GLI1 by Notch-CSL-HES/HEY, and GPCR-Gs-PKA signals. Int J Oncol 2009;35:187-192.

98. Dennler S, Andre J, Alexaki I, Li A, Magnaldo T, ten Dijke P, Wang XJ, et al. Induction of sonic hedgehog mediators by transforming growth factor-beta: Smad3-dependent activation of Gli2 and Gli1 expression in vitro and in vivo. Cancer Res 2007;67:6981-6986.

99. Maitah MY, Ali S, Ahmad A, Gadgeel S, Sarkar FH. Up-regulation of sonic hedgehog contributes to TGF-beta1-induced epithelial to mesenchymal transition in NSCLC cells. PLoS One 2011;6:e16068.

100. Derynck R, Zhang YE. Smad-dependent and Smad-independent pathways in TGF-beta family signalling. Nature 2003;425:577-584.

101. Omenetti A, Choi S, Michelotti G, Diehl AM. Hedgehog signaling in the liver. J Hepatol 2011;54:366-373.

102. Pereira Tde A, Witek RP, Syn WK, Choi SS, Bradrick S, Karaca GF, Agboola KM, et al. Viral factors induce Hedgehog pathway activation in humans with viral hepatitis, cirrhosis, and hepatocellular carcinoma. Lab Invest 2010;90:1690-1703.

103. Gressner AM, Weiskirchen R, Breitkopf K, Dooley S. Roles of TGF-beta in hepatic fibrosis. Front Biosci 2002;7:d793-807.

104. Roth S, Michel K, Gressner AM. (Latent) transforming growth factor beta in liver parenchymal cells, its injury-dependent release, and paracrine effects on rat hepatic stellate cells. Hepatology 1998;27:1003-1012.

105. Eguchi S, Kamlot A, Ljubimova J, Hewitt WR, Lebow LT, Demetriou AA, Rozga J. Fulminant hepatic failure in rats: survival and effect on blood chemistry and liver regeneration. Hepatology 1996;24:1452-1459.

106. Bosoi CR, Parent-Robitaille C, Anderson K, Tremblay M, Rose CF. AST-120 (spherical carbon adsorbent) lowers ammonia levels and attenuates brain edema in bile duct-ligated rats. Hepatology 2011;53:1995-2002.

107. Frampton G, Invernizzi P, Bernuzzi F, Pae HY, Quinn M, Horvat D, Galindo C, et al. Interleukin-6-driven progranulin expression increases cholangiocarcinoma growth by an Akt-dependent mechanism. Gut 2012;61:268-277.

108. DeMorrow S, Francis H, Gaudio E, Venter J, Franchitto A, Kopriva S, Onori P, et al. The endocannabinoid anandamide inhibits cholangiocarcinoma

growth via activation of the noncanonical Wnt signaling pathway. Am J Physiol Gastrointest Liver Physiol 2008;295:G1150-1158.

109. Livak KJ, Schmittgen TD. Analysis of relative gene expression data using real-time quantitative PCR and the 2(-Delta Delta C(T)) Method. Methods 2001;25:402-408.

110. Goodenough S, Davidson M, Kidd G, Matsumoto I, Wilce P. Cell death and immunohistochemistry of p53, c-Fos and c-Jun after spermine injection into the rat striatum. Exp Brain Res 2000;131:126-134.

111. Amankulor NM, Hambardzumyan D, Pyonteck SM, Becher OJ, Joyce JA, Holland EC. Sonic hedgehog pathway activation is induced by acute brain injury and regulated by injury-related inflammation. J Neurosci 2009;29:10299-10308.

112. Omenetti A, Diehl AM. The adventures of sonic hedgehog in development and repair. II. Sonic hedgehog and liver development, inflammation, and cancer. Am J Physiol Gastrointest Liver Physiol 2008;294:G595-598.

113. Omenetti A, Yang L, Li YX, McCall SJ, Jung Y, Sicklick JK, Huang J, et al. Hedgehog-mediated mesenchymal-epithelial interactions modulate hepatic response to bile duct ligation. Lab Invest 2007;87:499-514.

114. Yang L, Wang Y, Mao H, Fleig S, Omenetti A, Brown KD, Sicklick JK, et al. Sonic hedgehog is an autocrine viability factor for myofibroblastic hepatic stellate cells. J Hepatol 2008;48:98-106.

115. Jung Y, Brown KD, Witek RP, Omenetti A, Yang L, Vandongen M, Milton RJ, et al. Accumulation of hedgehog-responsive progenitors parallels alcoholic

liver disease severity in mice and humans. Gastroenterology 2008;134:1532-1543.

116. Ochoa B, Syn WK, Delgado I, Karaca GF, Jung Y, Wang J, Zubiaga AM, et al. Hedgehog signaling is critical for normal liver regeneration after partial hepatectomy in mice. Hepatology 2010;51:1712-1723.

117. Seth D, Haber PS, Syn WK, Diehl AM, Day CP. Pathogenesis of alcohol-induced liver disease: classical concepts and recent advances. J Gastroenterol Hepatol 2011;26:1089-1105.

118. Sicklick JK, Li YX, Choi SS, Qi Y, Chen W, Bustamante M, Huang J, et al. Role for hedgehog signaling in hepatic stellate cell activation and viability. Lab Invest 2005;85:1368-1380.

119. Lipinski RJ, Hutson PR, Hannam PW, Nydza RJ, Washington IM, Moore RW, Girdaukas GG, et al. Dose- and route-dependent teratogenicity, toxicity, and pharmacokinetic profiles of the hedgehog signaling antagonist cyclopamine in the mouse. Toxicol Sci 2008;104:189-197.

120. Lanz TV, Ding Z, Ho PP, Luo J, Agrawal AN, Srinagesh H, Axtell R, et al. Angiotensin II sustains brain inflammation in mice via TGF-beta. J Clin Invest 2010;120:2782-2794.

121. Luo J, Ho PP, Buckwalter MS, Hsu T, Lee LY, Zhang H, Kim DK, et al. Glia-dependent TGF-beta signaling, acting independently of the TH17 pathway, is critical for initiation of murine autoimmune encephalomyelitis. J Clin Invest 2007;117:3306-3315.

122. Shahi MH, Afzal M, Sinha S, Eberhart CG, Rey JA, Fan X, Castresana JS. Regulation of sonic hedgehog-GLI1 downstream target genes PTCH1, Cyclin D2, Plakoglobin, PAX6 and NKX2.2 and their epigenetic status in medulloblastoma and astrocytoma. BMC Cancer 2010;10:614.

123. Lockwood AH, Yap EW, Wong WH. Cerebral ammonia metabolism in patients with severe liver disease and minimal hepatic encephalopathy. J Cereb Blood Flow Metab 1991;11:337-341.

124. Chen F, Ohashi N, Li W, Eckman C, Nguyen JH. Disruptions of occludin and claudin-5 in brain endothelial cells in vitro and in brains of mice with acute liver failure. Hepatology 2009;50:1914-1923.

125. Pardridge WM. Blood-brain barrier delivery. Drug Discov Today 2007;12:54-61.

126. Welser JV, Li L, Milner R. Microglial activation state exerts a biphasic influence on brain endothelial cell proliferation by regulating the balance of TNF and TGF-beta1. J Neuroinflammation 2010;7:89.

127. Rama Rao KV, Norenberg MD. Brain energy metabolism and mitochondrial dysfunction in acute and chronic hepatic encephalopathy. Neurochem Int 2012;60:697-706.

128. Ballabh P, Braun A, Nedergaard M. The blood-brain barrier: an overview: structure, regulation, and clinical implications. Neurobiol Dis 2004;16:1-13.

129. Hawkins BT, Davis TP. The blood-brain barrier/neurovascular unit in health and disease. Pharmacol Rev 2005;57:173-185.

130. Yang Y, Estrada EY, Thompson JF, Liu W, Rosenberg GA. Matrix metalloproteinase-mediated disruption of tight junction proteins in cerebral vessels is reversed by synthetic matrix metalloproteinase inhibitor in focal ischemia in rat. J Cereb Blood Flow Metab 2007;27:697-709.

131. Shimojima N, Eckman CB, McKinney M, Sevlever D, Yamamoto S, Lin W, Dickson DW, et al. Altered expression of zonula occludens-2 precedes increased blood-brain barrier permeability in a murine model of fulminant hepatic failure. J Invest Surg 2008;21:101-108.

132. Nguyen JH, Yamamoto S, Steers J, Sevlever D, Lin W, Shimojima N, Castanedes-Casey M, et al. Matrix metalloproteinase-9 contributes to brain extravasation and edema in fulminant hepatic failure mice. J Hepatol 2006;44:1105-1114.

133. Goldberg PL, MacNaughton DE, Clements RT, Minnear FL, Vincent PA. p38 MAPK activation by TGF-beta1 increases MLC phosphorylation and endothelial monolayer permeability. Am J Physiol Lung Cell Mol Physiol 2002;282:L146-154.

134. Behzadian MA, Wang XL, Windsor LJ, Ghaly N, Caldwell RB. TGF-beta increases retinal endothelial cell permeability by increasing MMP-9: possible role of glial cells in endothelial barrier function. Invest Ophthalmol Vis Sci 2001;42:853-859.

135. Manaenko A, Chen H, Kammer J, Zhang JH, Tang J. Comparison Evans Blue injection routes: Intravenous versus intraperitoneal, for measurement of

blood-brain barrier in a mice hemorrhage model. J Neurosci Methods 2011;195:206-210.

136. Yuan SY, Rigor RR: Methods for measuring permeability. In: Regulation of Endothelial Barrier Function. San Rafael (CA), 2010.

137. Yamamoto S, Nguyen JH. TIMP-1/MMP-9 imbalance in brain edema in rats with fulminant hepatic failure. J Surg Res 2006;134:307-314.

138. Rai V, Nath K, Saraswat VA, Purwar A, Rathore RK, Gupta RK. Measurement of cytotoxic and interstitial components of cerebral edema in acute hepatic failure by diffusion tensor imaging. J Magn Reson Imaging 2008;28:334-341.

139. Kale RA, Gupta RK, Saraswat VA, Hasan KM, Trivedi R, Mishra AM, Ranjan P, et al. Demonstration of interstitial cerebral edema with diffusion tensor MR imaging in type C hepatic encephalopathy. Hepatology 2006;43:698-706.

140. Bémeur C, Chastre A, Desjardins P, Butterworth R. No changes in expression of tight junction proteins or blood–brain barrier permeability in azoxymethane-induced experimental acute liver failure. Neurochem Int 2010;56:205-207.

141. Koto T, Takubo K, Ishida S, Shinoda H, Inoue M, Tsubota K, Okada Y, et al. Hypoxia disrupts the barrier function of neural blood vessels through changes in the expression of claudin-5 in endothelial cells. Am J Pathol 2007;170:1389-1397.

142. Inamura A, Adachi Y, Inoue T, He Y, Tokuda N, Nawata T, Shirao S, et al. Cooling treatment transiently increases the permeability of brain capillary endothelial cells through translocation of claudin-5. Neurochem Res 2013;38:1641-1647.

143. Jiao H, Wang Z, Liu Y, Wang P, Xue Y. Specific role of tight junction proteins claudin-5, occludin, and ZO-1 of the blood-brain barrier in a focal cerebral ischemic insult. J Mol Neurosci 2011;44:130-139.

144. Ronaldson PT, Demarco KM, Sanchez-Covarrubias L, Solinsky CM, Davis TP. Transforming growth factor-beta signaling alters substrate permeability and tight junction protein expression at the blood-brain barrier during inflammatory pain. J Cereb Blood Flow Metab 2009;29:1084-1098.

145. Kim HS, Luo L, Pflugfelder SC, Li DQ. Doxycycline inhibits TGF-beta1-induced MMP-9 via Smad and MAPK pathways in human corneal epithelial cells. Invest Ophthalmol Vis Sci 2005;46:840-848.

146. Huang HC, Liu SY, Liang Y, Liu Y, Li JZ, Wang HY. [Transforming growth factor-beta1 stimulates matrix metalloproteinase-9 production through ERK activation pathway and upregulation of Ets-1 protein]. Zhonghua Yi Xue Za Zhi 2005;85:328-331.

147. Skowronska M, Zielinska M, Wojcik-Stanaszek L, Ruszkiewicz J, Milatovic D, Aschner M, Albrecht J. Ammonia increases paracellular permeability of rat brain endothelial cells by a mechanism encompassing oxidative/nitrosative

stress and activation of matrix metalloproteinases. J Neurochem 2012;121:125-134.

148. Larsson J, Karlsson S. The role of Smad signaling in hematopoiesis. Oncogene 2005;24:5676-5692.

149. Watabe T, Nishihara A, Mishima K, Yamashita J, Shimizu K, Miyazawa K, Nishikawa S, et al. TGF-beta receptor kinase inhibitor enhances growth and integrity of embryonic stem cell-derived endothelial cells. J Cell Biol 2003;163:1303-1311.

150. Okamoto T, Takahashi S, Nakamura E, Nagaya K, Hayashi T, Fujieda K. Transforming growth factor-beta1 induces matrix metalloproteinase-9 expression in human meningeal cells via ERK and Smad pathways. Biochem Biophys Res Commun 2009;383:475-479.

151. Kato M, Putta S, Wang M, Yuan H, Lanting L, Nair I, Gunn A, et al. TGF-beta activates Akt kinase through a microRNA-dependent amplifying circuit targeting PTEN. Nat Cell Biol 2009;11:881-889.

152. Hu L, Hofmann J, Jaffe RB. Phosphatidylinositol 3-kinase mediates angiogenesis and vascular permeability associated with ovarian carcinoma. Clin Cancer Res 2005;11:8208-8212.

153. Yuan TL, Choi HS, Matsui A, Benes C, Lifshits E, Luo J, Frangioni JV, et al. Class 1A PI3K regulates vessel integrity during development and tumorigenesis. Proc Natl Acad Sci U S A 2008;105:9739-9744.

154. Kilic E, Kilic U, Wang Y, Bassetti CL, Marti HH, Hermann DM. The phosphatidylinositol-3 kinase/Akt pathway mediates VEGF's neuroprotective activity and induces blood brain barrier permeability after focal cerebral ischemia. FASEB J 2006;20:1185-1187.

155. Yang B, Singh S, Bressani R, Kanmogne GD. Cross-talk between STAT1 and PI3K/AKT signaling in HIV-1-induced blood-brain barrier dysfunction: role of CCR5 and implications for viral neuropathogenesis. J Neurosci Res 2010;88:3090-3101.

156. Tchantchou F, Zhang Y. Selective inhibition of alpha/beta-hydrolase domain 6 attenuates neurodegeneration, alleviates blood brain barrier breakdown, and improves functional recovery in a mouse model of traumatic brain injury. J Neurotrauma 2013;30:565-579.

157. Olson TS, Ley K. Chemokines and chemokine receptors in leukocyte trafficking. Am J Physiol Regul Integr Comp Physiol 2002;283:R7-28.

158. Banisor I, Leist TP, Kalman B. Involvement of beta-chemokines in the development of inflammatory demyelination. J Neuroinflammation 2005;2:7.

159. Dijkstra IM, Hulshof S, van der Valk P, Boddeke HW, Biber K. Cutting edge: activity of human adult microglia in response to CC chemokine ligand 21. J Immunol 2004;172:2744-2747.

160. Chastre A, Belanger M, Beauchesne E, Nguyen BN, Desjardins P, Butterworth RF. Inflammatory cascades driven by tumor necrosis factor-alpha

play a major role in the progression of acute liver failure and its neurological complications. PLoS One 2012;7:e49670.

161. Ramos CD, Canetti C, Souto JT, Silva JS, Hogaboam CM, Ferreira SH, Cunha FQ. MIP-1alpha[CCL3] acting on the CCR1 receptor mediates neutrophil migration in immune inflammation via sequential release of TNF-alpha and LTB4. J Leukoc Biol 2005;78:167-177.

162. Seki E, De Minicis S, Gwak GY, Kluwe J, Inokuchi S, Bursill CA, Llovet JM, et al. CCR1 and CCR5 promote hepatic fibrosis in mice. J Clin Invest 2009;119:1858-1870.

163. Vitner EB, Farfel-Becker T, Eilam R, Biton I, Futerman AH. Contribution of brain inflammation to neuronal cell death in neuronopathic forms of Gaucher's disease. Brain 2012;135:1724-1735.

164. Zhu XB, Wang YB, Chen O, Zhang DQ, Zhang ZH, Cao AH, Huang SY, et al. Characterization of the expression of macrophage inflammatory protein-1alpha (MIP-1alpha) and C-C chemokine receptor 5 (CCR5) after kainic acid-induced status epilepticus (SE) in juvenile rats. Neuropathol Appl Neurobiol 2012;38:602-616.

165. Han Y, Wang J, Zhou Z, Ransohoff RM. TGFbeta1 selectively up-regulates CCR1 expression in primary murine astrocytes. Glia 2000;30:1-10.

166. Eltayeb S, Berg AL, Lassmann H, Wallstrom E, Nilsson M, Olsson T, Ericsson-Dahlstrand A, et al. Temporal expression and cellular origin of CC

chemokine receptors CCR1, CCR2 and CCR5 in the central nervous system: insight into mechanisms of MOG-induced EAE. J Neuroinflammation 2007;4:14.

167. Etemad S, Zamin RM, Ruitenberg MJ, Filgueira L. A novel in vitro human microglia model: characterization of human monocyte-derived microglia. J Neurosci Methods 2012;209:79-89.

168. Harry GJ. Microglia during development and aging. Pharmacol Ther 2013;139:313-326.

169. Rose C, Michalak A, Pannunzio M, Chatauret N, Rambaldi A, Butterworth RF. Mild hypothermia delays the onset of coma and prevents brain edema and extracellular brain glutamate accumulation in rats with acute liver failure. Hepatology 2000;31:872-877.

170. Ajuebor MN, Hogaboam CM, Le T, Proudfoot AE, Swain MG. CCL3/MIP-1alpha is pro-inflammatory in murine T cell-mediated hepatitis by recruiting CCR1-expressing CD4(+) T cells to the liver. Eur J Immunol 2004;34:2907-2918.

171. Shi F, Zhang JY, Zeng Z, Tien P, Wang FS. Skewed ratios between CD3(+) T cells and monocytes are associated with poor prognosis in patients with HBV-related acute-on-chronic liver failure. Biochem Biophys Res Commun 2010;402:30-36.

172. Heinrichs D, Berres ML, Nellen A, Fischer P, Scholten D, Trautwein C, Wasmuth HE, et al. The chemokine CCL3 promotes experimental liver fibrosis in mice. PLoS One 2013;8:e66106.

173. Shawcross DL, Wright GA, Stadlbauer V, Hodges SJ, Davies NA, Wheeler-Jones C, Pitsillides AA, et al. Ammonia impairs neutrophil phagocytic function in liver disease. Hepatology 2008;48:1202-1212.

174. Shawcross DL, Shabbir SS, Taylor NJ, Hughes RD. Ammonia and the neutrophil in the pathogenesis of hepatic encephalopathy in cirrhosis. Hepatology 2010;51:1062-1069.

175. Reichel CA, Puhr-Westerheide D, Zuchtriegel G, Uhl B, Berberich N, Zahler S, Wymann MP, et al. C-C motif chemokine CCL3 and canonical neutrophil attractants promote neutrophil extravasation through common and distinct mechanisms. Blood 2012;120:880-890.

176. Kim IS, Jang SW, Sung HJ, Lee JS, Ko J. Differential CCR1-mediated chemotaxis signaling induced by human CC chemokine HCC-4/CCL16 in HOS cells. FEBS Lett 2005;579:6044-6048.

177. Ko J, Kim IS, Jang SW, Lee YH, Shin SY, Min DS, Na DS. Leukotactin-1/CCL15-induced chemotaxis signaling through CCR1 in HOS cells. FEBS Lett 2002;515:159-164.

178. Kim IS, Ryang YS, Kim YS, Jang SW, Sung HJ, Lee YH, Kim J, et al. Leukotactin-1-induced ERK activation is mediated via Gi/Go protein/PLC/PKC delta/Ras cascades in HOS cells. Life Sci 2003;73:447-459.

179. Lu DY, Tang CH, Yeh WL, Wong KL, Lin CP, Chen YH, Lai CH, et al. SDF-1alpha up-regulates interleukin-6 through CXCR4, PI3K/Akt, ERK, and NF-kappaB-dependent pathway in microglia. Eur J Pharmacol 2009;613:146-154.

180. Sometani A, Kataoka H, Nitta A, Fukumitsu H, Nomoto H, Furukawa S. Transforming growth factor-beta1 enhances expression of brain-derived neurotrophic factor and its receptor, TrkB, in neurons cultured from rat cerebral cortex. J Neurosci Res 2001;66:369-376.

181. Brionne TC, Tesseur I, Masliah E, Wyss-Coray T. Loss of TGF-beta 1 leads to increased neuronal cell death and microgliosis in mouse brain. Neuron 2003;40:1133-1145.

182. Berahovich RD, Miao Z, Wang Y, Premack B, Howard MC, Schall TJ. Proteolytic activation of alternative CCR1 ligands in inflammation. J Immunol 2005;174:7341-7351.

183. Sundaram V, Shaikh OS. Acute liver failure: current practice and recent advances. Gastroenterol Clin North Am 2011;40:523-539.

184. Chung HS, Jung DH, Park CS. Intraoperative predictors of short-term mortality in living donor liver transplantation due to acute liver failure. Transplant Proc 2013;45:236-240.

185. Mpabanzi L, Jalan R. Neurological complications of acute liver failure: pathophysiological basis of current management and emerging therapies. Neurochem Int 2012;60:736-742.

186. Mumtaz K, Azam Z, Hamid S, Abid S, Memon S, Ali Shah H, Jafri W. Role of N-acetylcysteine in adults with non-acetaminophen-induced acute liver failure in a center without the facility of liver transplantation. Hepatol Int 2009;3:563-570.

187. Ringe B, Lubbe N, Kuse E, Frei U, Pichlmayr R. Total hepatectomy and liver transplantation as two-stage procedure. Ann Surg 1993;218:3-9.

188. Jalan R, Pollok A, Shah SH, Madhavan K, Simpson KJ. Liver derived pro-inflammatory cytokines may be important in producing intracranial hypertension in acute liver failure. J Hepatol 2002;37:536-538.

189. Riobo NA, Saucy B, Dilizio C, Manning DR. Activation of heterotrimeric G proteins by Smoothened. Proc Natl Acad Sci U S A 2006;103:12607-12612.

190. Mahoney WM, Jr., Gunaje J, Daum G, Dong XR, Majesky MW. Regulator of G-protein signaling - 5 (RGS5) is a novel repressor of hedgehog signaling. PLoS One 2013;8:e61421.

191. Park K, Hong SW, Hur W, Lee MY, Yang JA, Kim SW, Yoon SK, et al. Target specific systemic delivery of TGF-beta siRNA/(PEI-SS)-g-HA complex for the treatment of liver cirrhosis. Biomaterials 2011;32:4951-4958.

192. Birukova AA, Adyshev D, Gorshkov B, Birukov KG, Verin AD. ALK5 and Smad4 are involved in TGF-beta1-induced pulmonary endothelial permeability. FEBS Lett 2005;579:4031-4037.

193. Skowronska M, Albrecht J. Alterations of blood brain barrier function in hyperammonemia: an overview. Neurotox Res 2012;21:236-244.

194. Lv S, Song HL, Zhou Y, Li LX, Cui W, Wang W, Liu P. Tumour necrosis factor-alpha affects blood-brain barrier permeability and tight junction-associated occludin in acute liver failure. Liver Int 2010;30:1198-1210.

195. Baeck C, Wehr A, Karlmark KR, Heymann F, Vucur M, Gassler N, Huss S, et al. Pharmacological inhibition of the chemokine CCL2 (MCP-1) diminishes liver macrophage infiltration and steatohepatitis in chronic hepatic injury. Gut 2012;61:416-426.

196. Degre D, Lemmers A, Gustot T, Ouziel R, Trepo E, Demetter P, Verset L, et al. Hepatic expression of CCL2 in alcoholic liver disease is associated with disease severity and neutrophil infiltrates. Clin Exp Immunol 2012;169:302-310.

197. Leifeld L, Dumoulin FL, Purr I, Janberg K, Trautwein C, Wolff M, Manns MP, et al. Early up-regulation of chemokine expression in fulminant hepatic failure. J Pathol 2003;199:335-344.

198. Antoniades CG, Quaglia A, Taams LS, Mitry RR, Hussain M, Abeles R, Possamai LA, et al. Source and characterization of hepatic macrophages in acetaminophen-induced acute liver failure in humans. Hepatology 2012;56:735-746.

199. D'Mello C, Le T, Swain MG. Cerebral microglia recruit monocytes into the brain in response to tumor necrosis factoralpha signaling during peripheral organ inflammation. J Neurosci 2009;29:2089-2102.